

Supporting Information for

**Crustal seismic structure and anisotropy of Madagascar and southeastern Africa using  
receiver function harmonics: interplay of inherited local heterogeneity and current regional  
stress**

E. Tsang-Hin-Sun<sup>1,2</sup>, M. Evain<sup>1</sup>, J. Julia<sup>3</sup>, G. Lamarque<sup>1,2</sup>, P. Schnurle<sup>1</sup>

<sup>1</sup>Ifremer, Marine Geosciences, Centre de Brest, CS 10070 - 29280 Plouzane - France

<sup>2</sup>Université de Bretagne Occidentale (UBO), Institut Universitaire Européen de la Mer (IUEM), Laboratoire Geosciences Ocean, UMR 6538, 29280 Plouzané, France

<sup>3</sup>Departamento de Geofísica, Universidade Federal do Rio Grande do Norte, Natal, RN CEP 59078-970, Brazil

Corresponding authors: Eve Tsang-Hin-Sun (eve.tsang.hin.sun@ifremer.fr); Mikael Evain (mikael.evain@ifremer.fr)

Abbreviated title: Crustal seismic structure and anisotropy under SE-Africa and Madagascar

**Contents of this file**

Text S1 to S2

Figures S1 to S3

Tables S1

## **Introduction**

This supporting information contains additional details on the data processing, in particular concerning the estimation of the crustal thickness by the H- $\kappa$  stacking method and on the expected uncertainties in using the harmonic decomposition method.

- Text S1 explores the effect of noise and azimuthal coverage on the uncertainty of the harmonic decomposition method;
- Text S2 details the data processing for estimating the crustal thickness using the H- $\kappa$  stacking method;
- Figures S1 and S2 illustrate Text S1;
- Figures S3 compiles for each stations stacked radial and transverse RF sorted in back-azimuth, calculated harmonic components and rotated harmonic components.
- Table S1 summarizes the results of the H- $\kappa$  stacking method.

### **Text S1.**

In theory, the harmonic decomposition method is able to retrieve the orientation of anisotropy for a minimum of 9 bins, no matter the azimuthal distribution of the bins. In previous studies, uncertainties on the angle have been estimated through misfit in the particle motion of harmonics (e;g. Bianchi et al., 2010) or through bootstrap-like resampling of the stacked RFs (Lamarque & Julia, 2019). These two methods, however, quantify the level of noise in the data, rather than the true uncertainty on the angle estimation. Firstly, the uncertainty of the angle estimation should be in the order of the size of the bin ( $5^\circ$  for bins of  $10^\circ$ ). Secondly, the quality of the estimation depends on the position of the azimuthal gaps with respect to the symmetry axis and the level of noise in the RFs.

To quantify both effects (noise and azimuthal coverage), synthetic RFs were computed using the Raysum code (Frederiksen & Bostock, 2000) for a simple model composed of one anisotropic layer (figure S1a). RFs were computed in all directions in non overlapping  $10^\circ$  bins (figure S1b). Realistic noise was modeled as a series of spikes with random amplitudes, width and arrival times. These three criteria were extracted from the real data set: the amplitude of the spikes are normally distributed and do not exceed 20 percent of the maximum amplitude of the RFs; the recurrence of the spikes follows a normal distribution with 1 s mean and 0.5 s standard deviation. The series of spikes was then convoluted with a Gaussian pulse and the resulting noisy time series in each direction were then added to the RFs. Then, the orientation of the fast axis in the crust was estimated from the noisy RFs decomposed into back-azimuth harmonics for different number of bins. For each test, 500 realizations were made in order to get a robust estimation of the error.

First, we tested the effect of decimating the number of bins in randomly chosen back-azimuths. When no noise is added, decimating the RF data set has a low impact on the quality of the estimation, even when only 9 bins are selected (figure S2). Adding realistic noise to the RFs still allows a quite satisfying estimation of the fast-axis orientation with standard errors reaching  $\sim 15^\circ$  though, when a minimum of 9 bins are selected.

Then, the data set were decimated in a particular direction rather than in different random azimuths, while decreasing the number of bins, to mimic an azimuthal gap in the data set. In this case, the standard error is much more sensitive to the position of the gap with respect to the orientation of the fast axis. In particular, the error is expected to be larger when the gap is in the direction normal to the fast axis. In the absence of noise, the standard error increases starting from 20 bins and reach  $20^\circ$  when only 9 bins are selected. Adding noise emphasizes this trend, with uncertainties up to  $25^\circ$  when 15 bins are selected and reaching  $50^\circ$  for only 9 bins.

In our data set, only stations with more than 10 RFs bins were considered (table S1) and the average number of bins is 30, while the average gap is  $77^\circ$ . Thus, in average, the estimation are not expected to be strongly influenced by the azimuthal gap. However, there is not necessarily a direct relationship between the azimuthal gap and the number of RF bins. Thus, the combination of randomly and focused gap might contribute to increase the level of uncertainty in comparison with the theoretical value. Temporary stations deployed in Madagascar and Mozambique are mostly concerned by gaps in the azimuthal coverage and the interpretation of their harmonics must thus take into account the possible large uncertainties there.

## Text S2.

We used the H-k stacking method (Zhu & Kanamori, 2000) to estimate the crustal thickness beneath the stations for which no data were previously published (mainly in South Africa and Mozambique). First, we selected only the best quality RFs as those reproducing at least 95% of the observed initial seismogram.

The technique stacks the Pms and PpPms phases to determine the crustal thickness and mean vp/vs ratio:

$$s(H, \kappa) = \sum w_1 r_i(t_1) + w_2 r_i(t_2) - w_3 r_i(t_3) \quad (1)$$

where  $r_i$  is the i-th radial RF;  $t_1$ ,  $t_2$  and  $t_3$  are the predicted arrival times of the Ps, PpPs and PpSs+PsPs phases, respectively;  $w_1$ ,  $w_2$ ,  $w_3$  are weights and  $\sum w_i = 1$ . The maximum of  $s$  is reached when all phases are stacked coherently, with the best estimate of  $H$  and  $\kappa$ . Two sets of weighing factors were tested:

- set 1:  $w_1=0.6$ ,  $w_2=0.3$ ,  $w_3=0.1$ ;
- set 2:  $w_1=0.4$ ,  $w_2=0.3$ ,  $w_3=0.3$ .

The uncertainty on the estimated parameters was quantify through a bootstrap approach (Julia & Mejia, 2004) for 100 realizations. Finally,  $v_p$  was set to the average value of 6.5 km/s. The results are summarized in the table S2. For some temporary stations, especially in Mozambique and Madagascar, the H-k stacking failed to produce a coherent solution. For those stations, the Moho depth was extracted from the crust1.0 model (Laske et al., 2013).

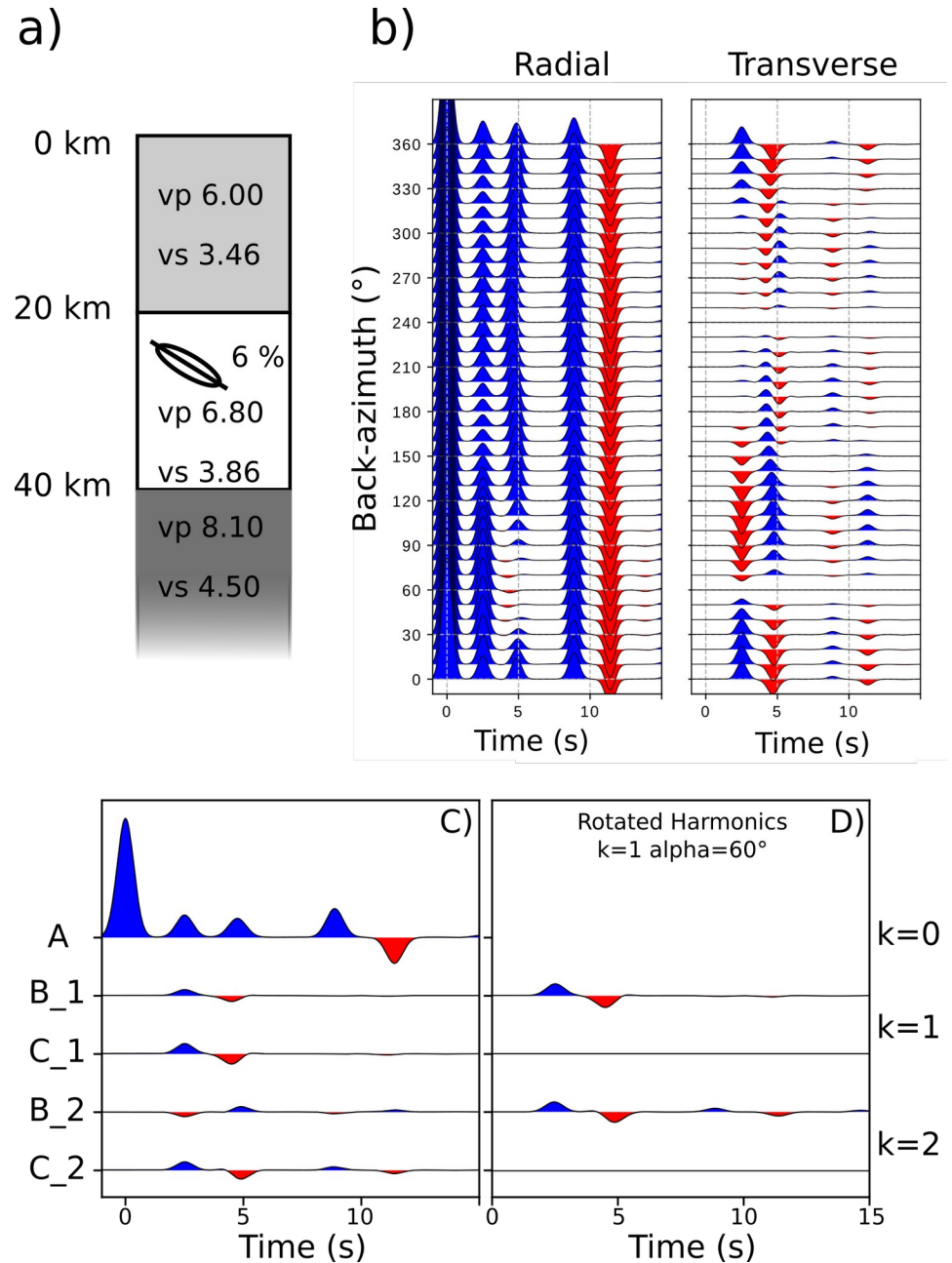


**Figure S1.** Model (a) and RF synthetics (b) used to test the effect of noise and azimuthal coverage on the uncertainty of the harmonic decomposition method. In the model (a), the anisotropy is 6 % and the fast axis trends N60° and plunges of 30°. Polarity reversals are clearly visible in the transverse RF at 60° and 240° (b). C) and D) are respectively as in figure 2 and 3 the resulting harmonics and rotated harmonics.

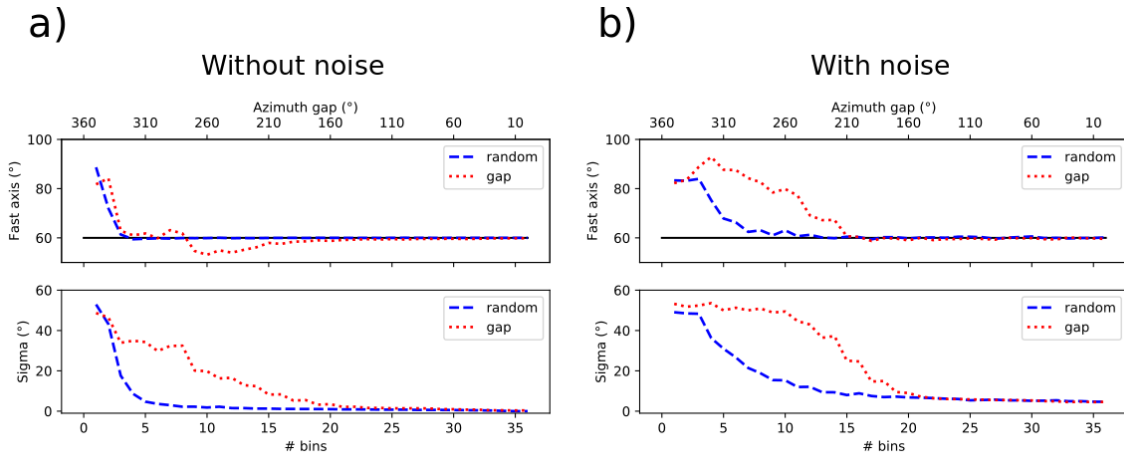


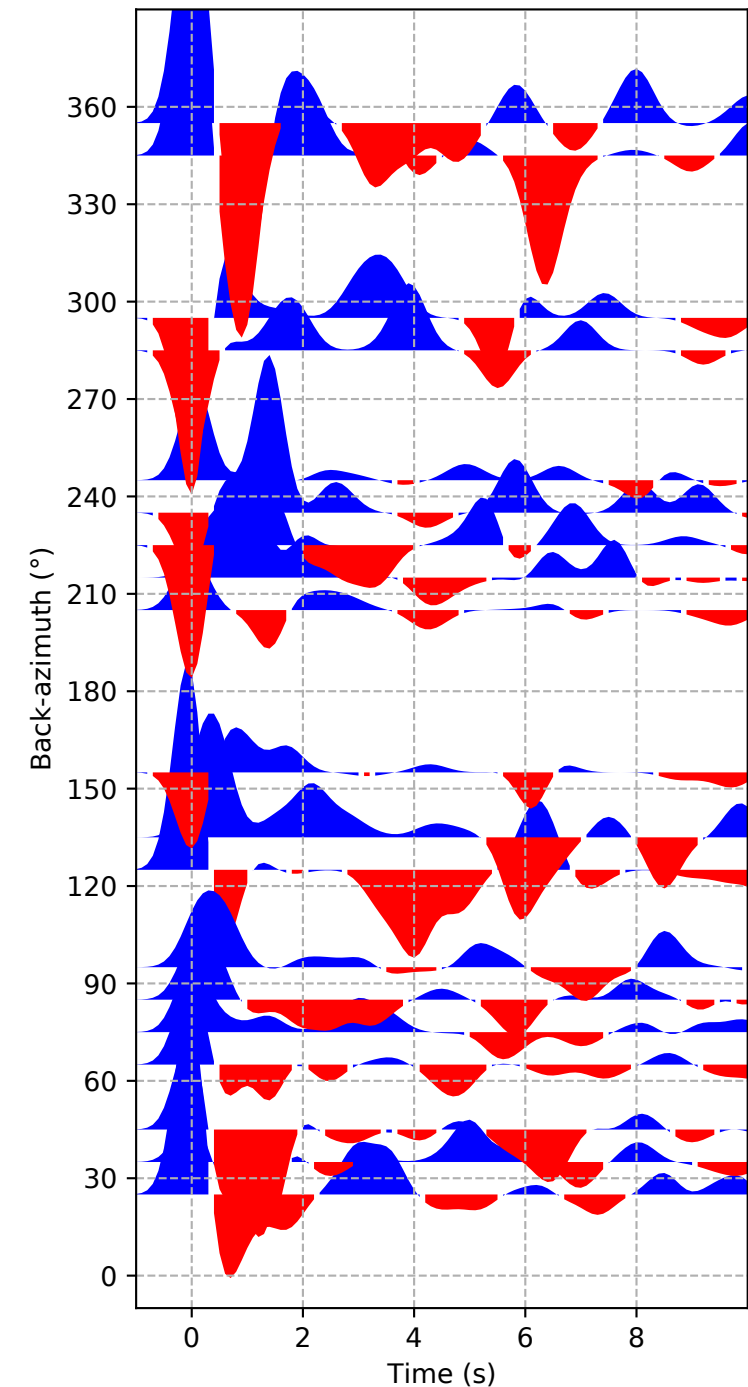
**Figure S2.** Effect of noise and azimuthal coverage on the harmonic decomposition method.

a) The evolution of the estimated angle (mean of the 500 realizations, top panel) and of the uncertainty on the angle sigma (standard deviation of the 500 realizations, bottom panel) as a function of the azimuthal gap/number of bins, in case where no noise was added to the synthetic RFs. b) the same as a) when noise was added to the synthetic RFs. In both case, the tests were proceed for randomly chosen bins (dashed lines) and focused azimuthal gap (dotted lines).

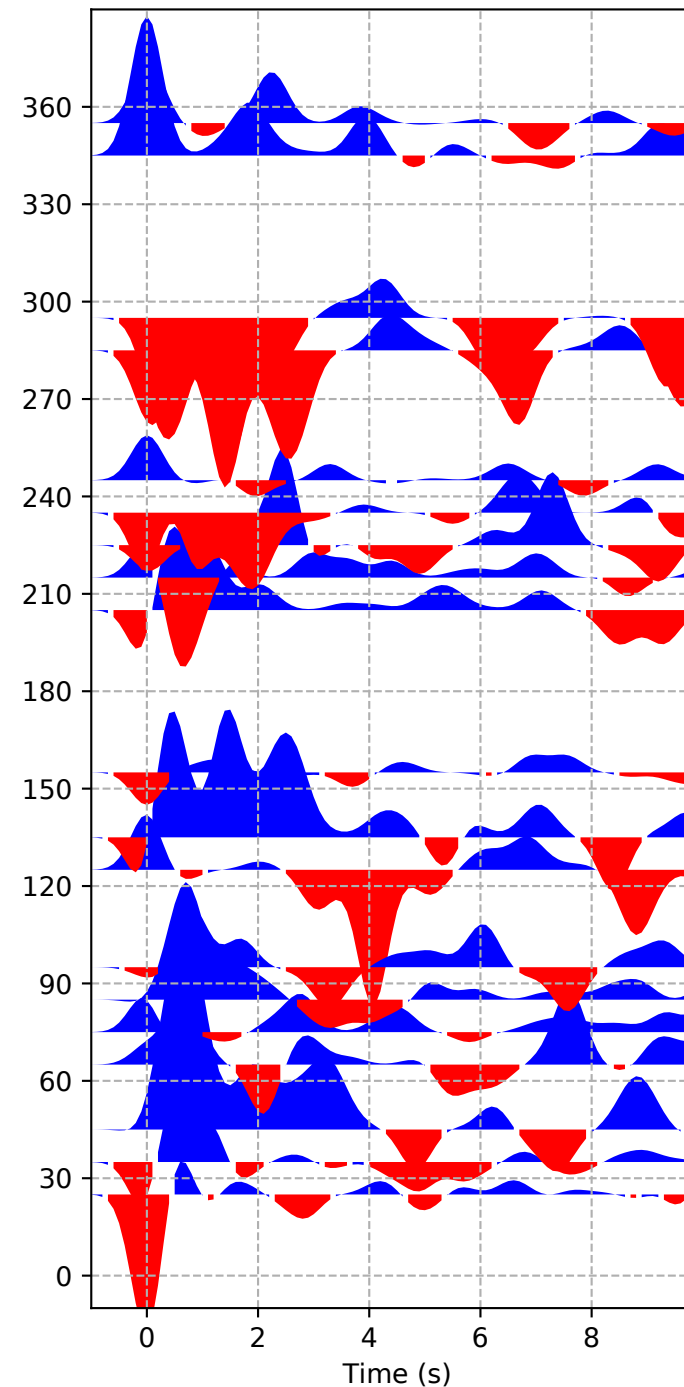
**Figure S3.** For each stations radial (a) and transverse (b) receiver functions stacked in back-azimuth bins of  $10^\circ$  without overlap; c) resulting harmonics corresponding to the degrees  $k=0$  (A),  $k=1$  ( $B_1, C_1$ ) and  $k=2$  ( $B_2, C_2$ ); d) rotated harmonics according to angle provided in Table 1: degree  $k=0$  (A) is repeated then rotated harmonics for degree  $k=1$  ( $Br_1, Cr_1$ ) and  $k=2$  ( $Br_2, Cr_2$ ).

## AF-CNG

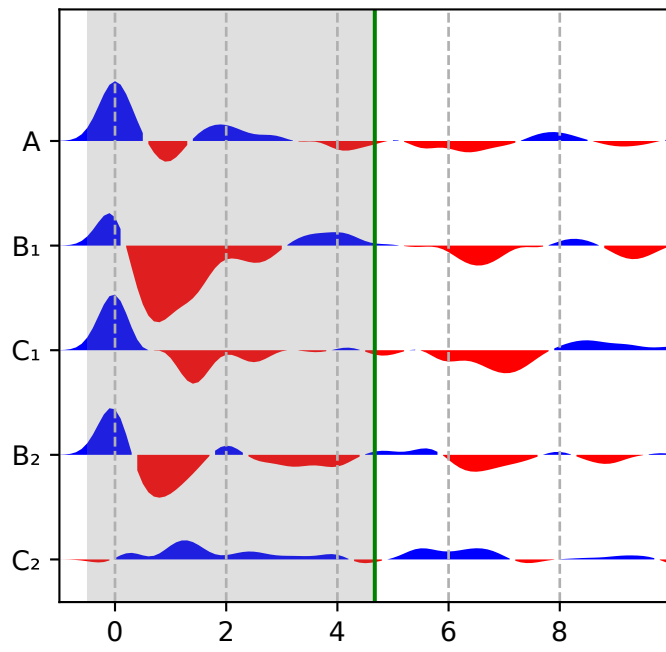
A) Radial



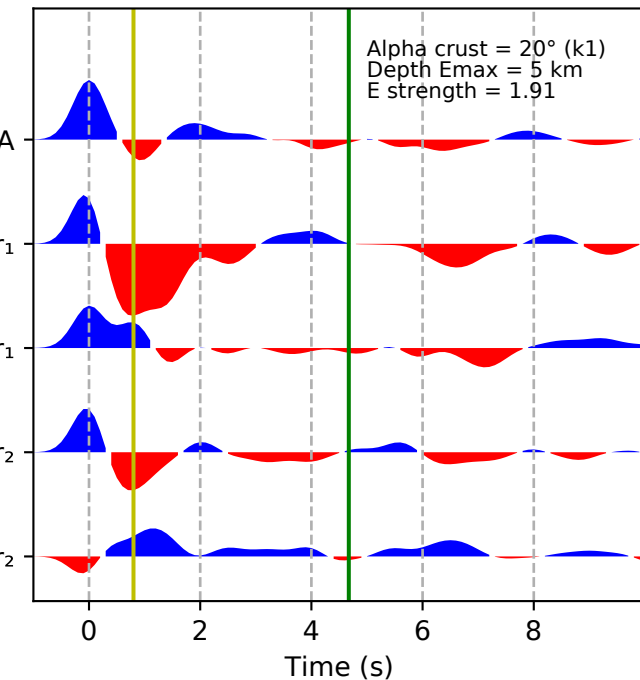
B) Transverse



C) Harmonics components

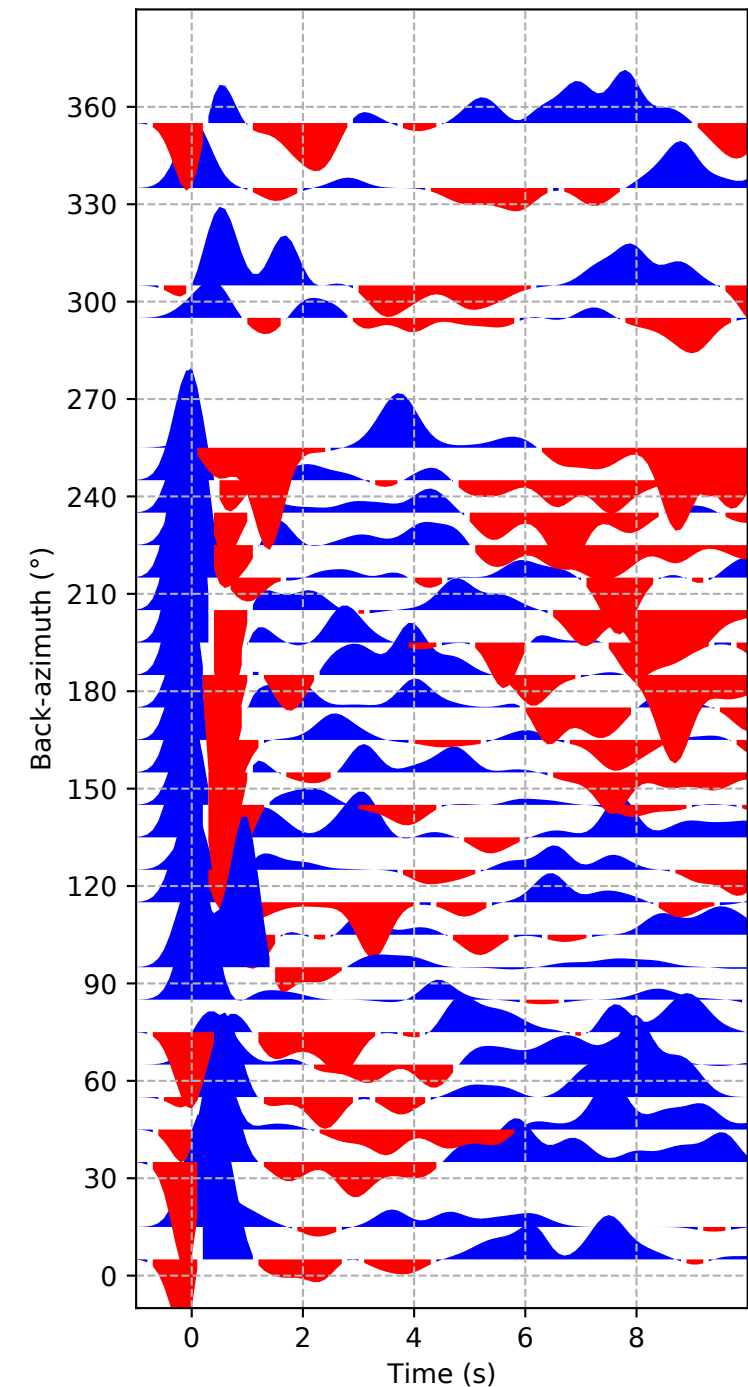


D) Rotated Harmonics components

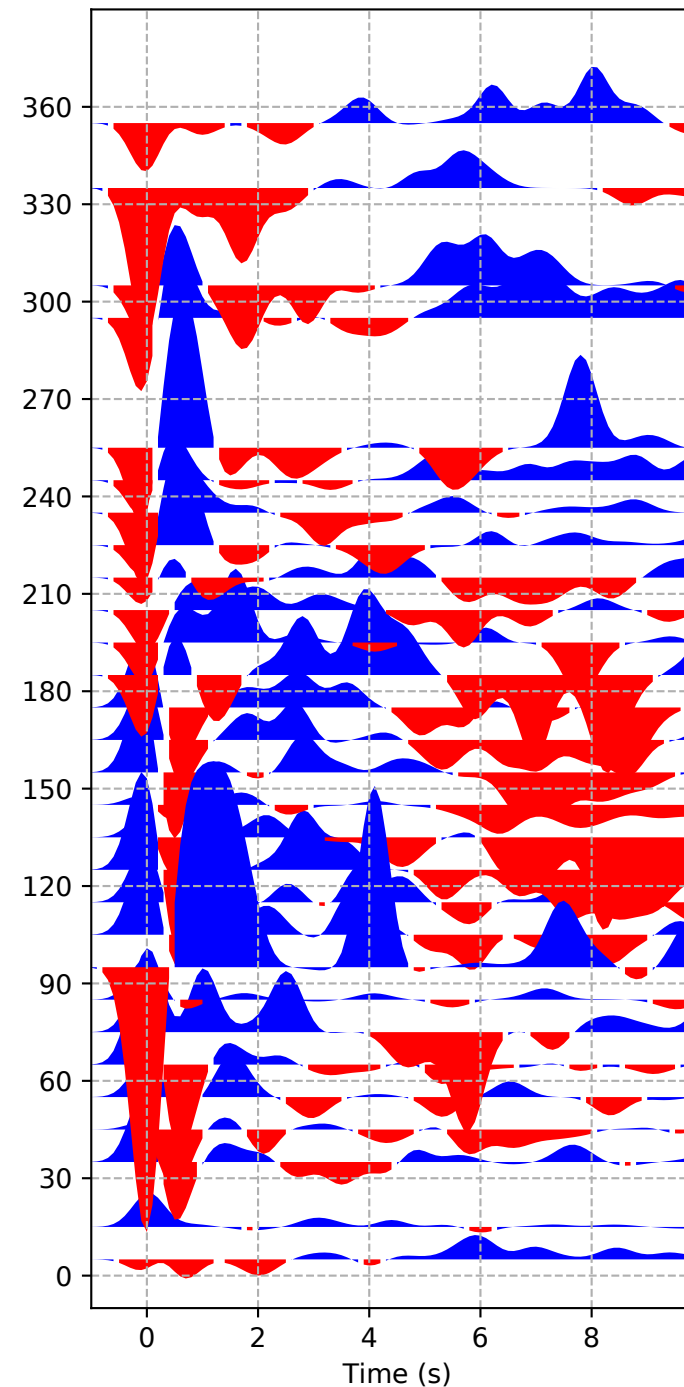


## AF-GRM

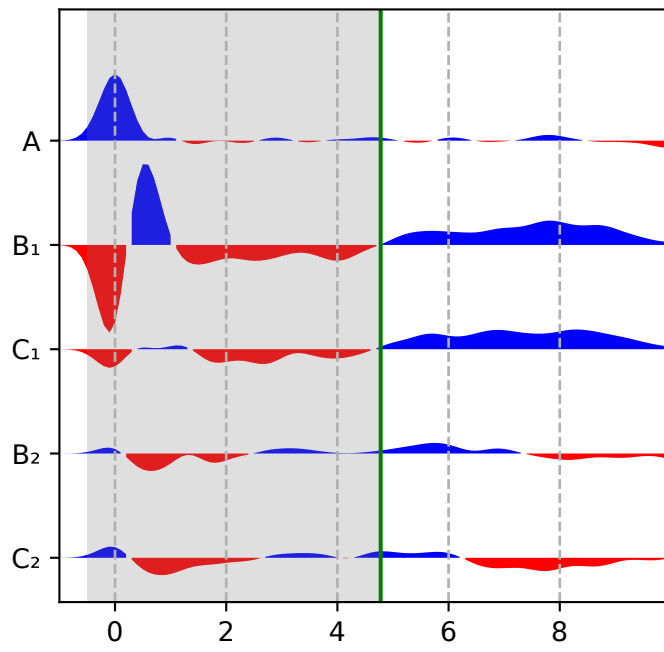
A) Radial



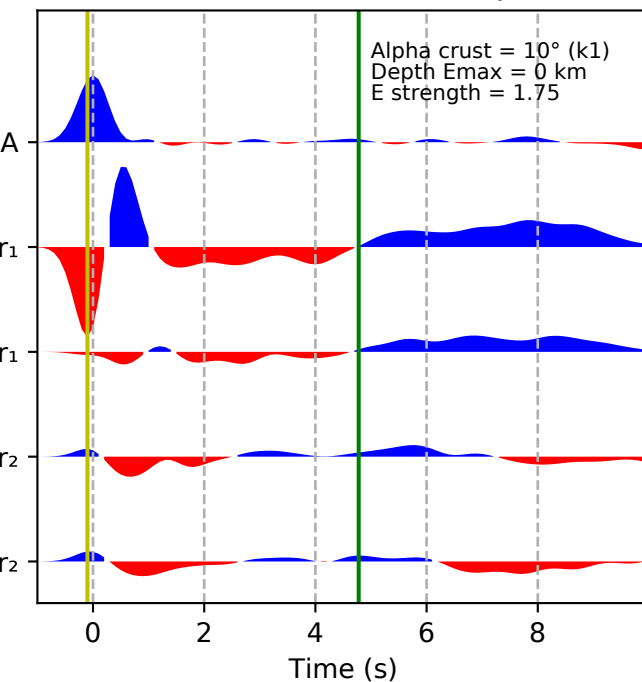
B) Transverse

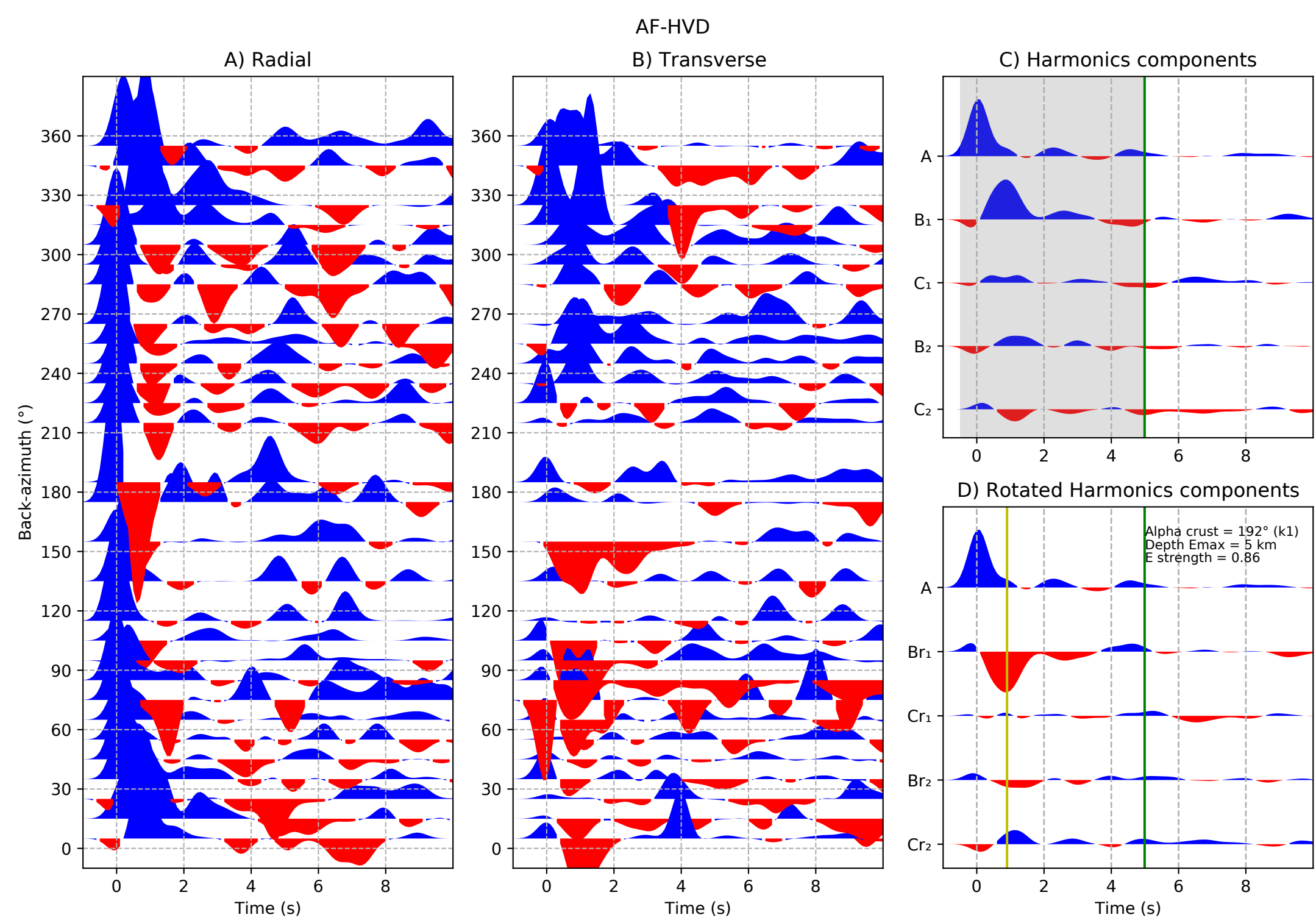


C) Harmonics components



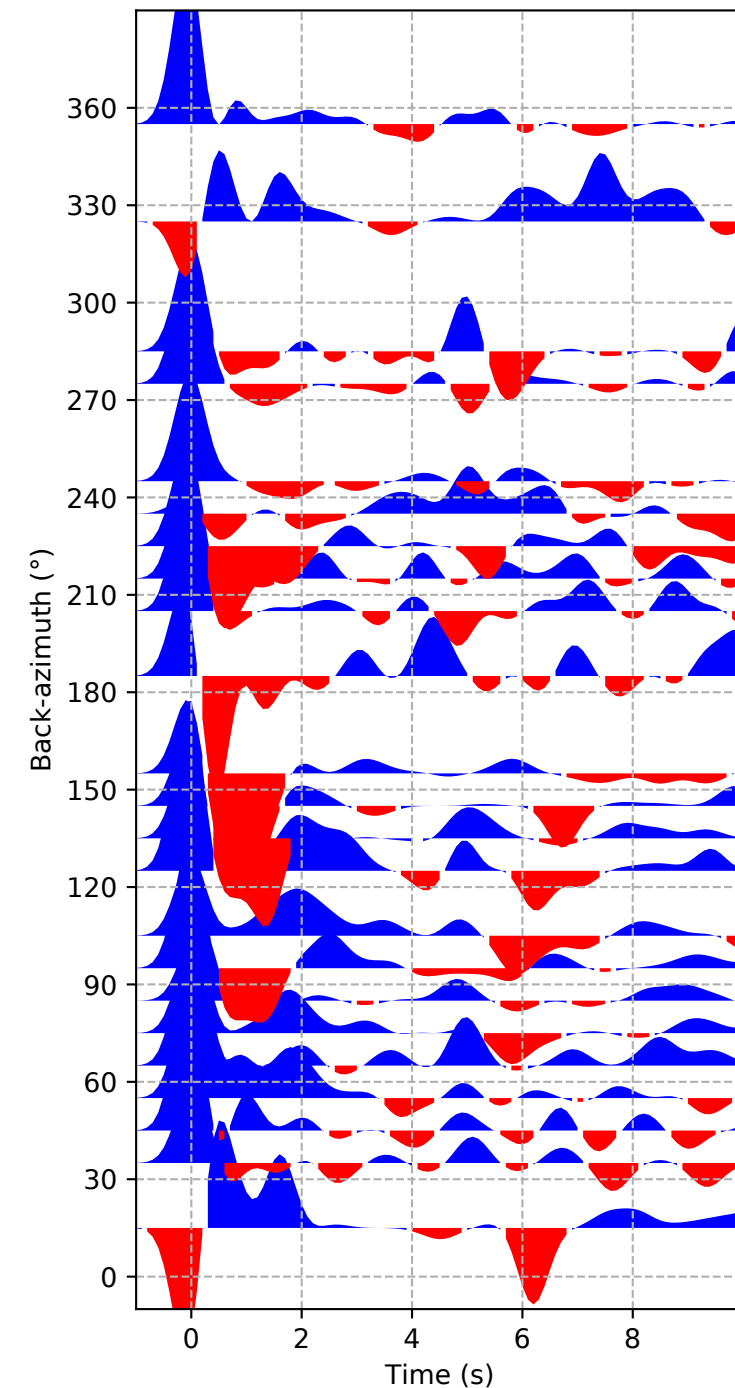
D) Rotated Harmonics components



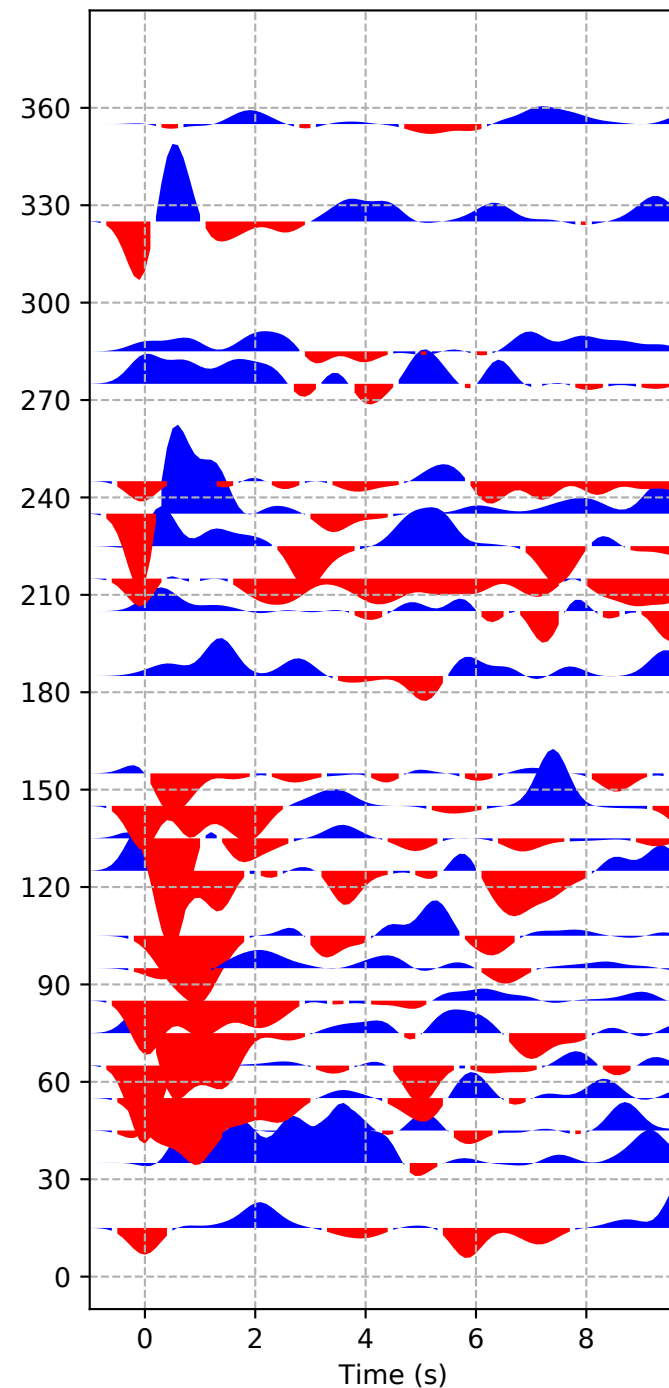


# AF-MOPA

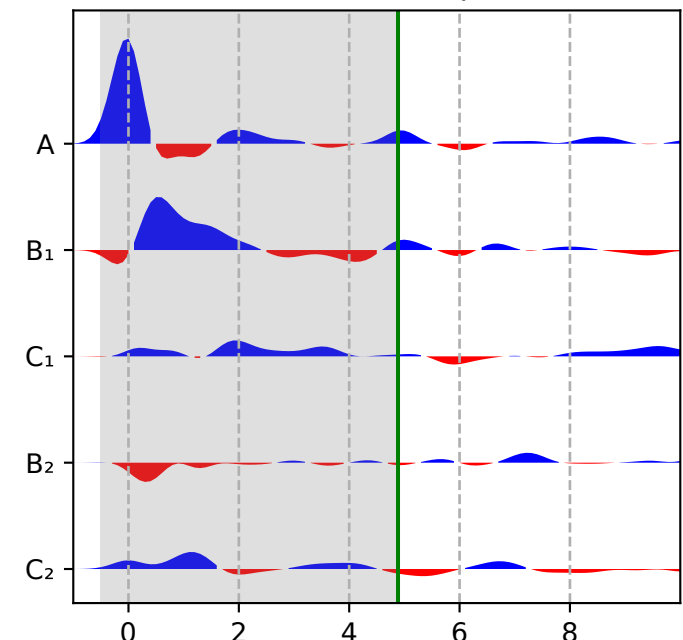
A) Radial



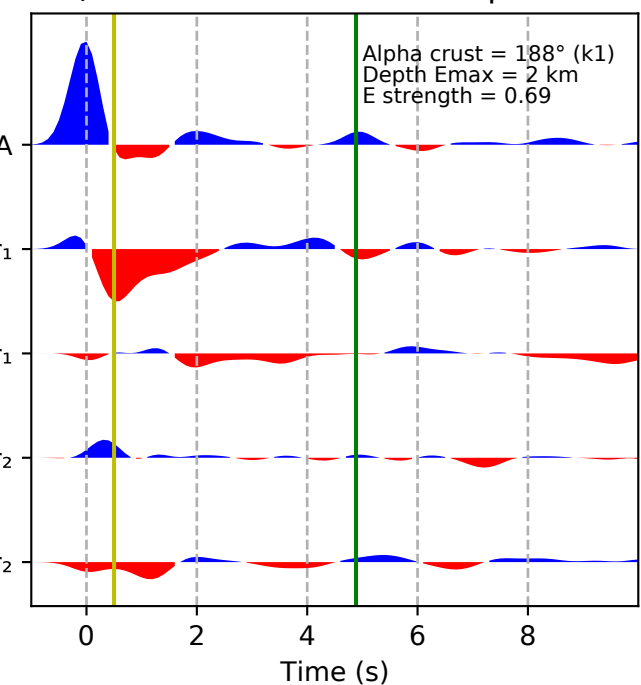
B) Transverse



C) Harmonics components

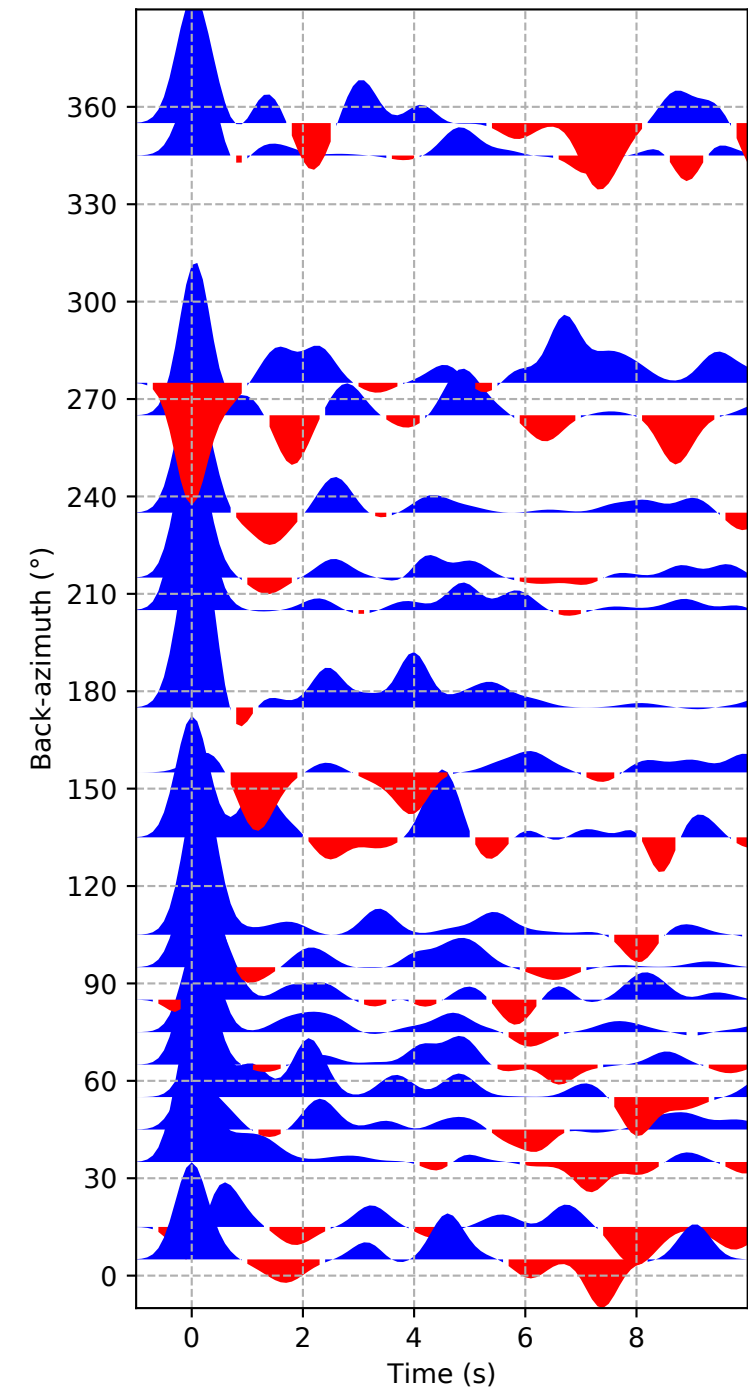


D) Rotated Harmonics components

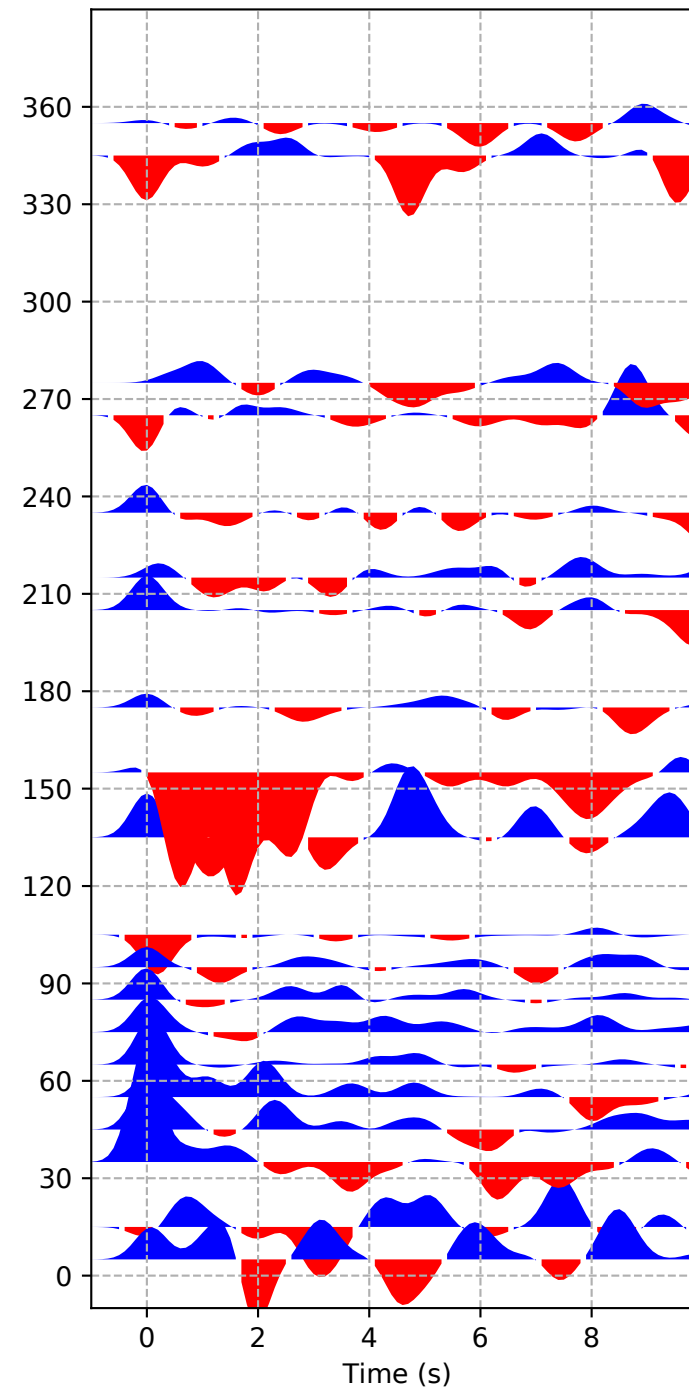


## AF-MZM

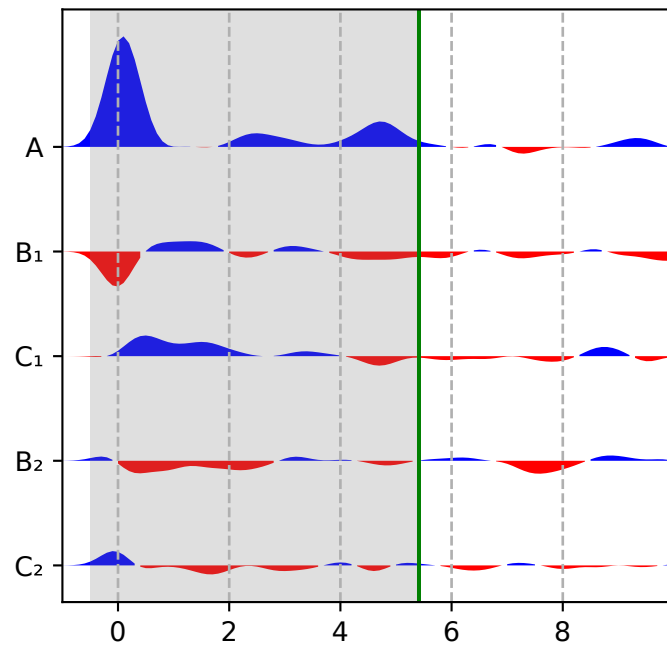
A) Radial



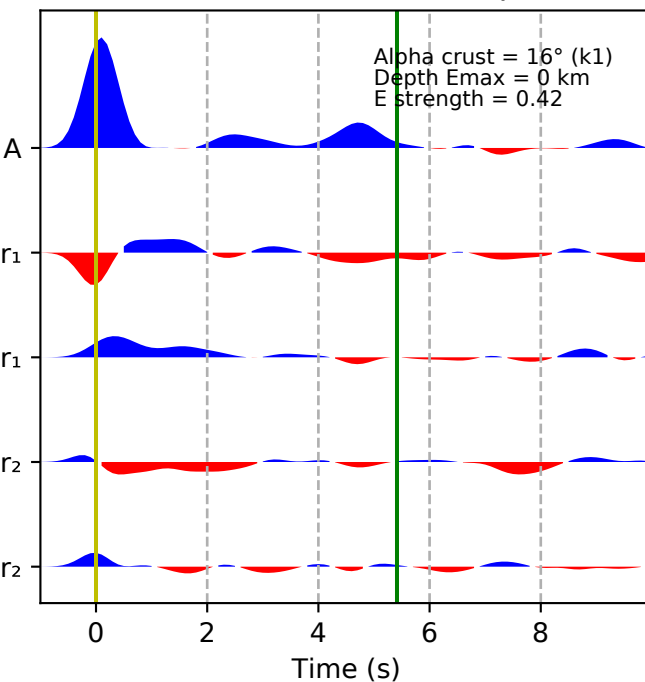
B) Transverse



C) Harmonics components

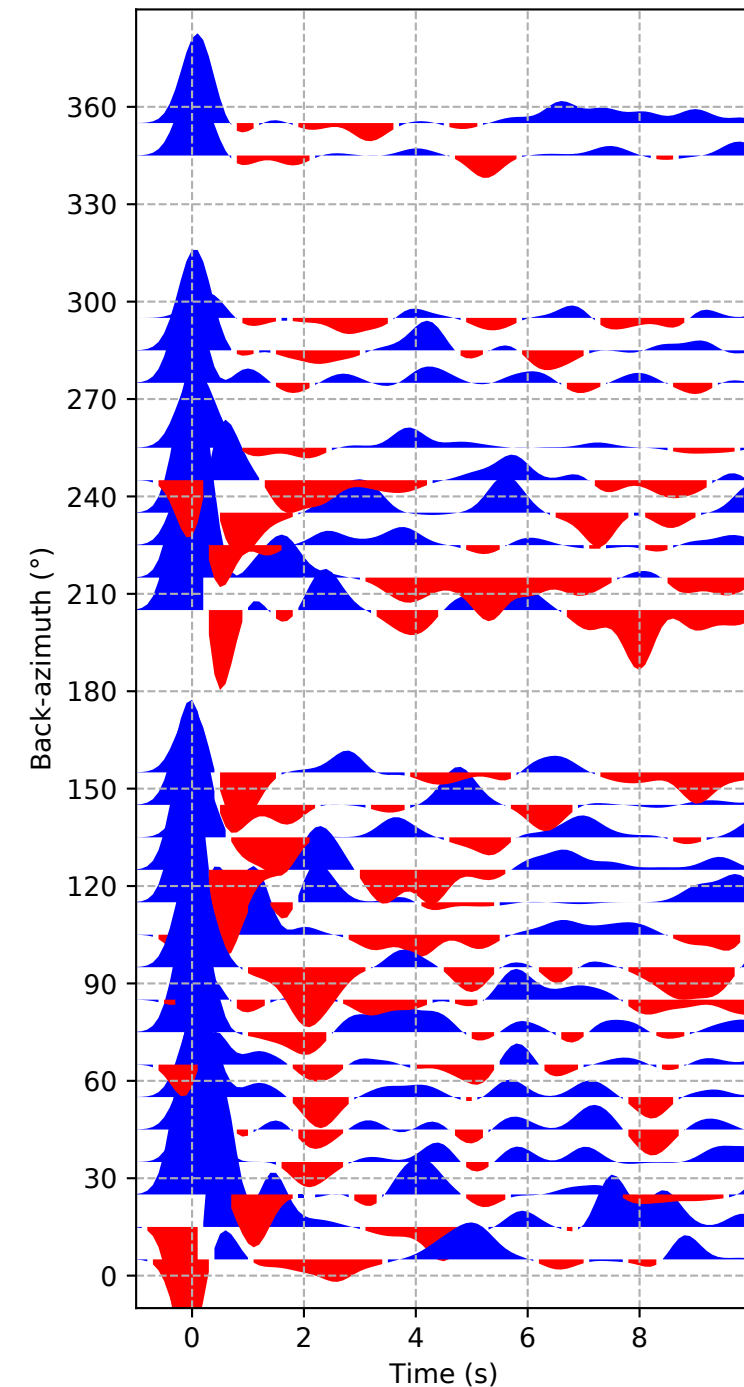


D) Rotated Harmonics components

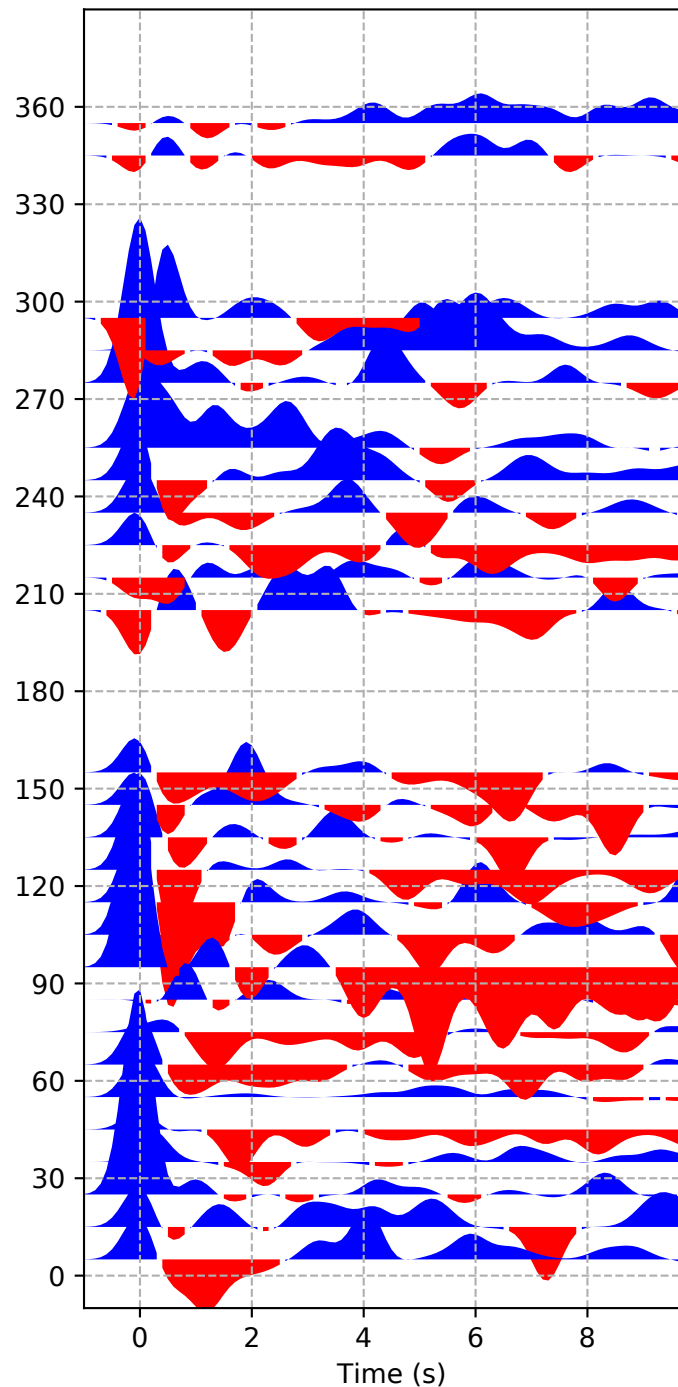


# AF-POGA

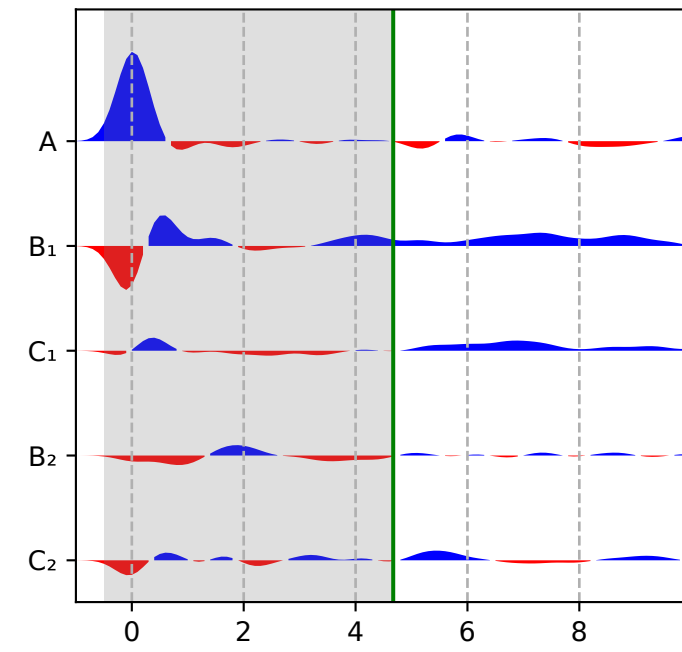
**A) Radial**



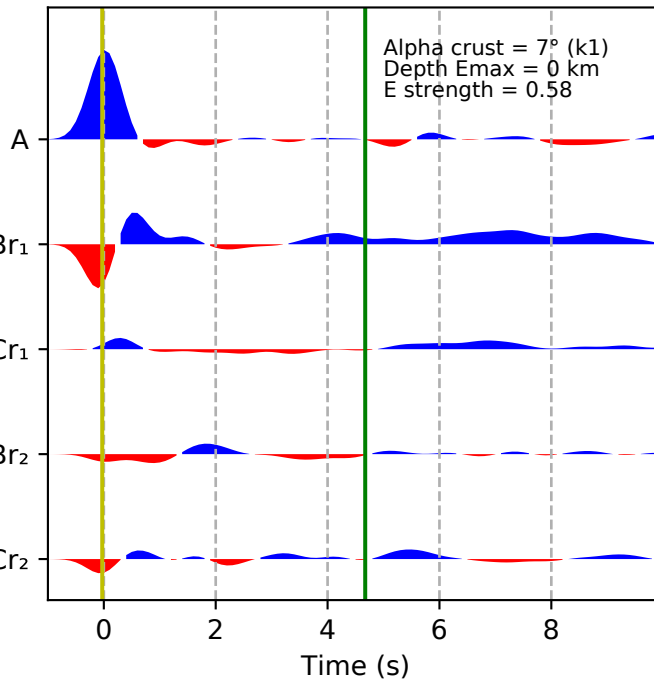
**B) Transverse**



**C) Harmonics components**



**D) Rotated Harmonics components**

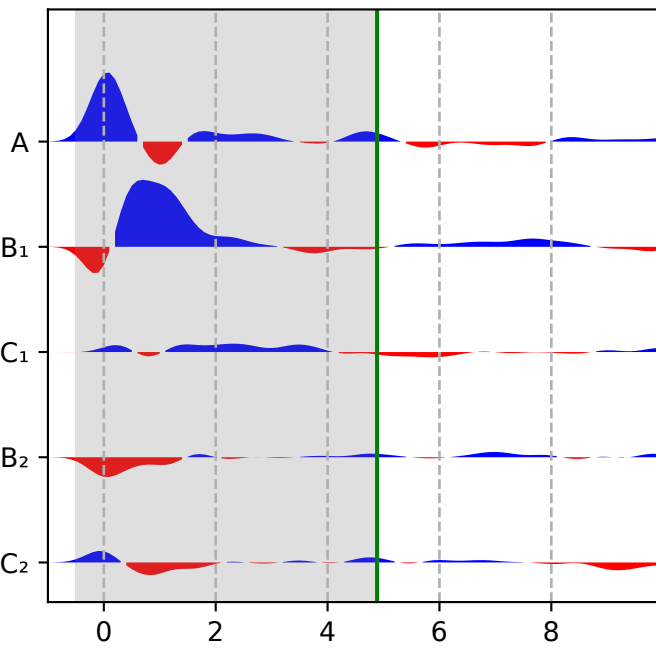
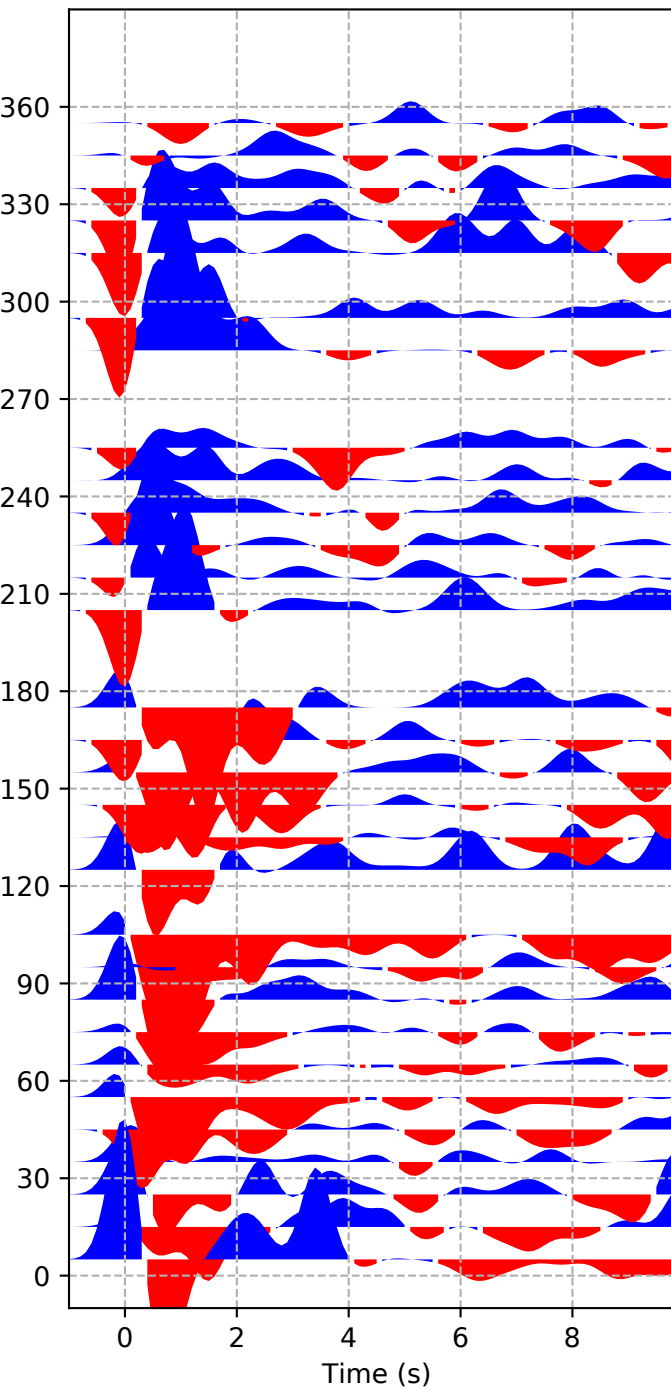
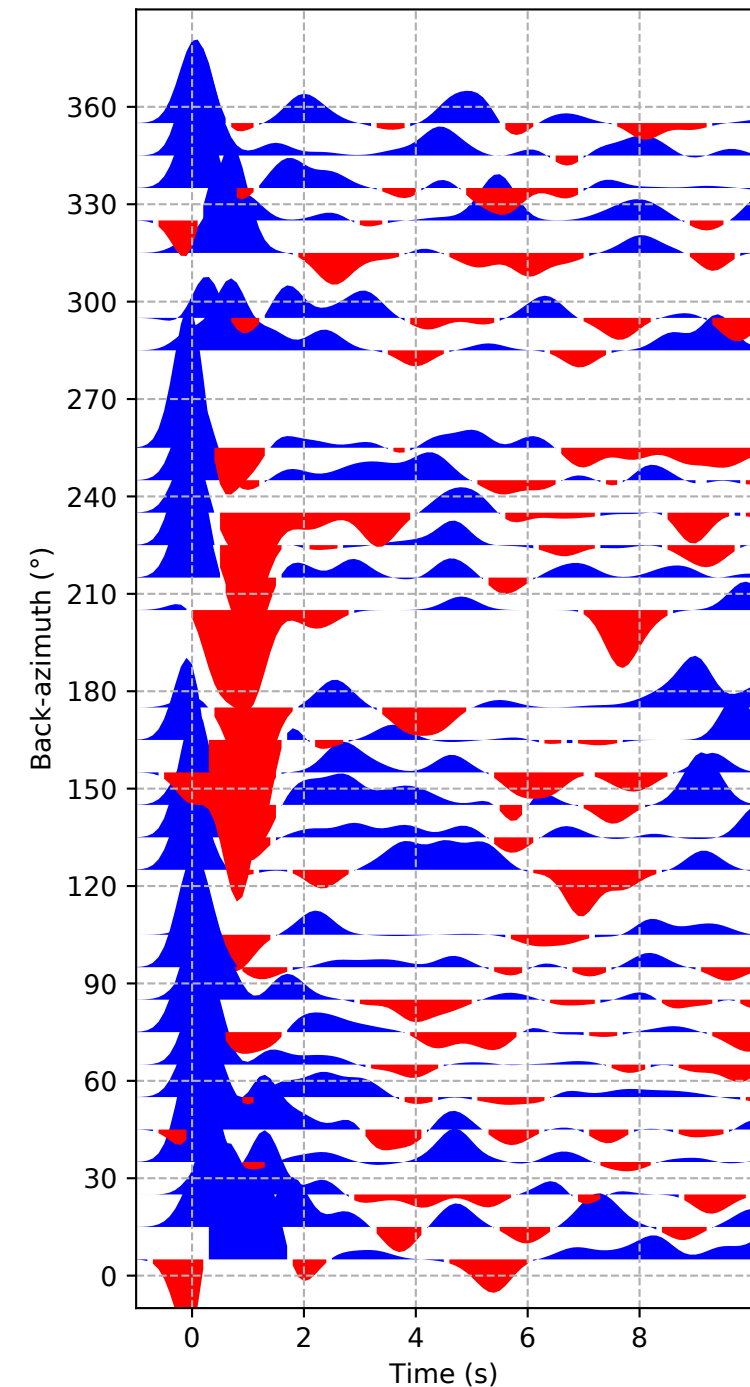


## AF-SEK

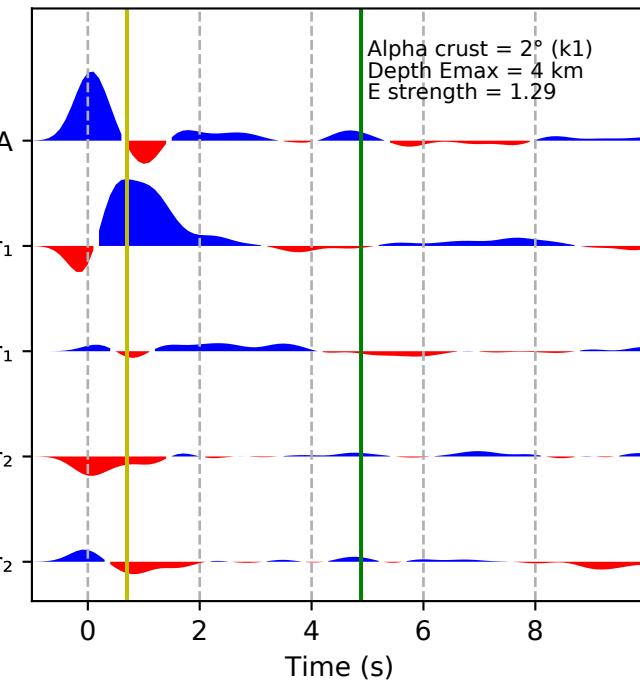
## B) Transverse

## C) Harmonics components

## A) Radial

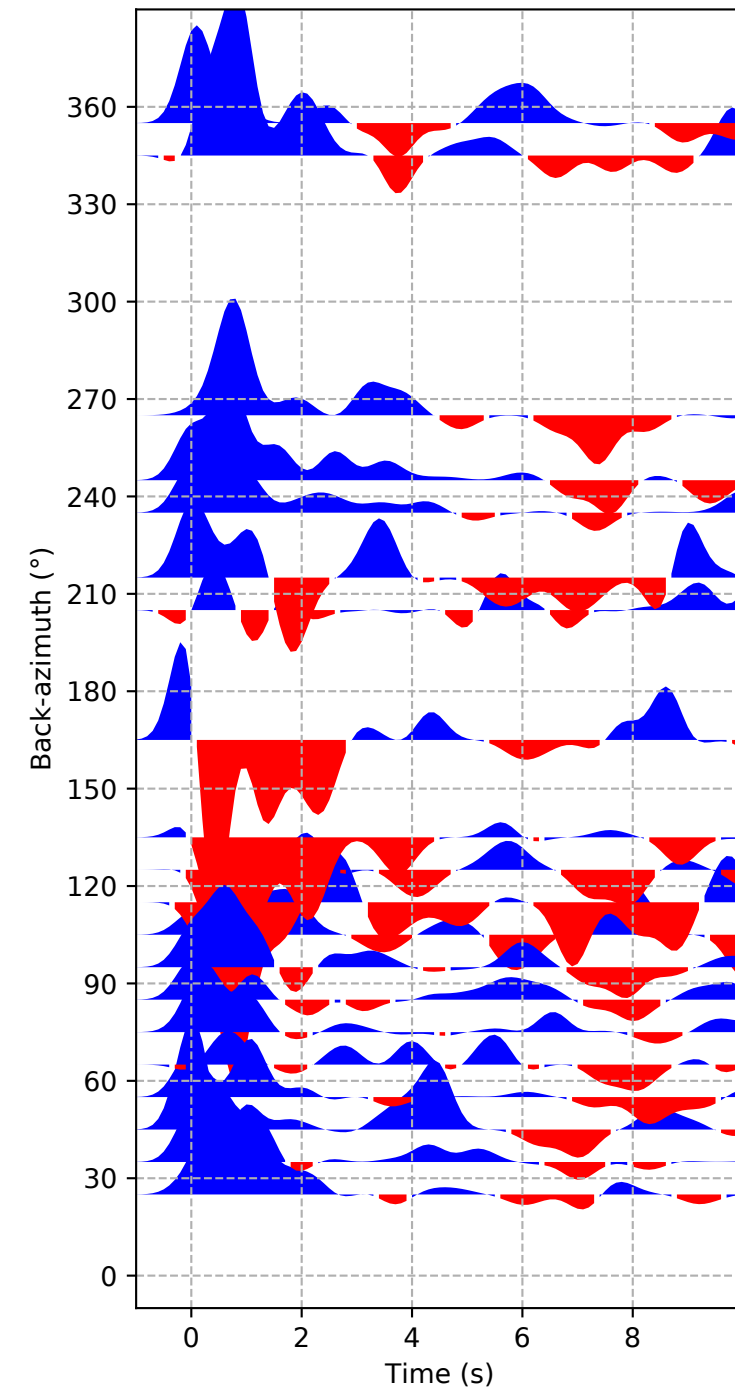


## D) Rotated Harmonics components

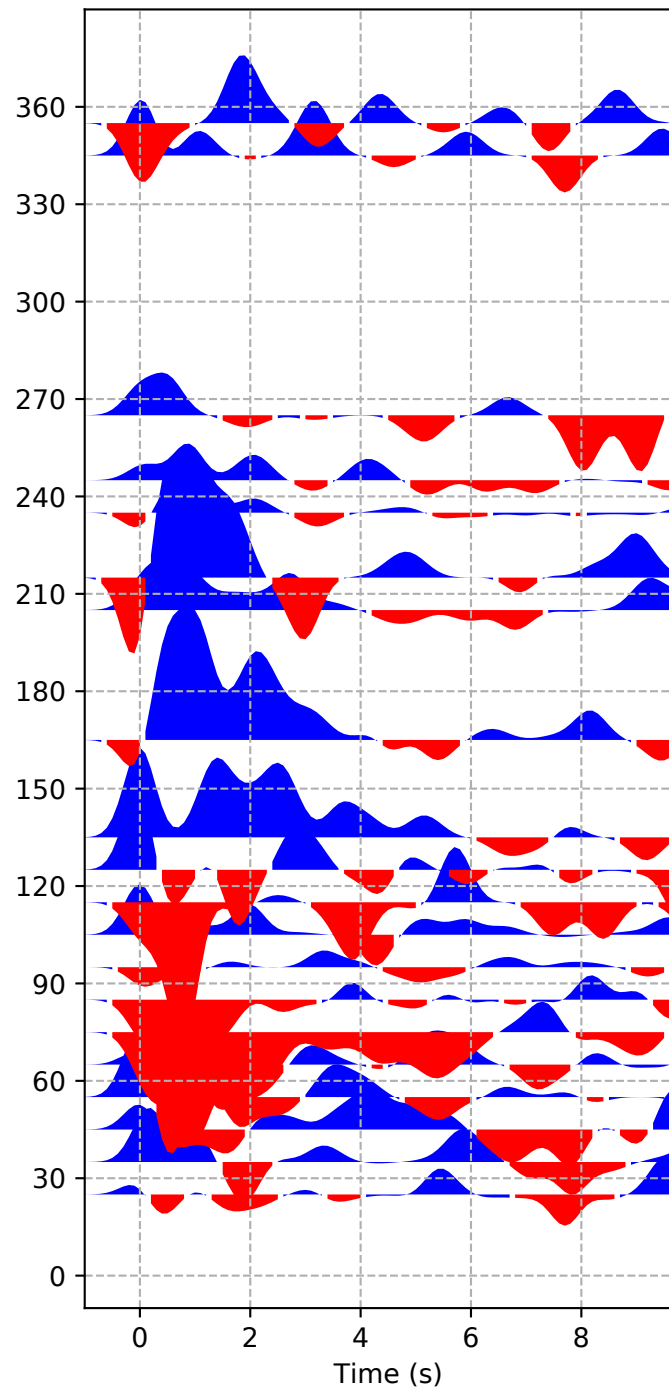


## AF-SKRH

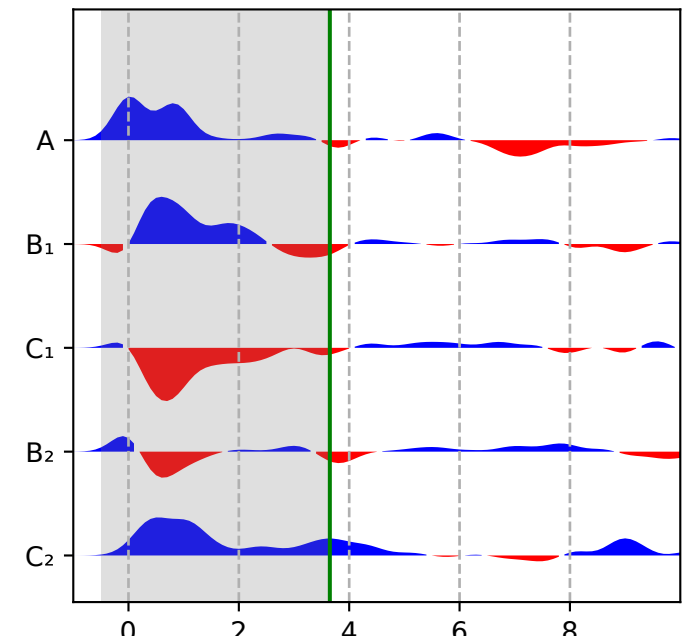
A) Radial



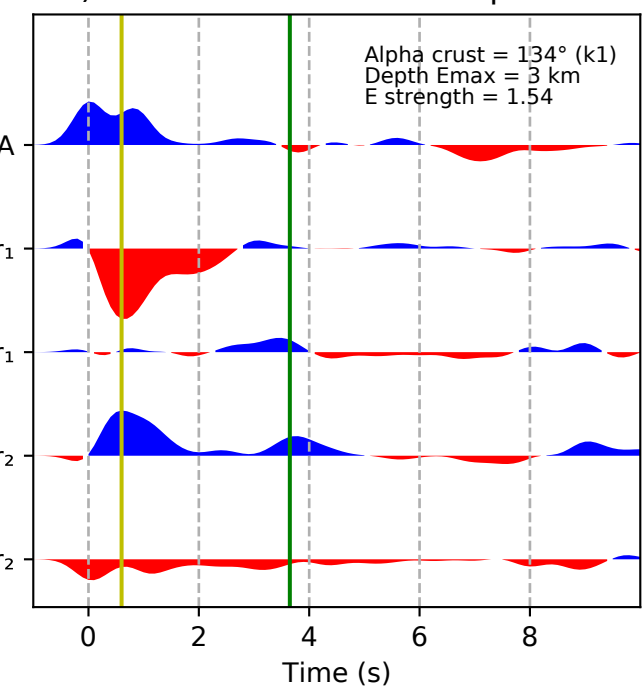
B) Transverse



C) Harmonics components



D) Rotated Harmonics components

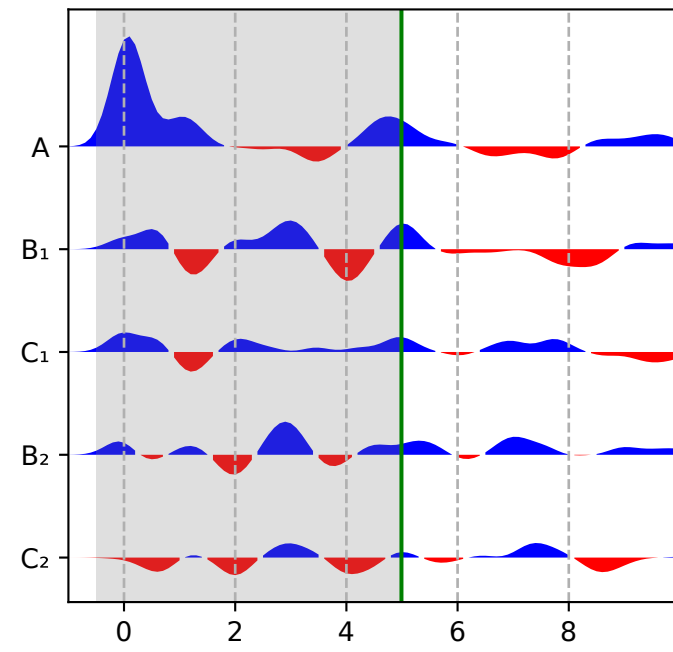
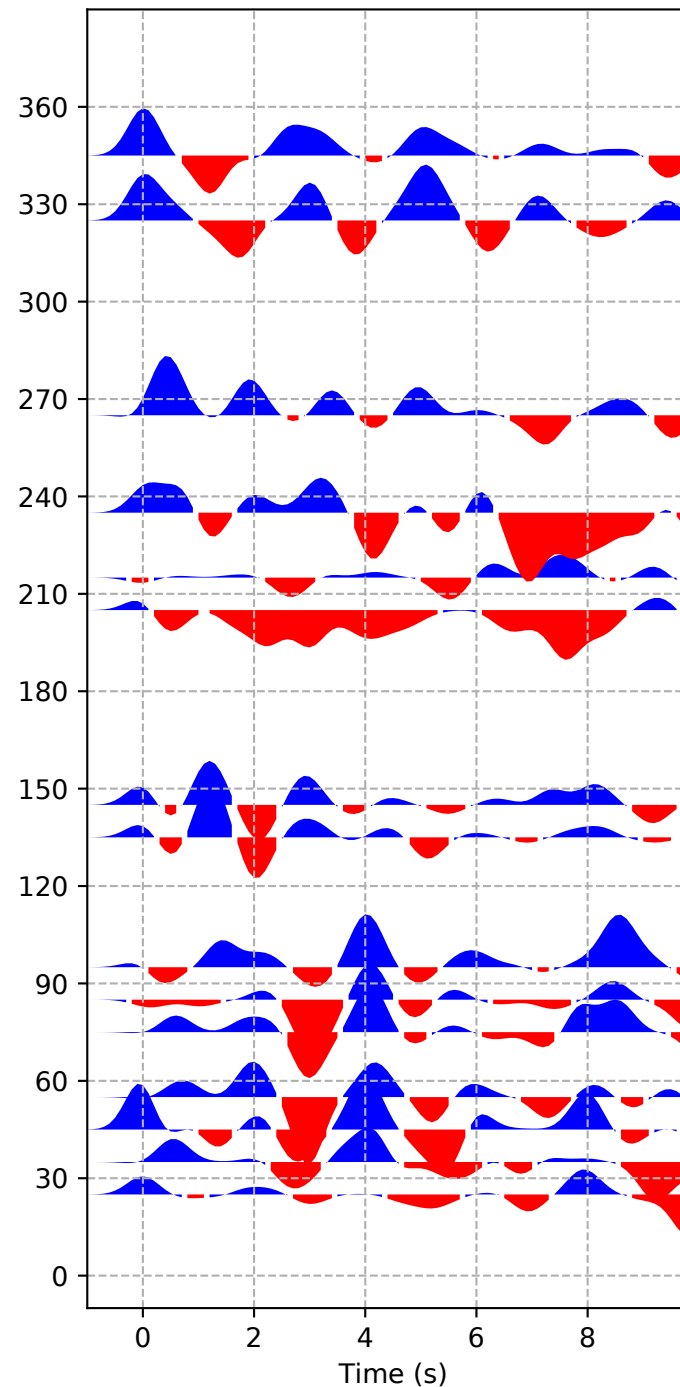
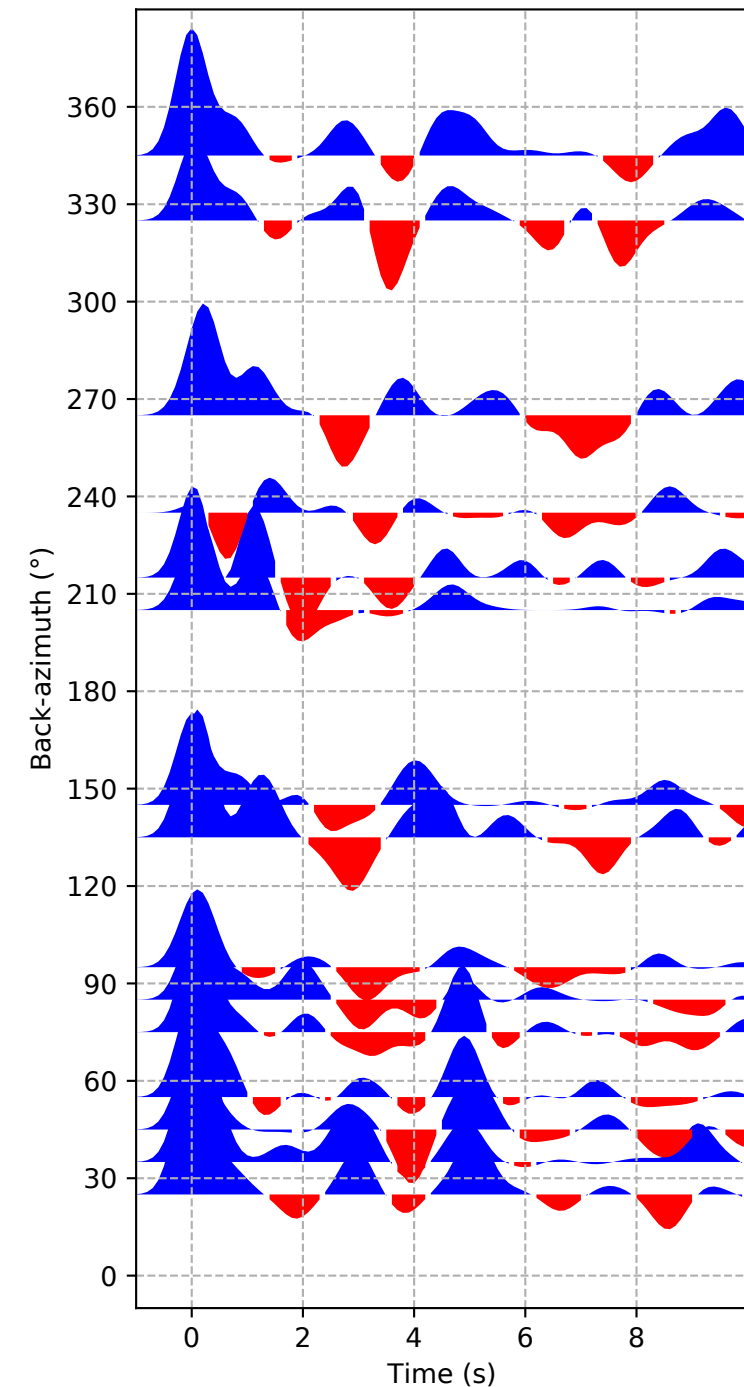


## AF-TETE

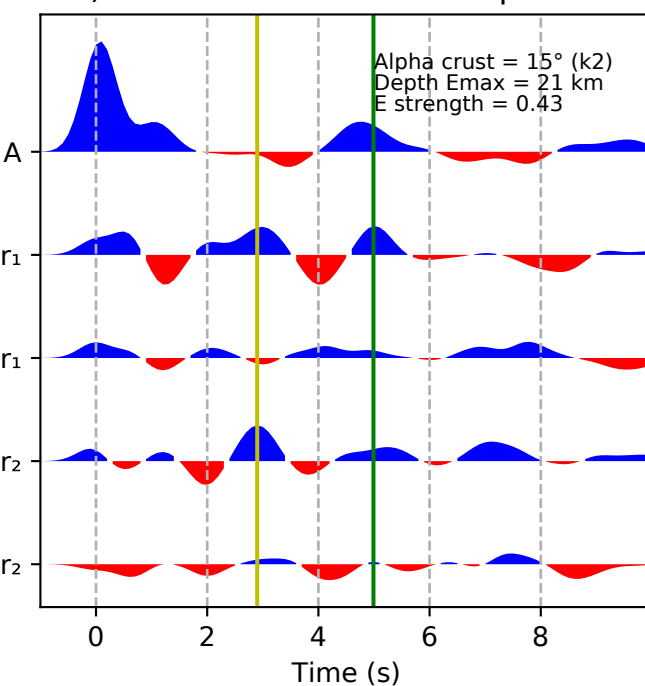
## B) Transverse

## C) Harmonics components

## A) Radial

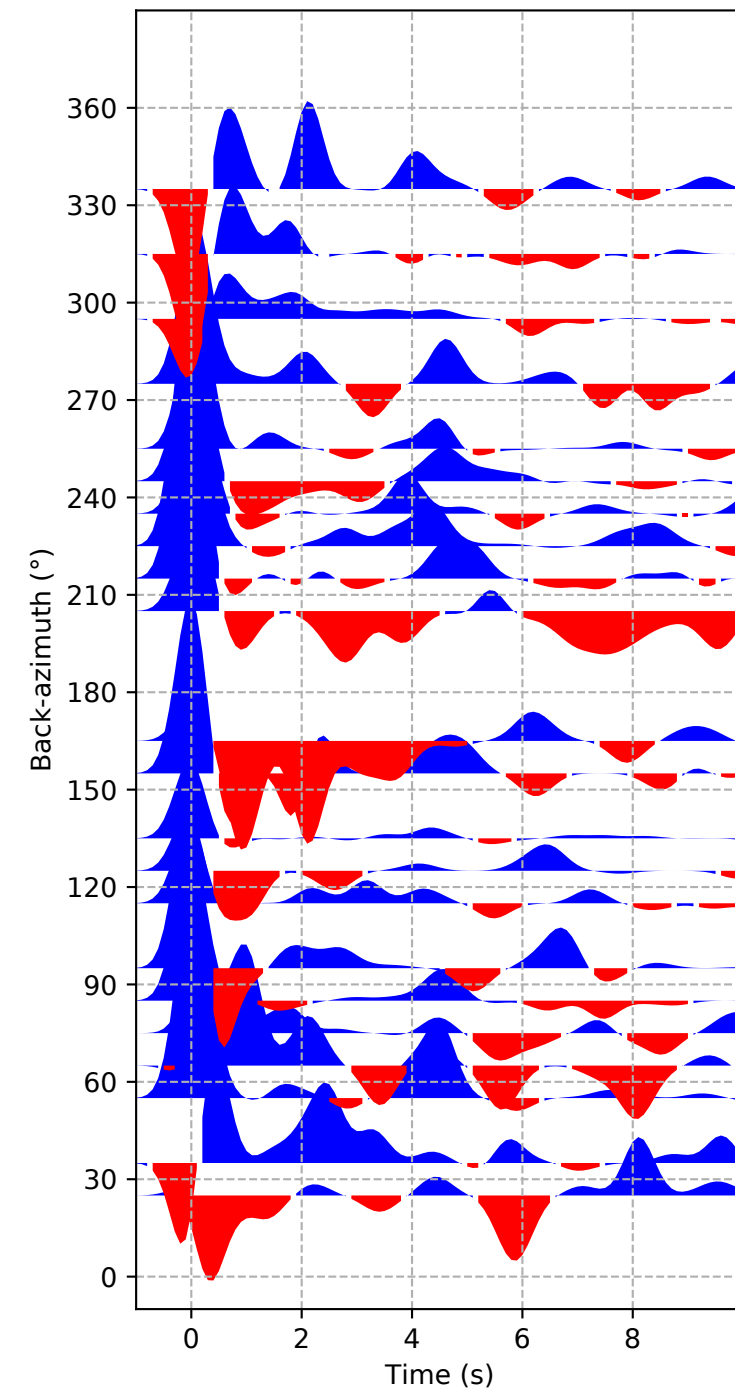


## D) Rotated Harmonics components

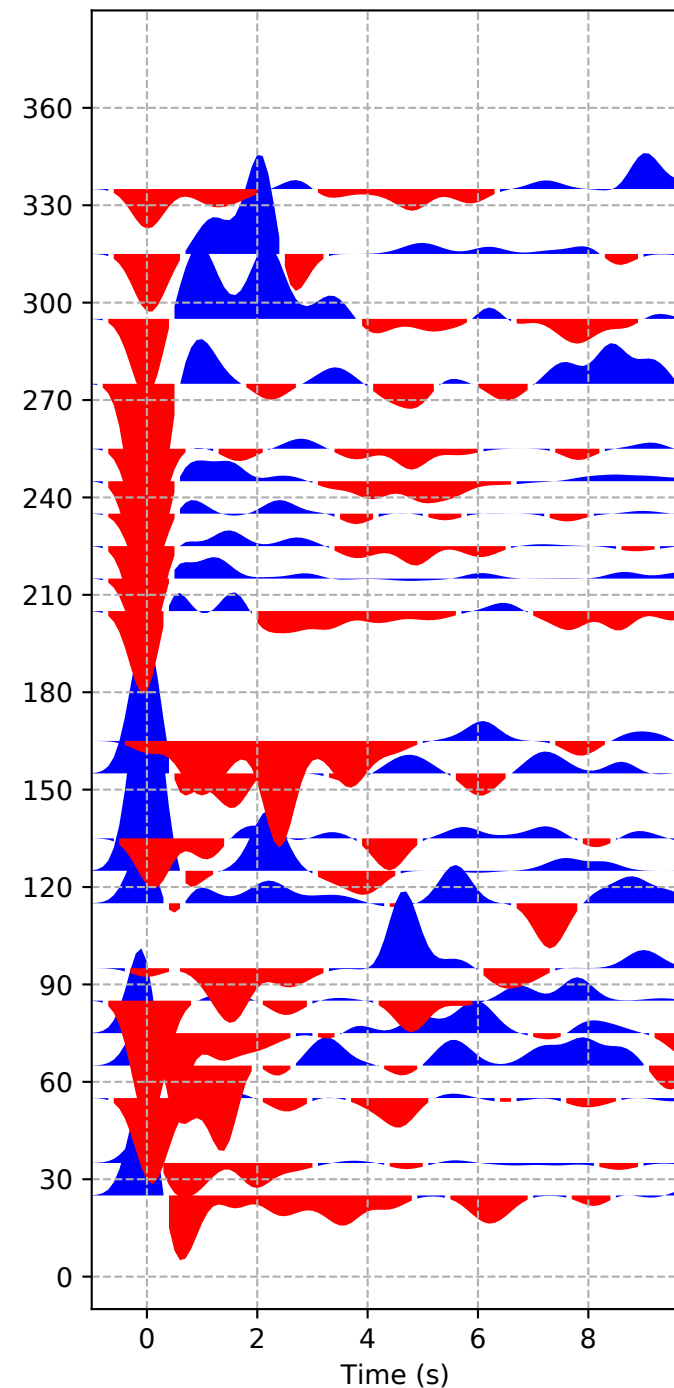


# AF-WDLM

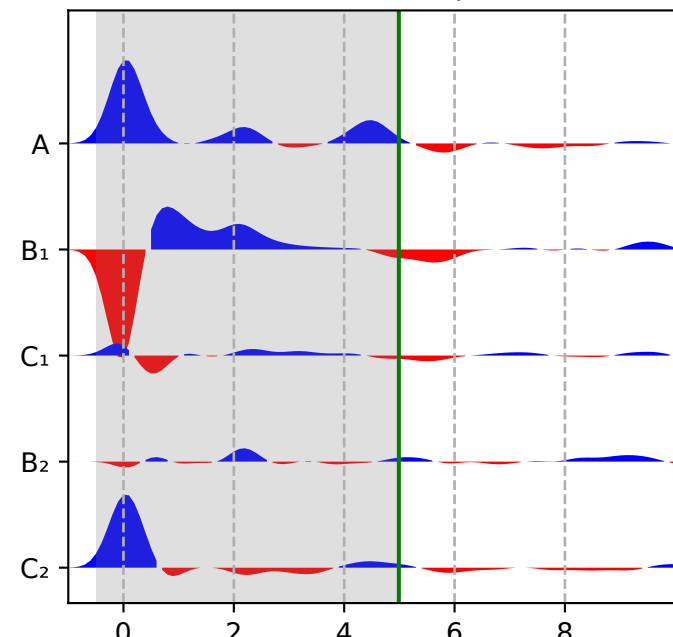
A) Radial



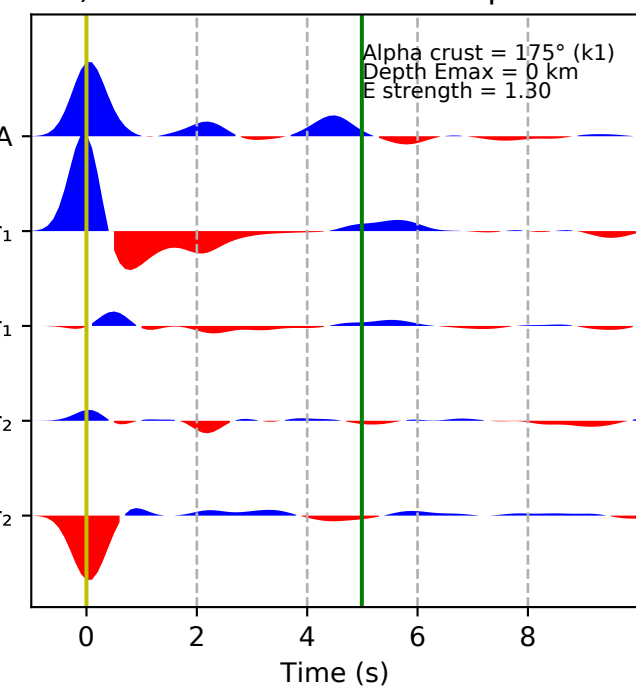
B) Transverse



C) Harmonics components

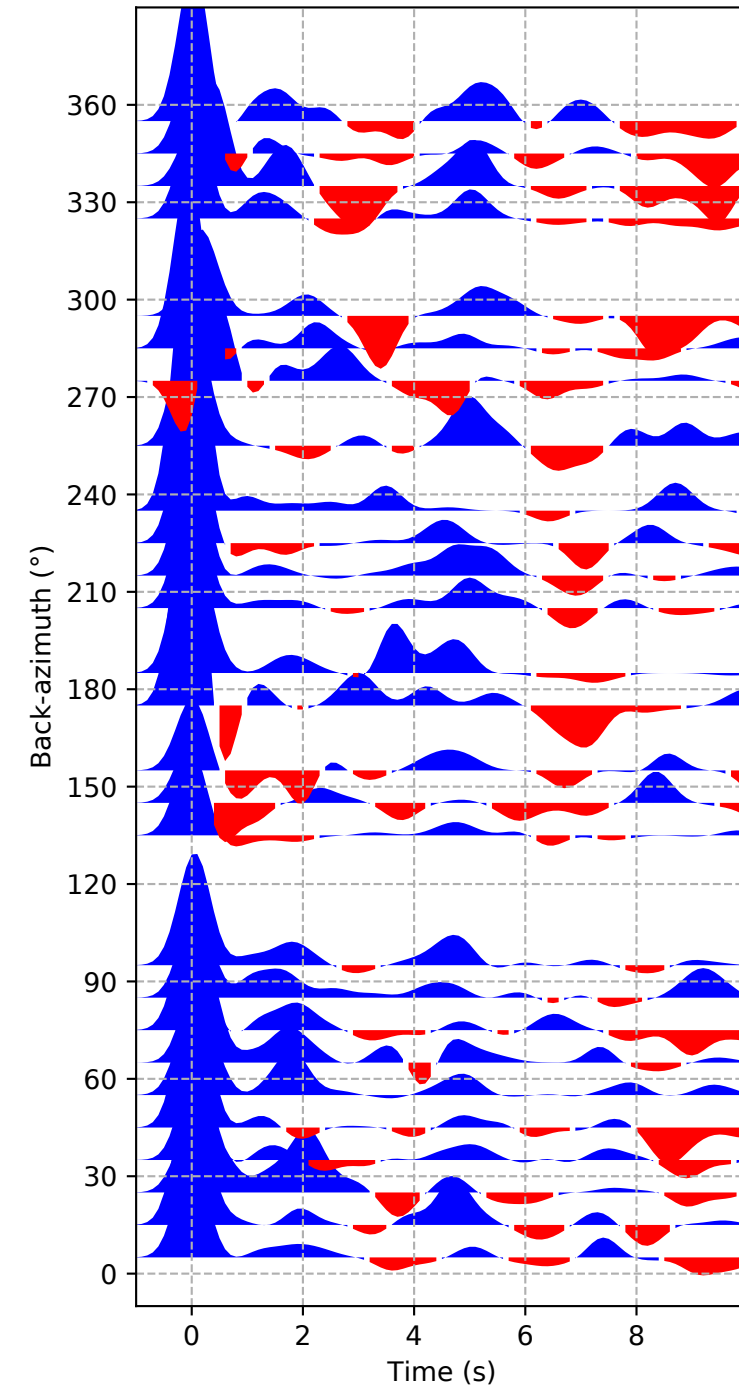


D) Rotated Harmonics components

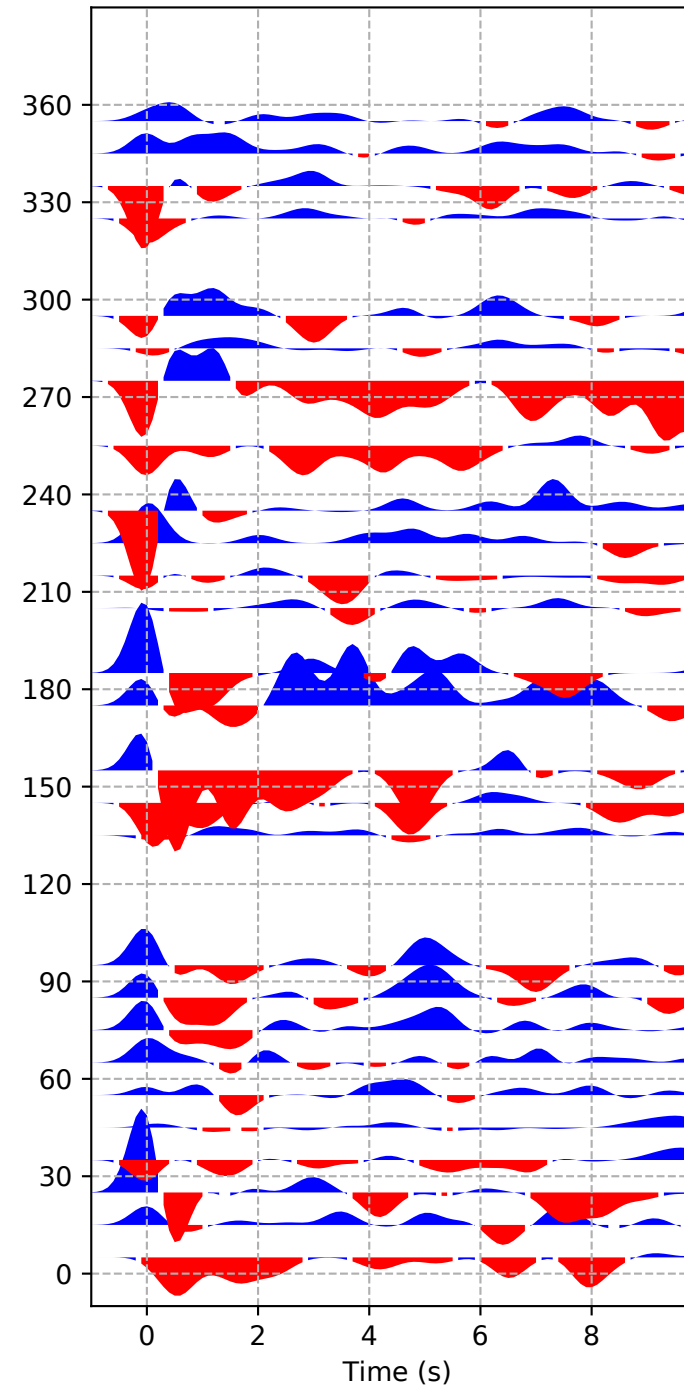


# AF-ZOMB

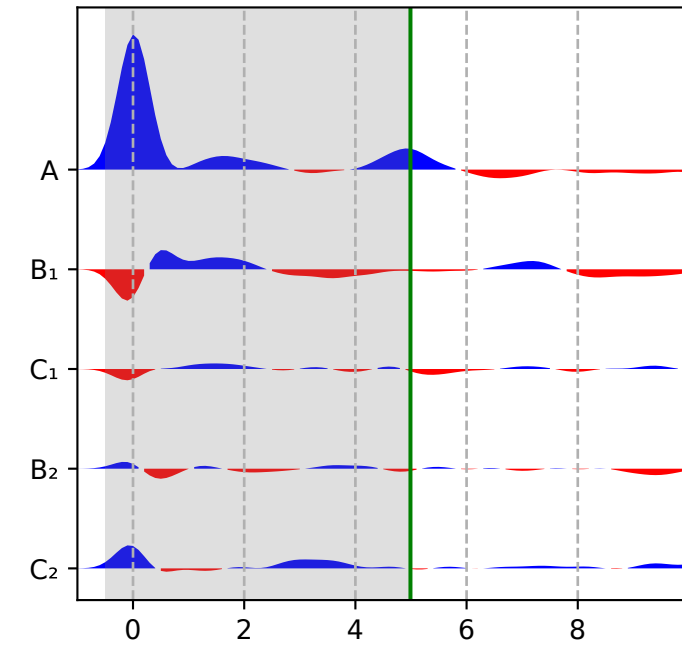
A) Radial



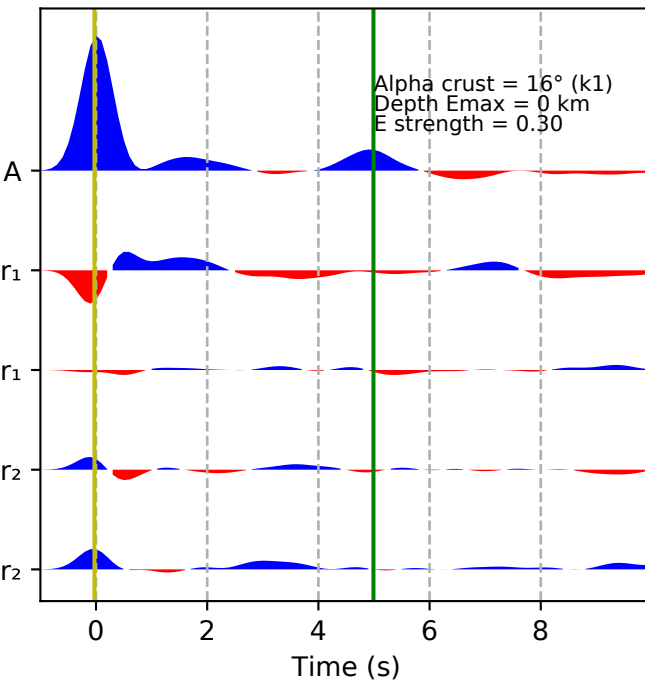
B) Transverse

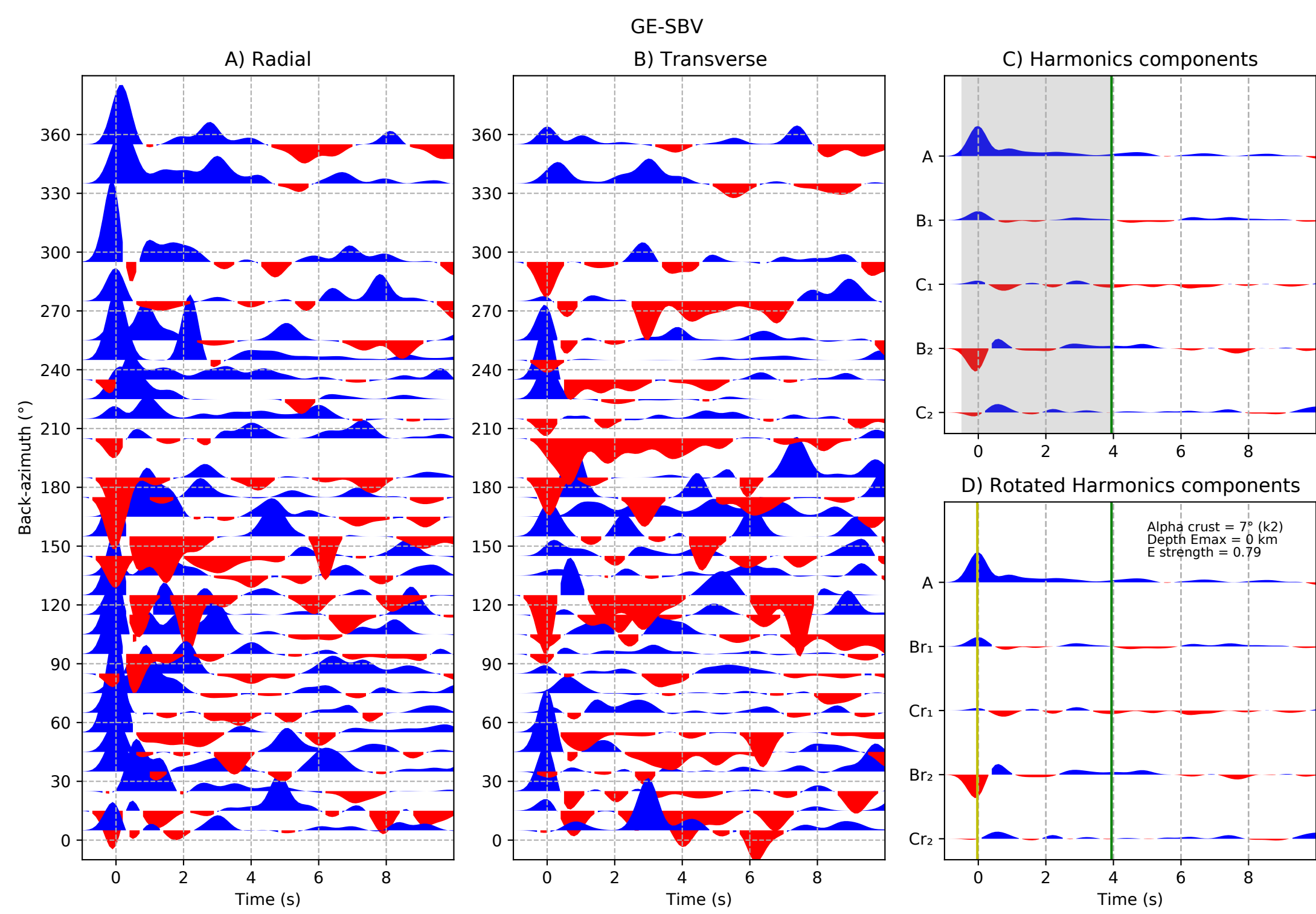


C) Harmonics components



D) Rotated Harmonics components



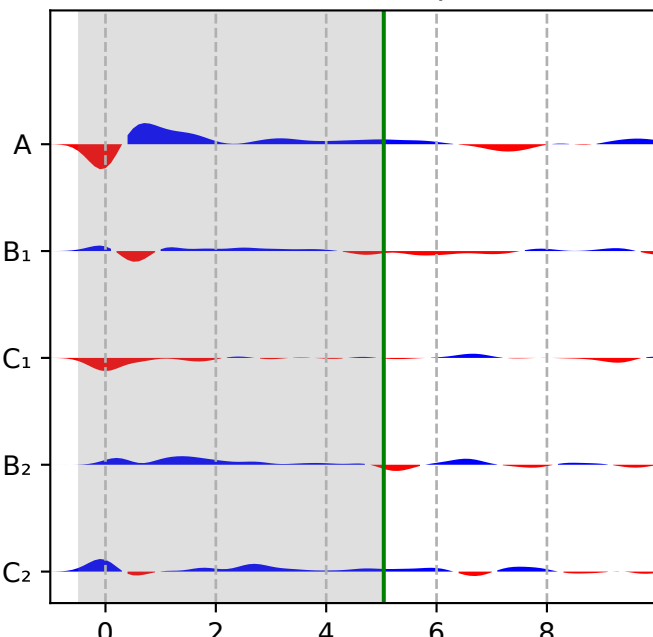
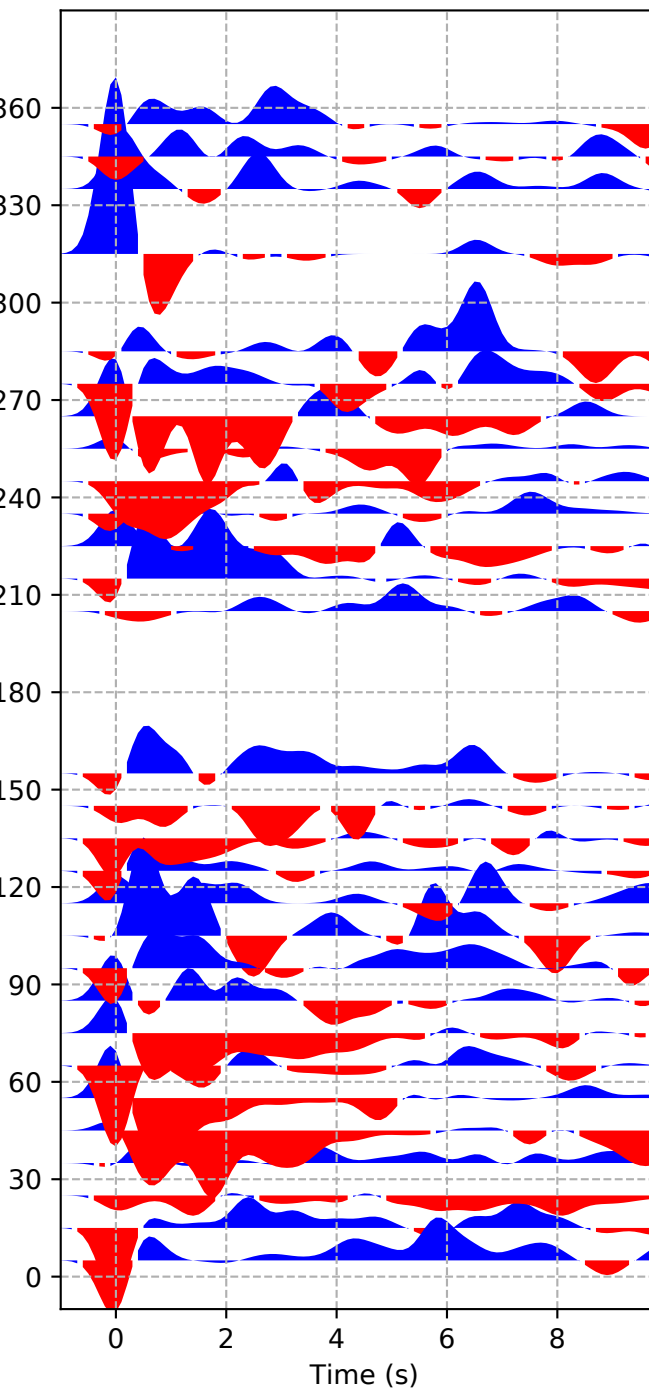
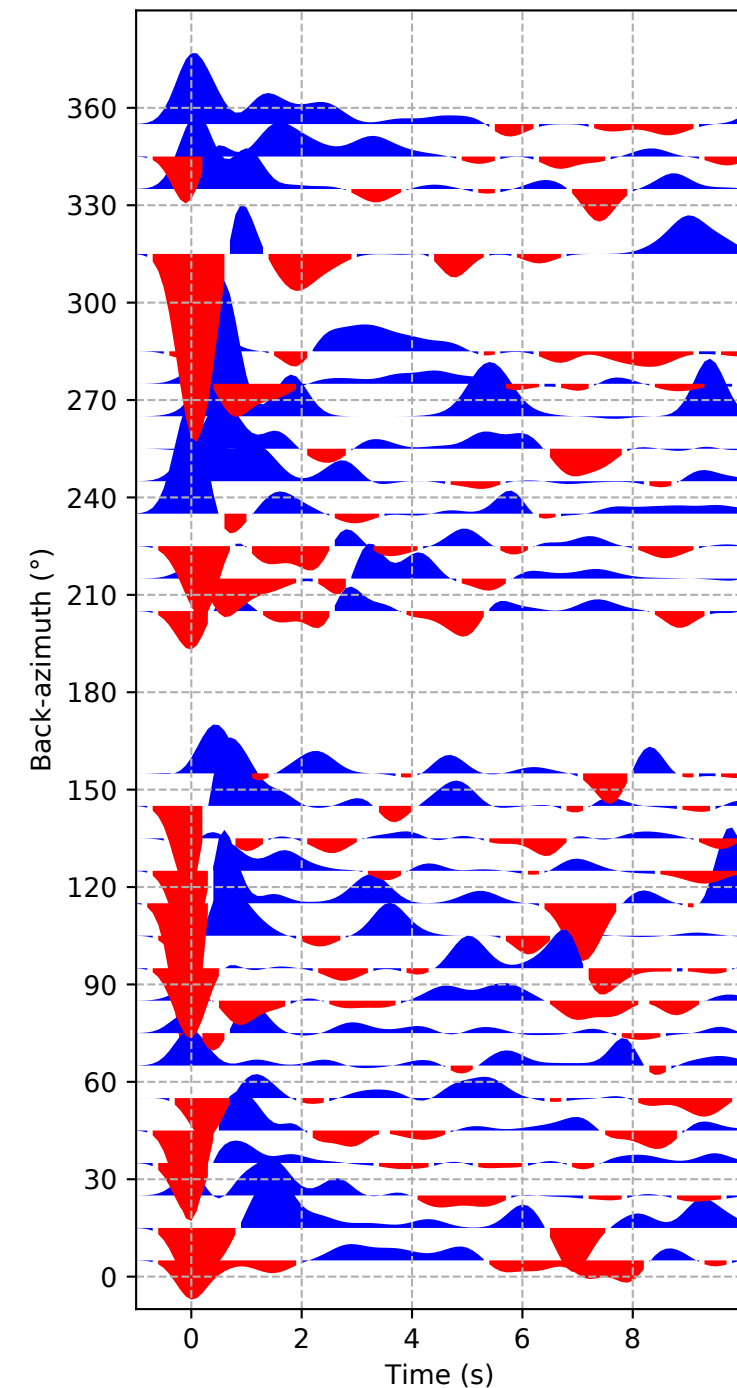


## GE-VOI

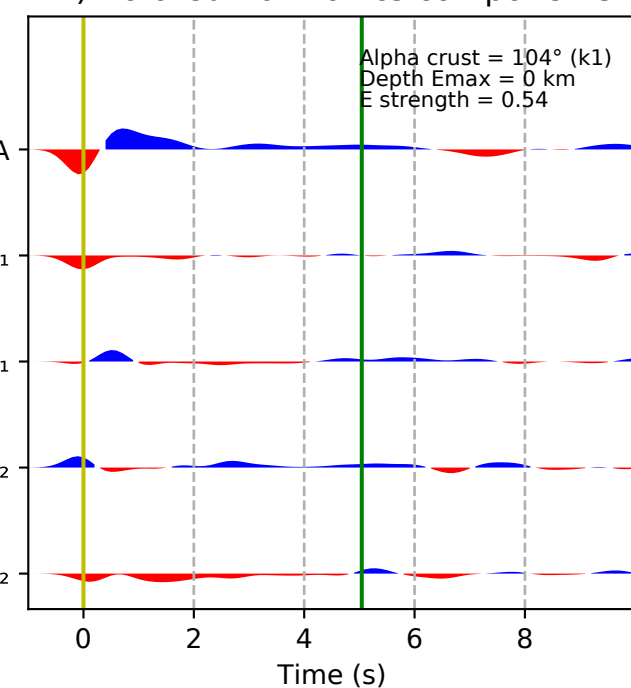
## B) Transverse

## C) Harmonics components

## A) Radial

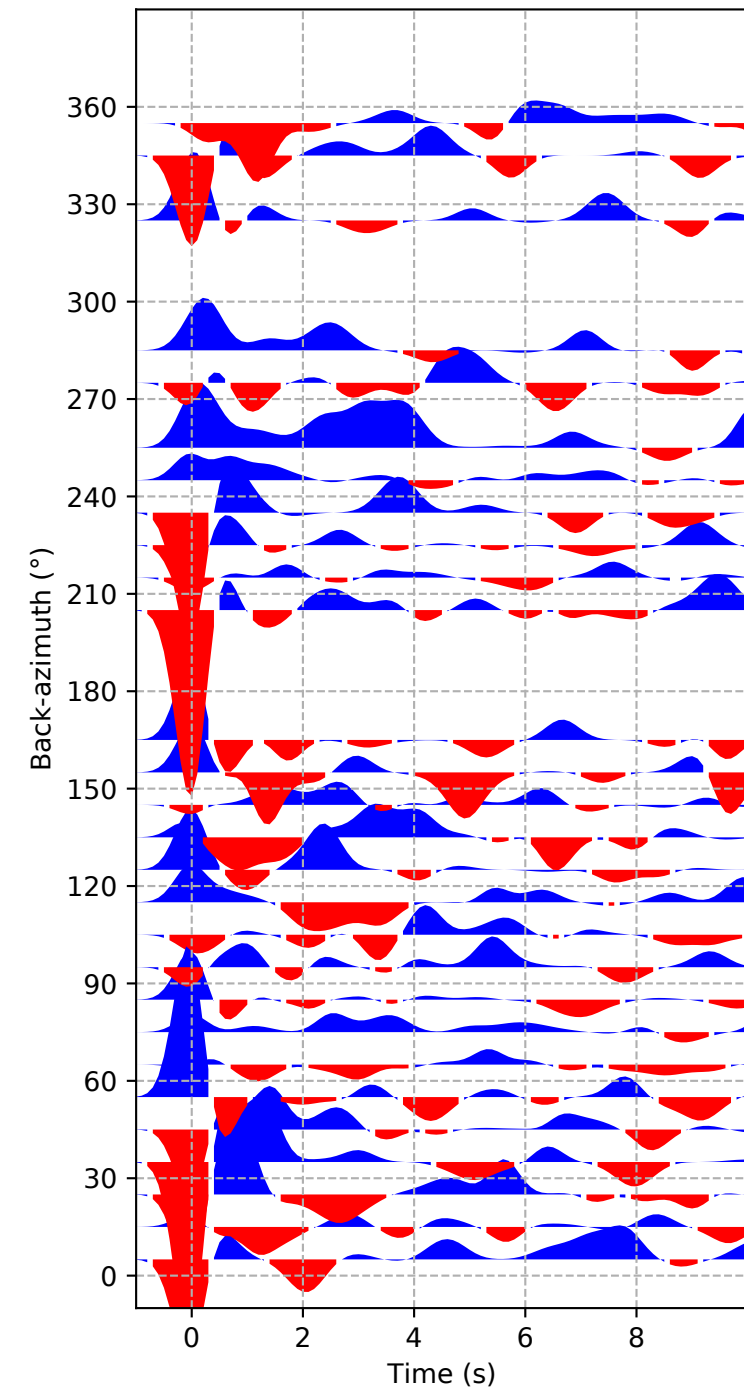


## D) Rotated Harmonics components

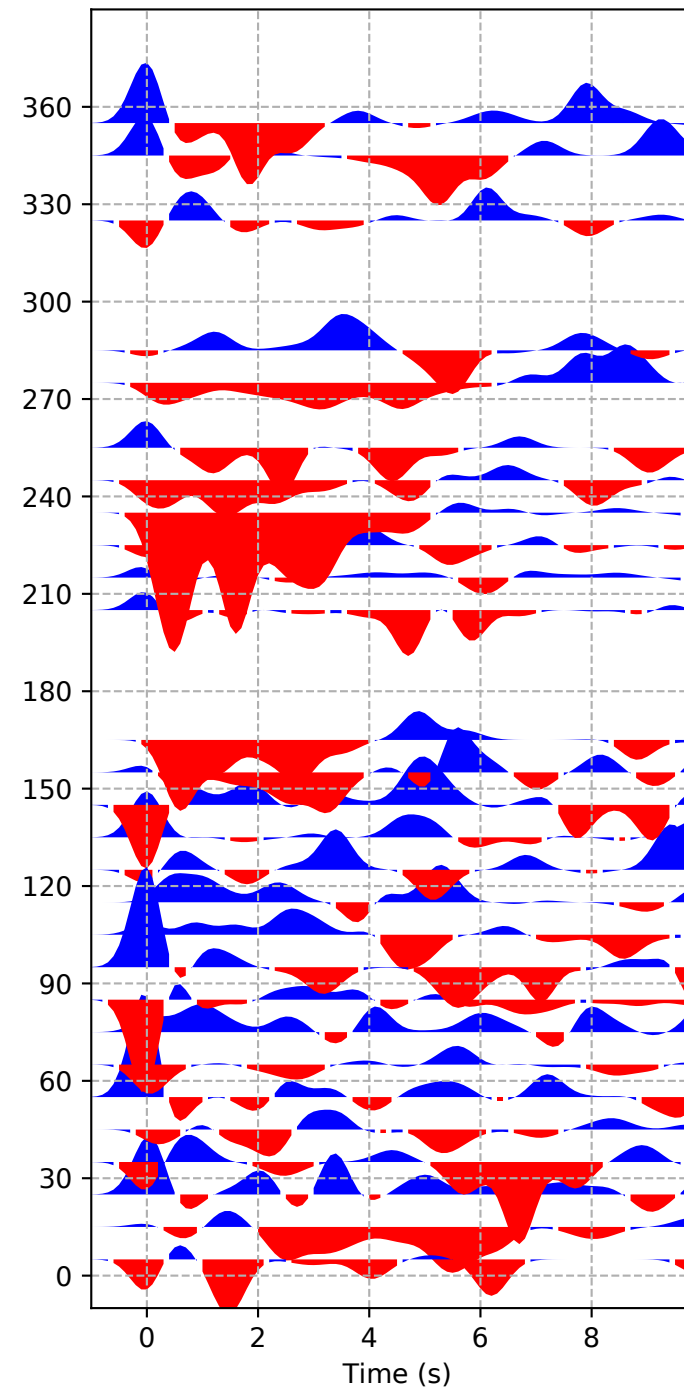


# G-FOMA

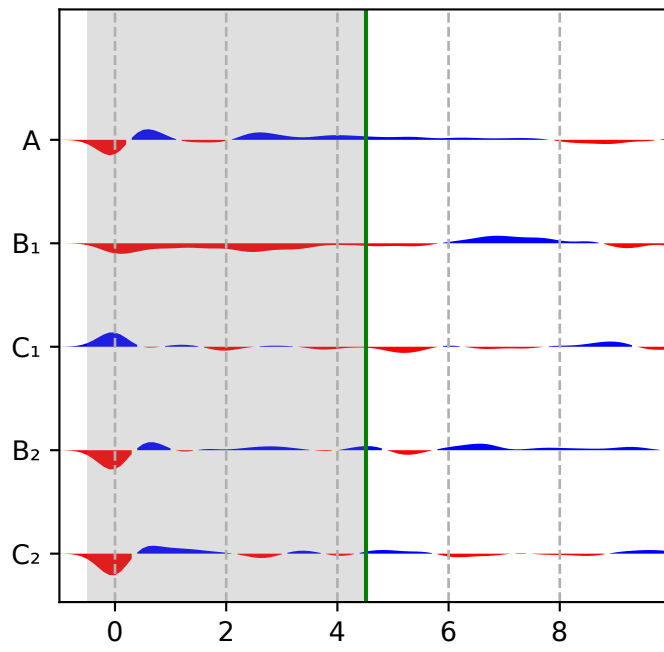
A) Radial



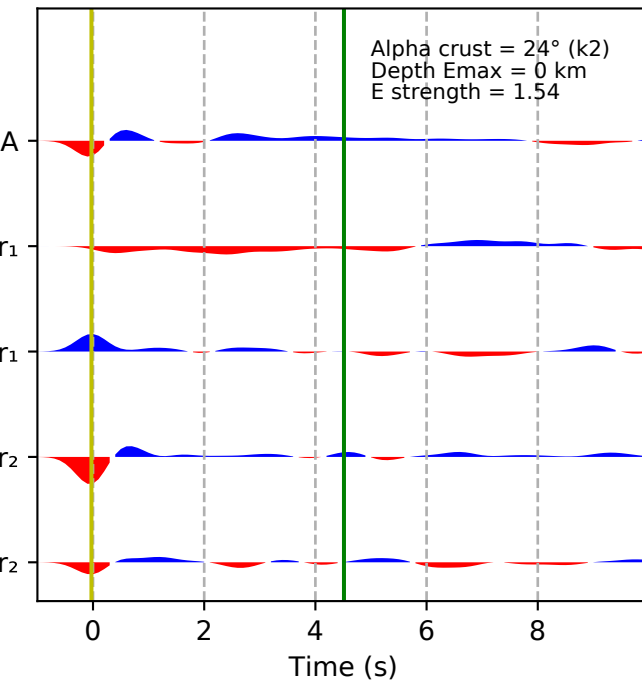
B) Transverse



C) Harmonics components

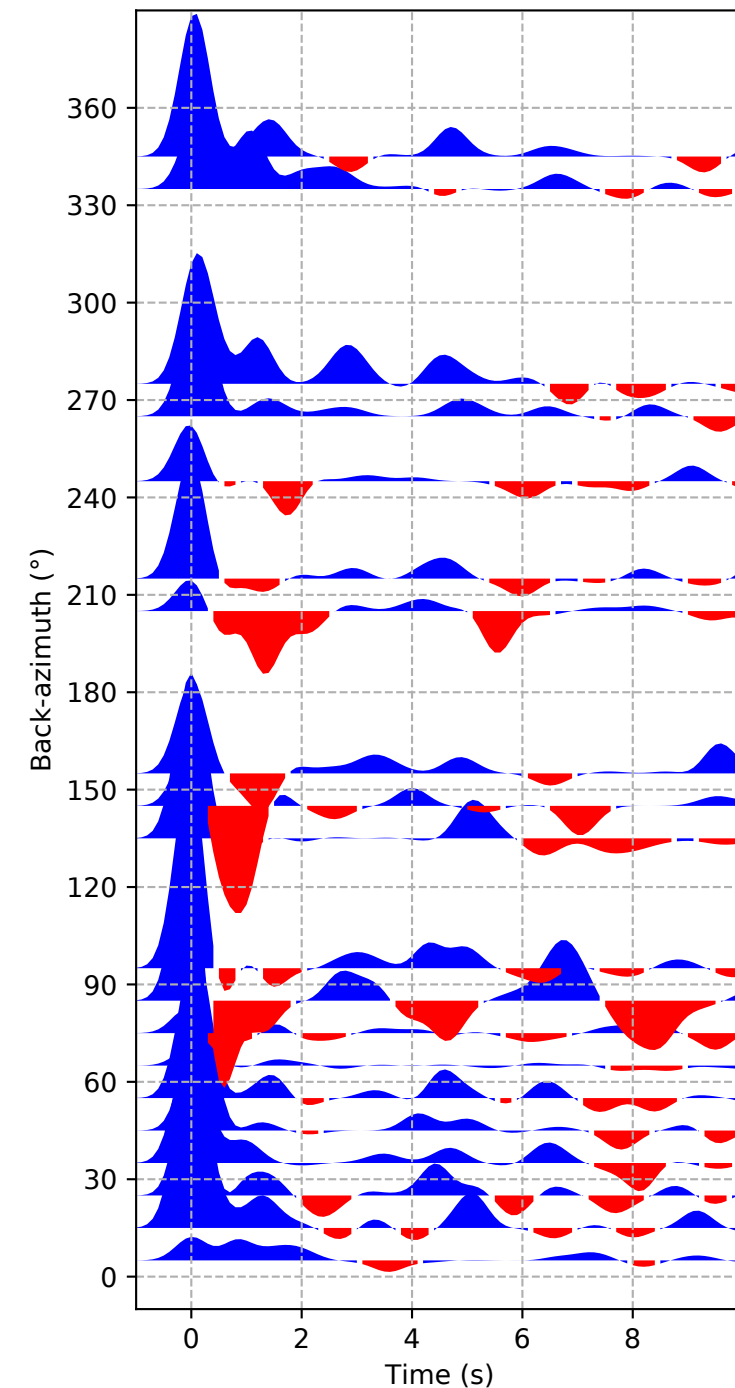


D) Rotated Harmonics components

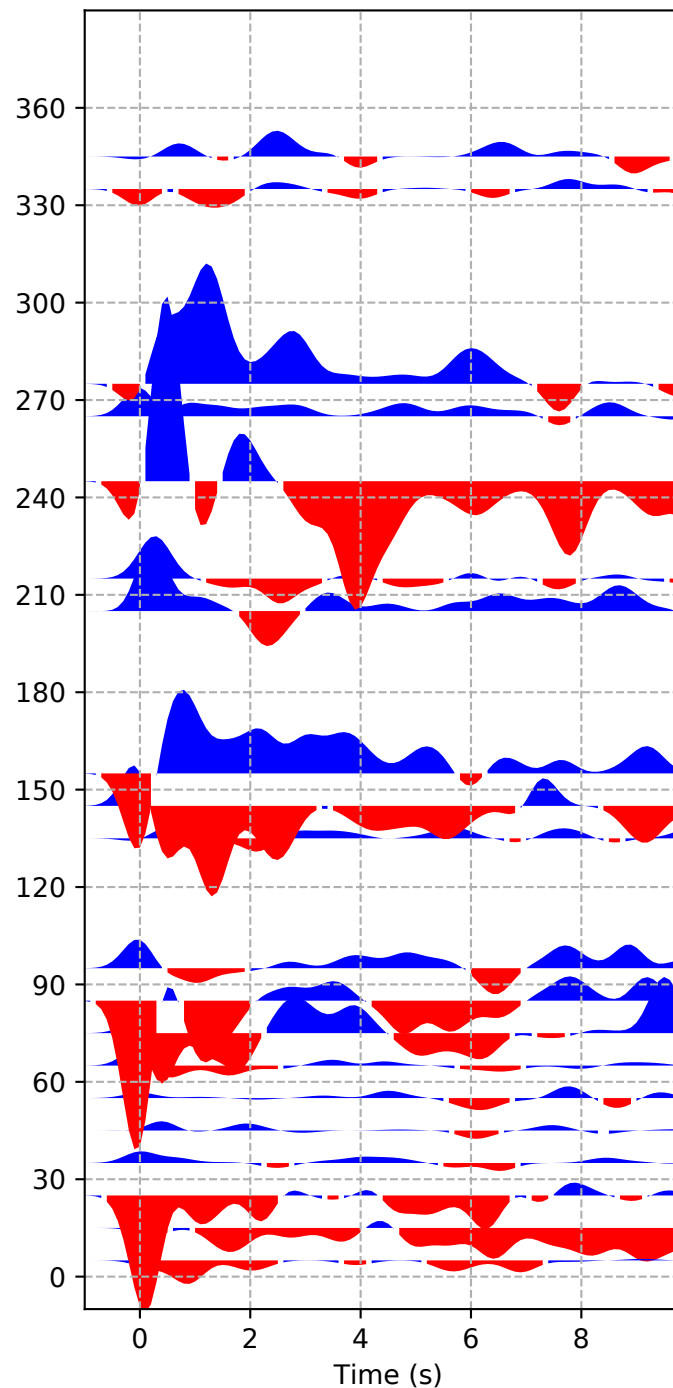


# II-ABPO

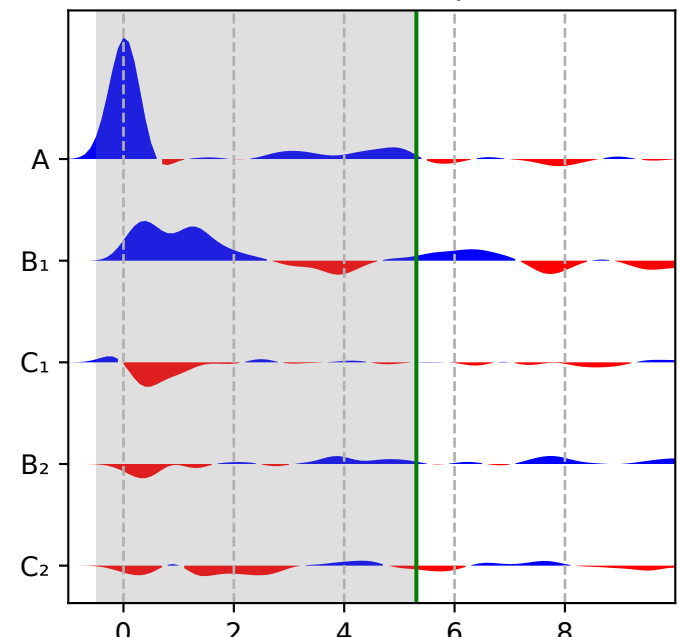
A) Radial



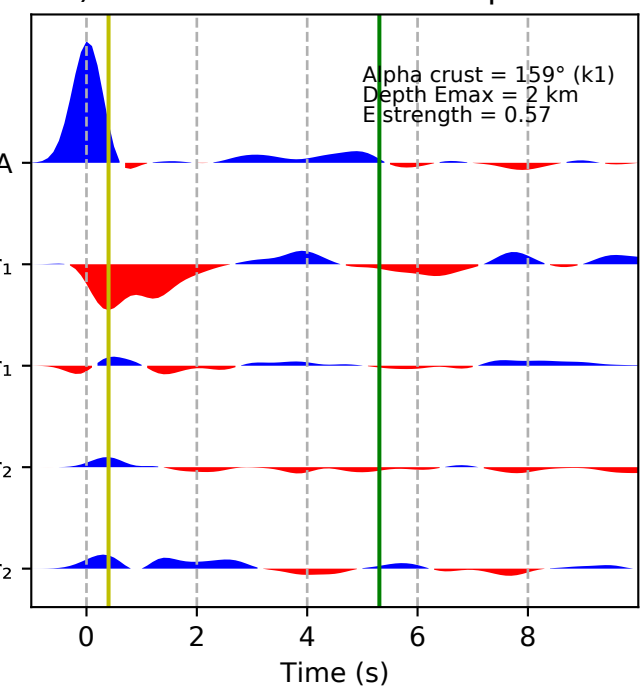
B) Transverse



C) Harmonics components

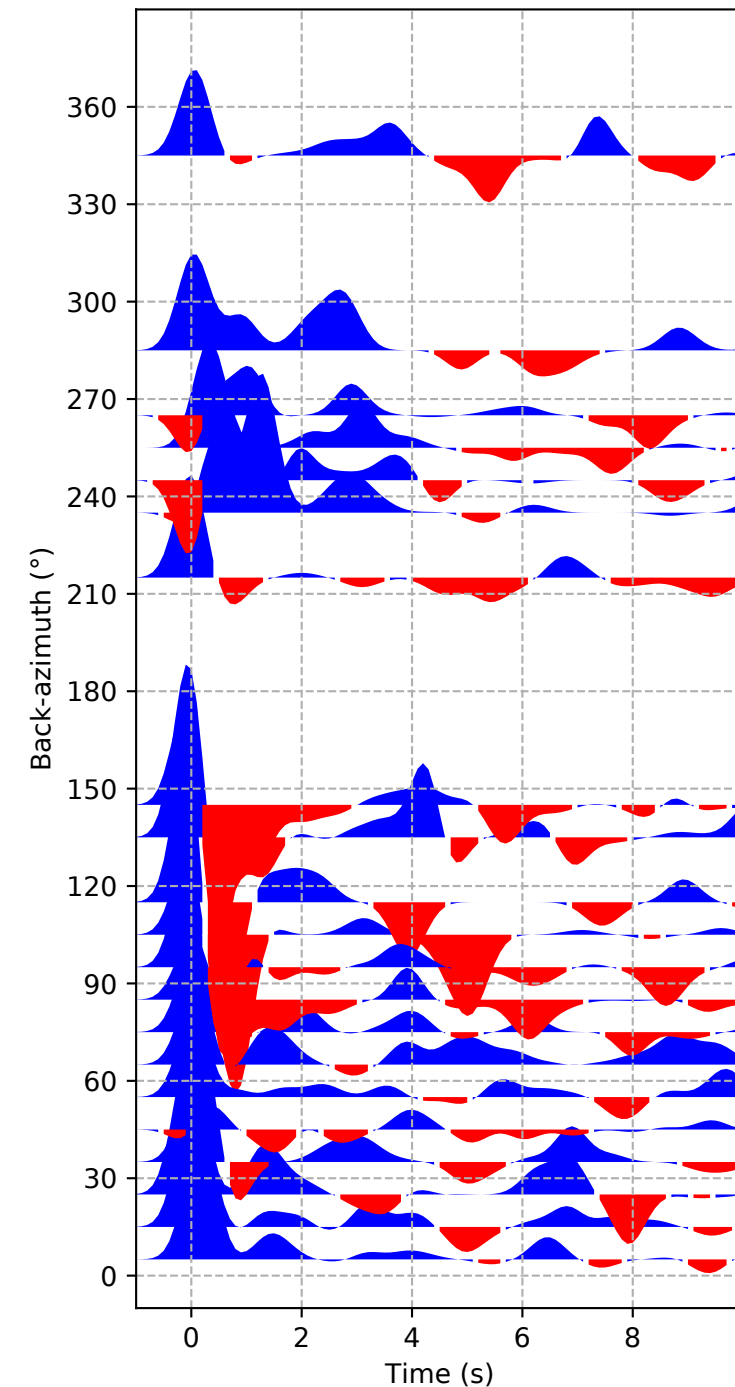


D) Rotated Harmonics components

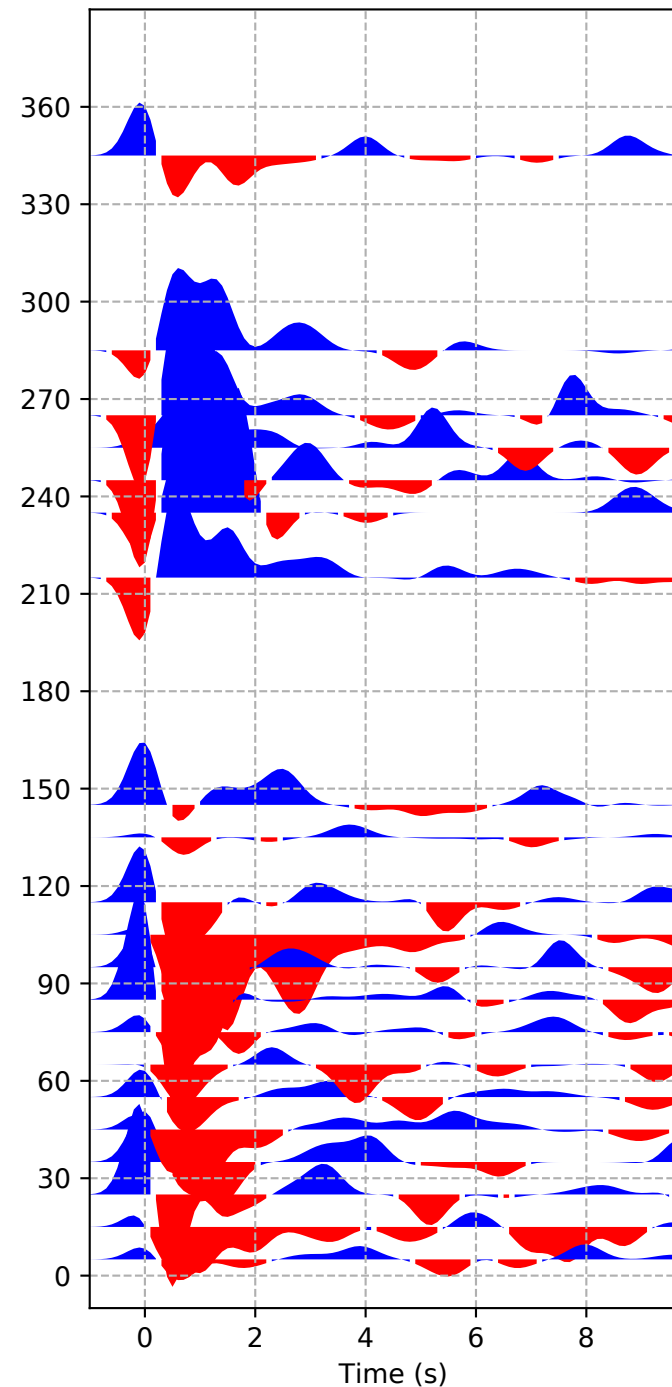


## XV-AMPY

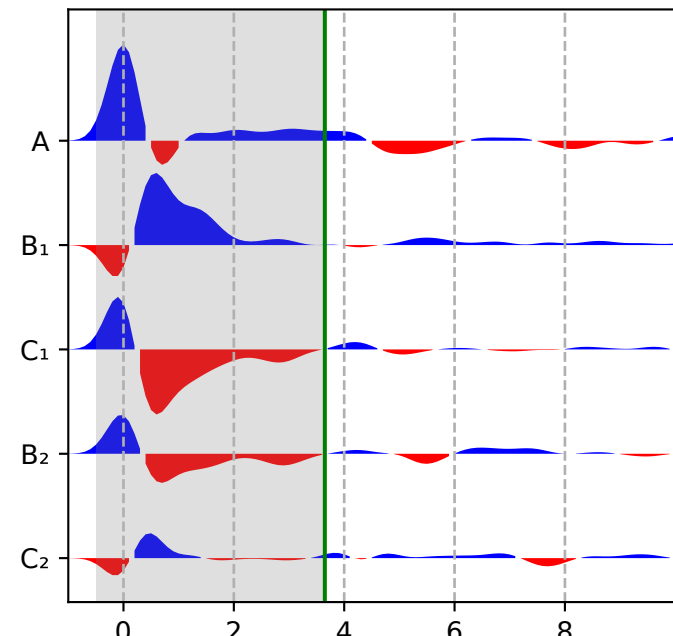
A) Radial



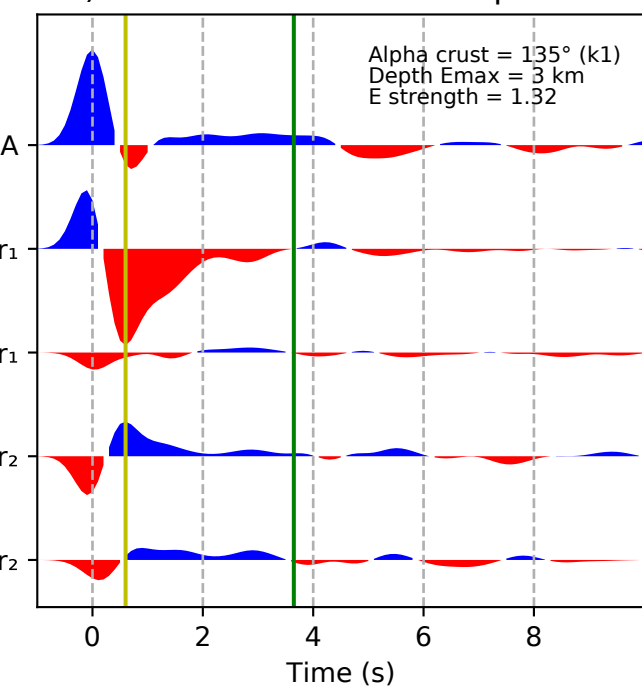
B) Transverse



C) Harmonics components

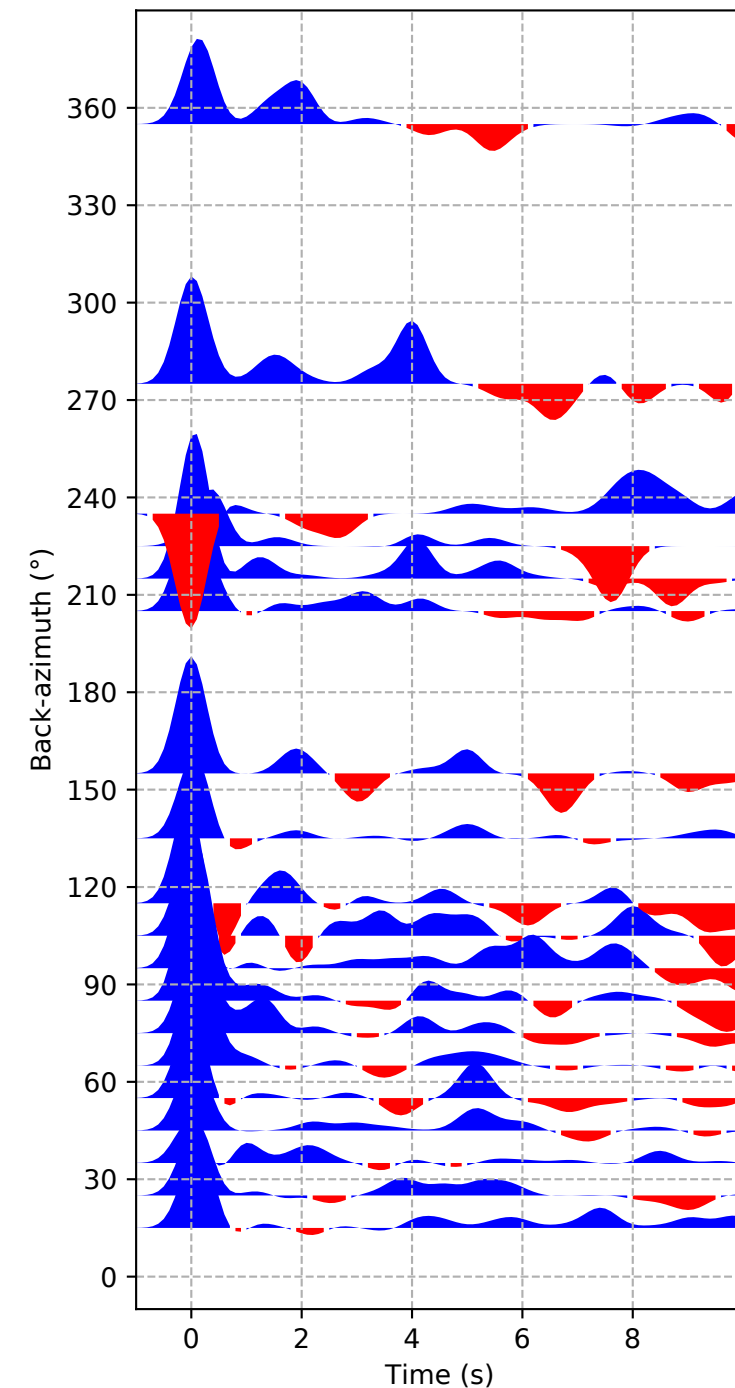


D) Rotated Harmonics components

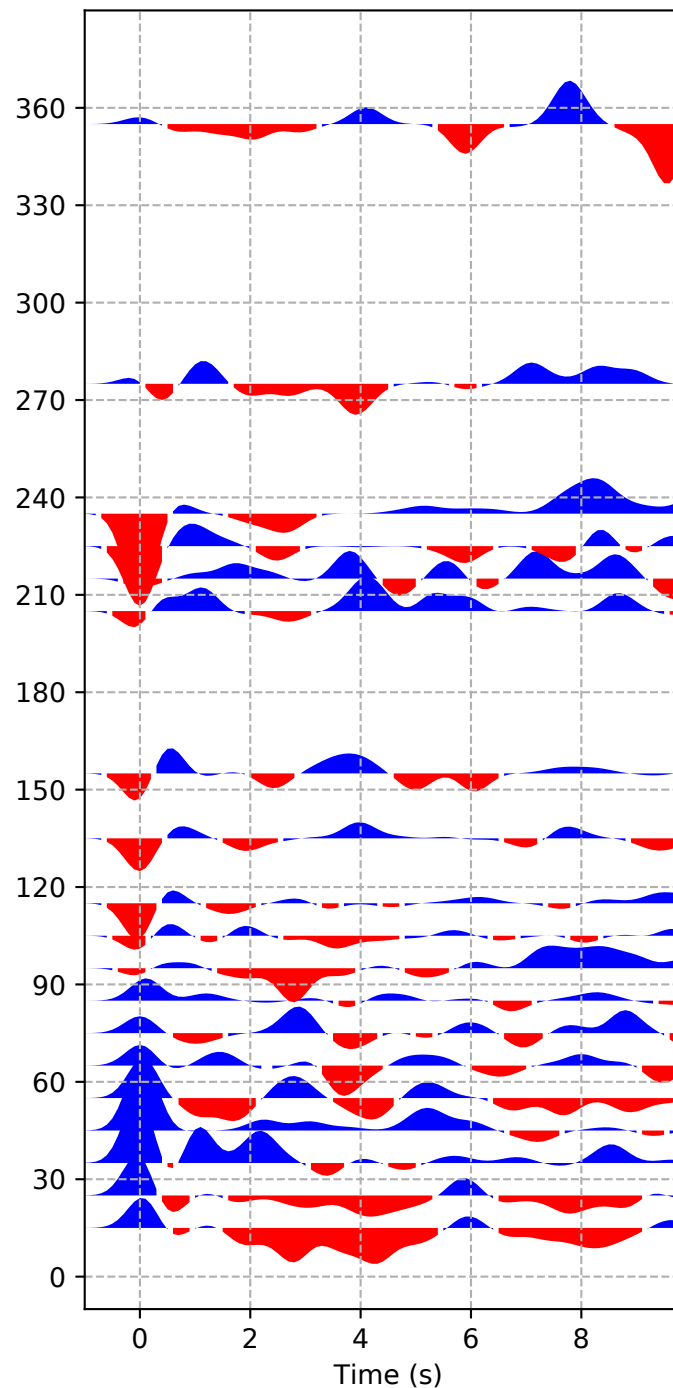


## XV-ANLA

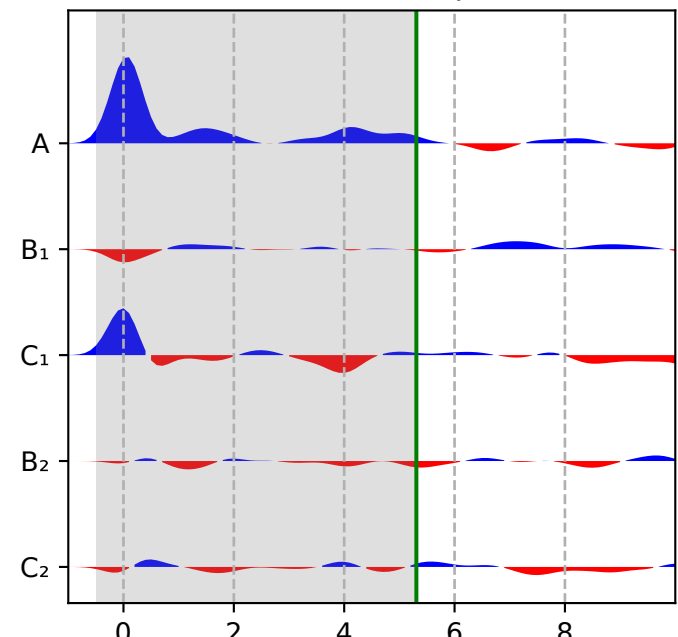
A) Radial



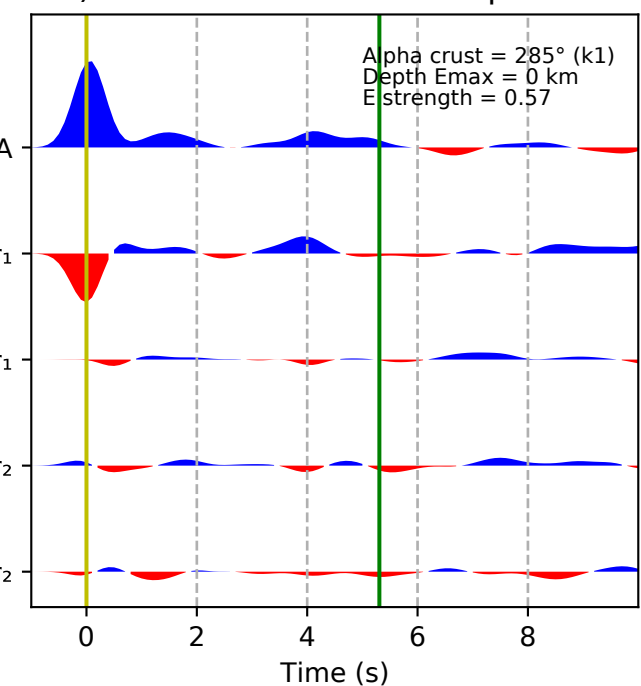
B) Transverse



C) Harmonics components

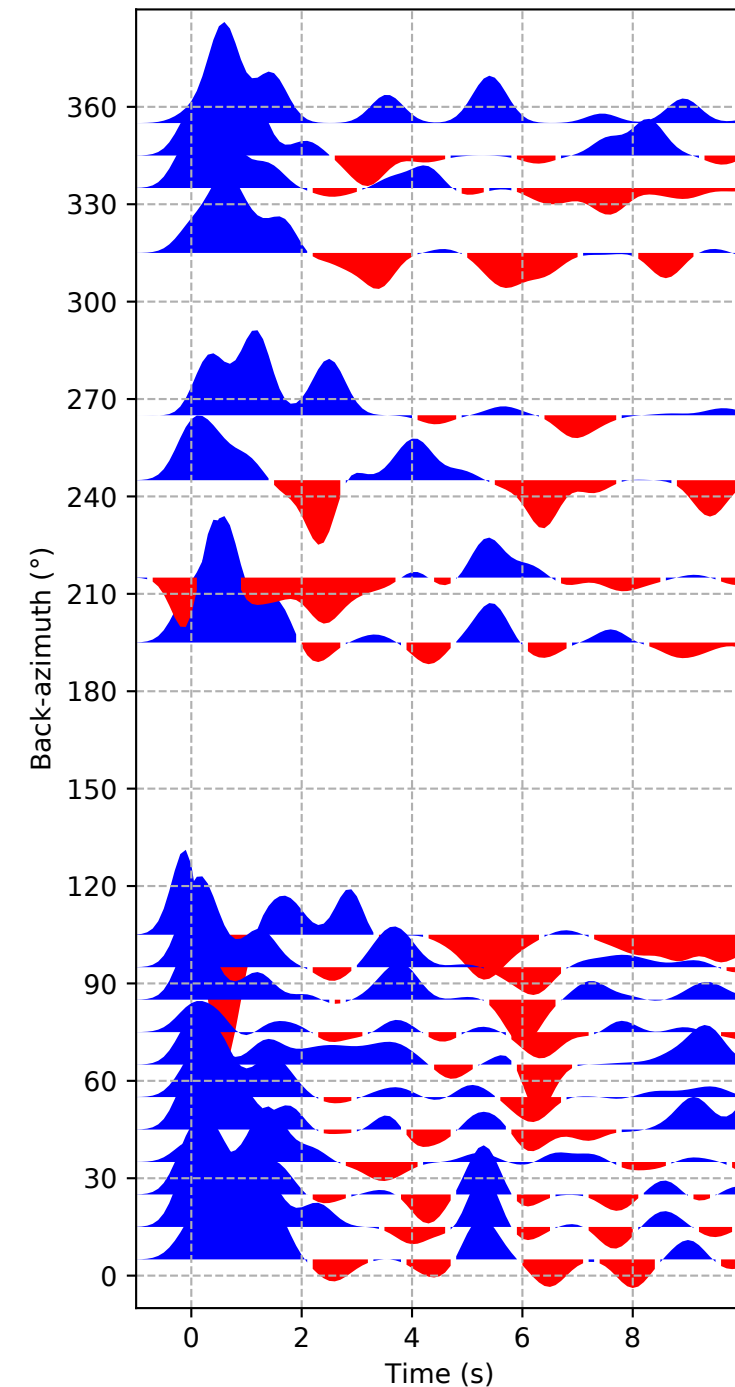


D) Rotated Harmonics components

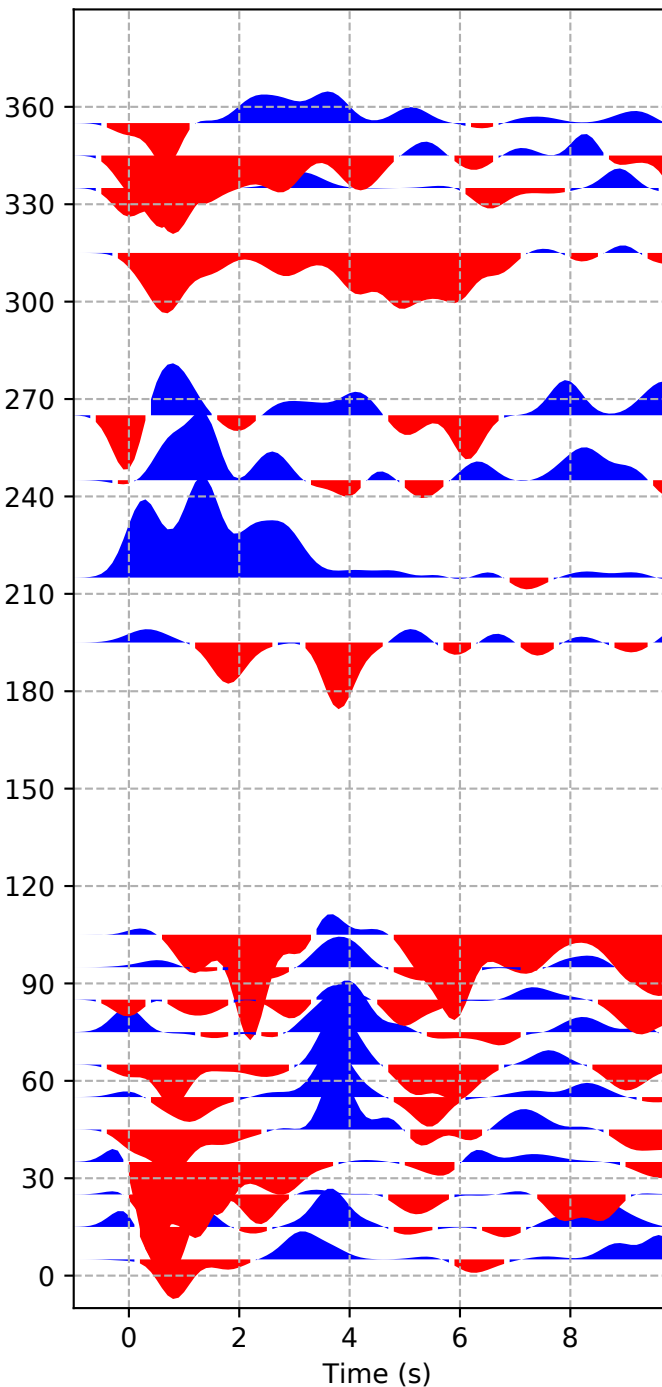


# XV-ANTS

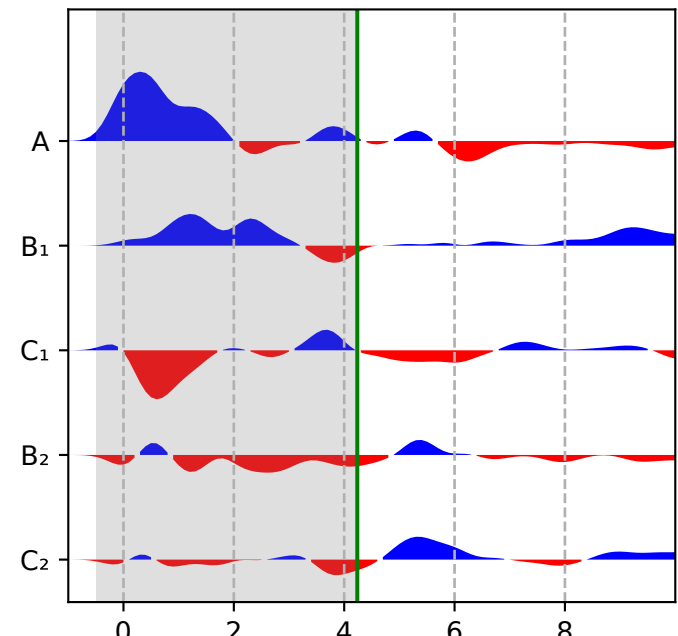
A) Radial



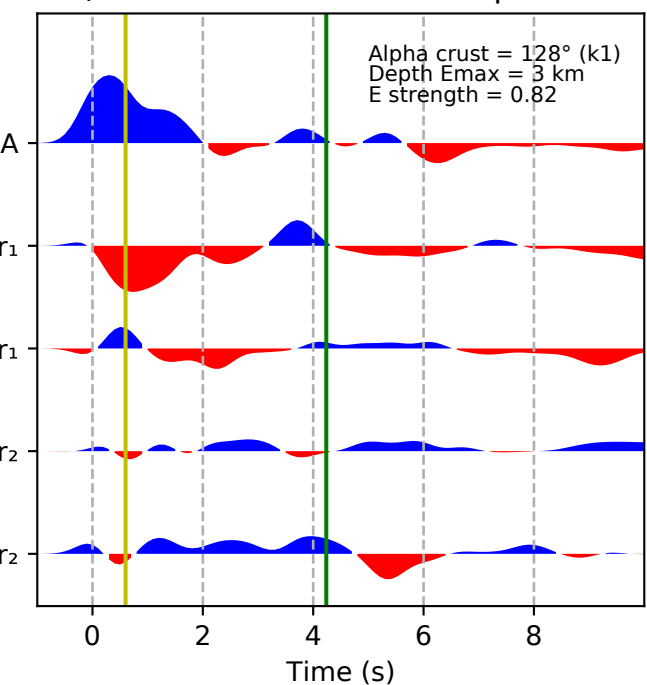
B) Transverse



C) Harmonics components

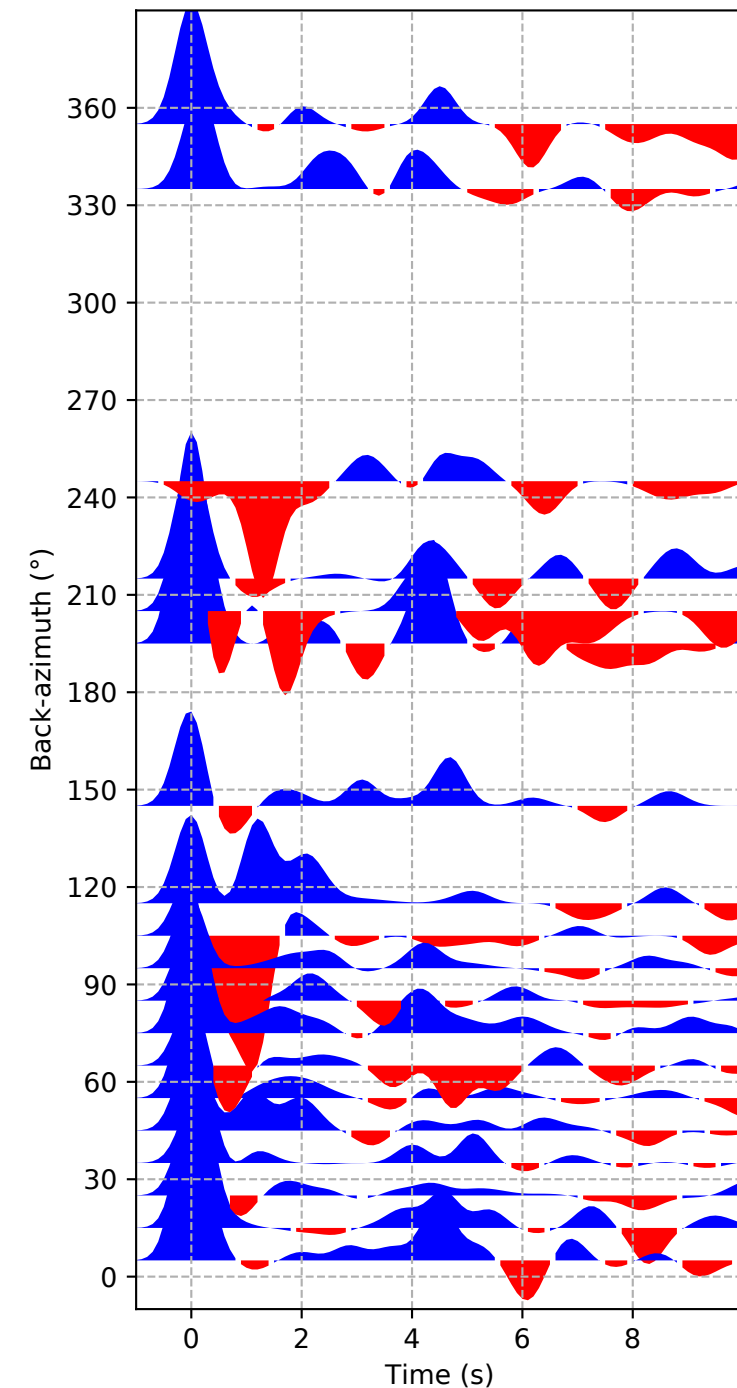


D) Rotated Harmonics components

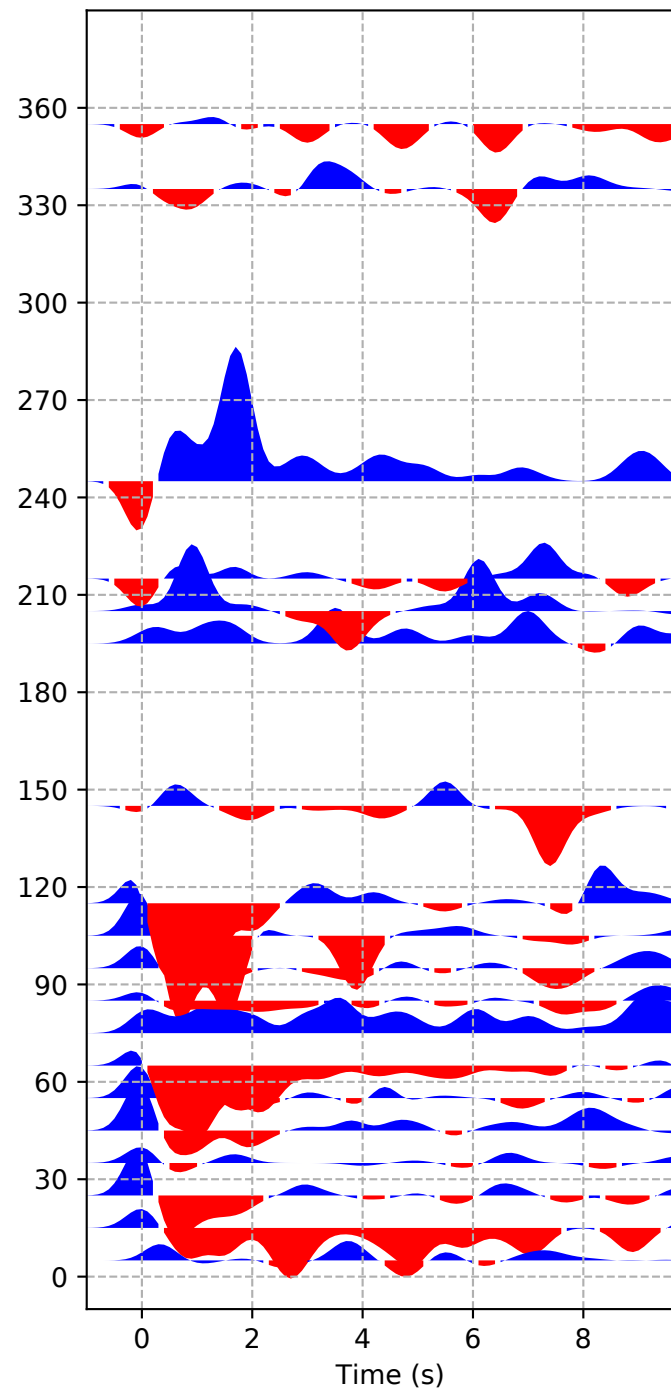


# XV-BAEL

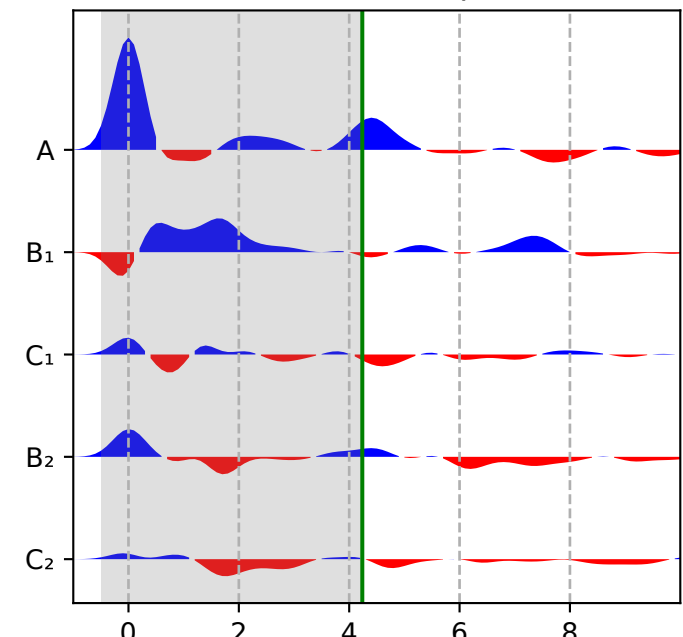
A) Radial



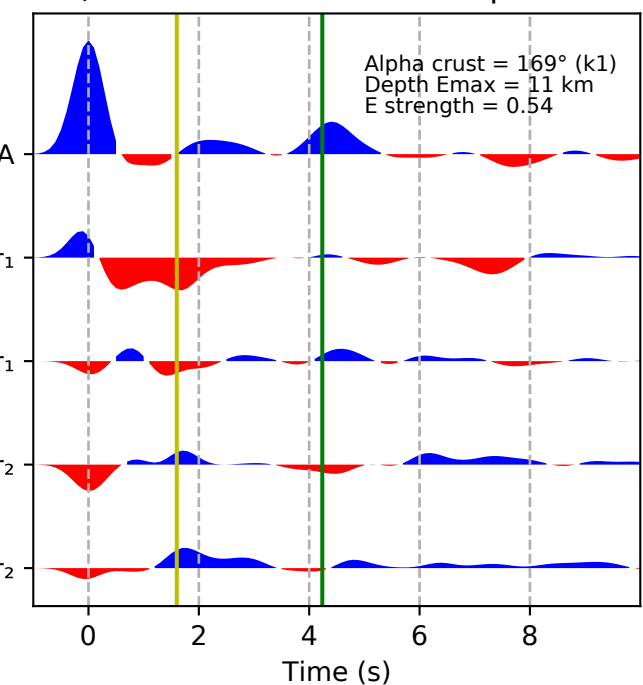
B) Transverse



C) Harmonics components

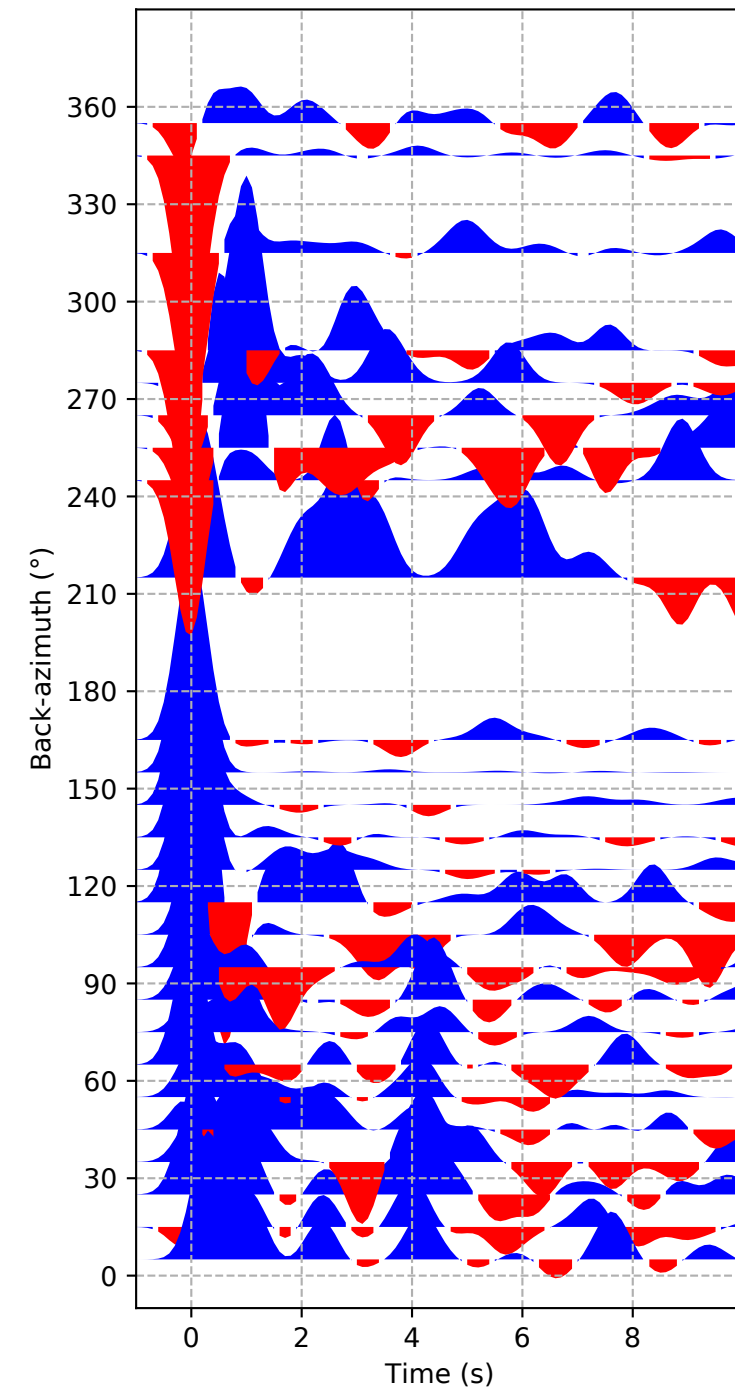


D) Rotated Harmonics components

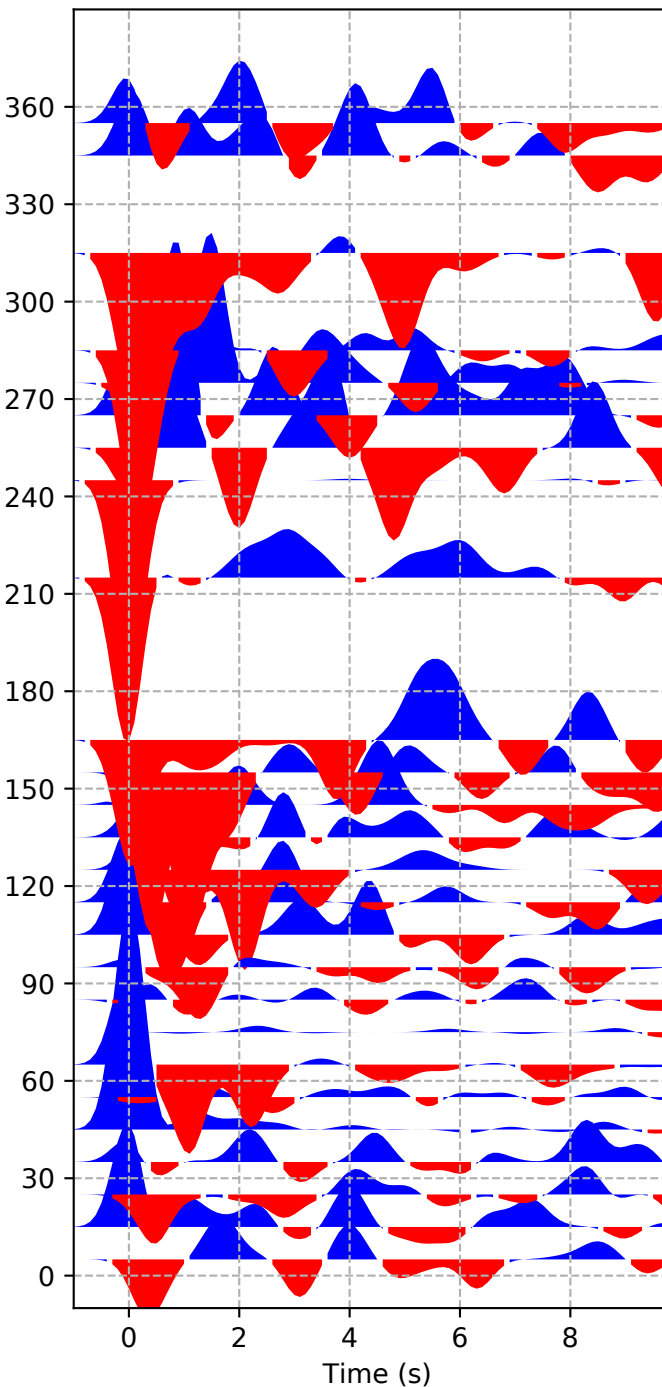


## XV-BAND

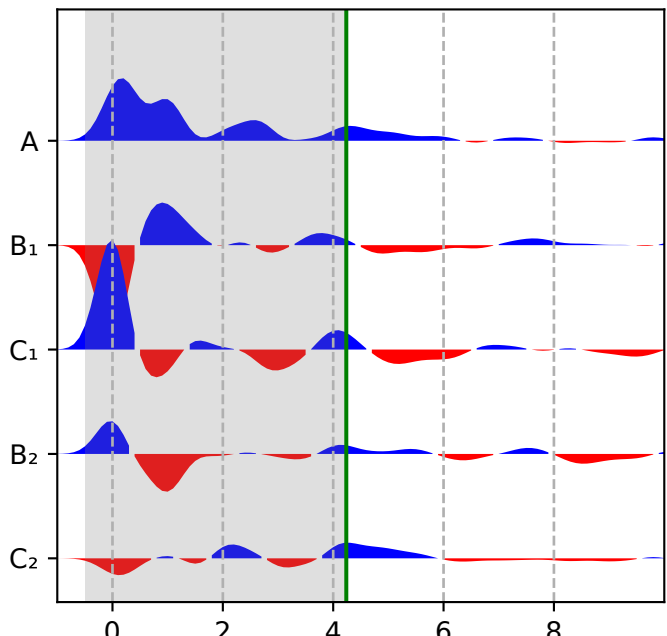
A) Radial



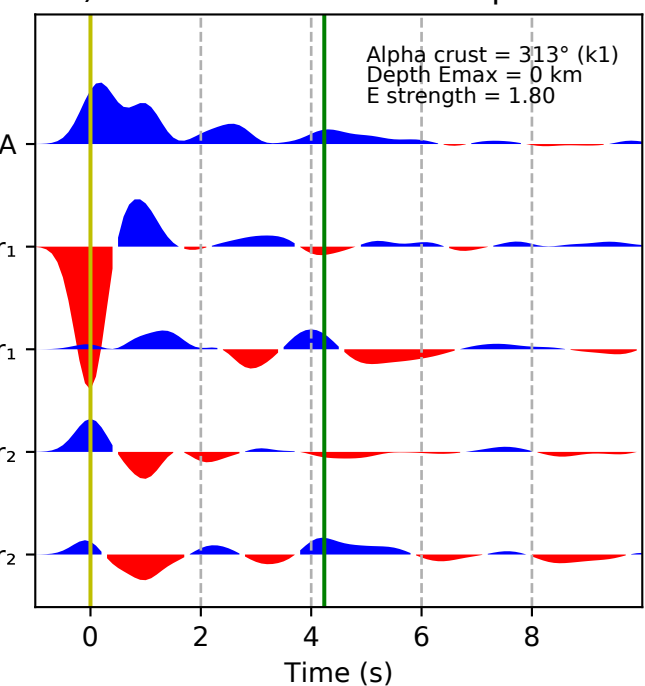
B) Transverse



C) Harmonics components

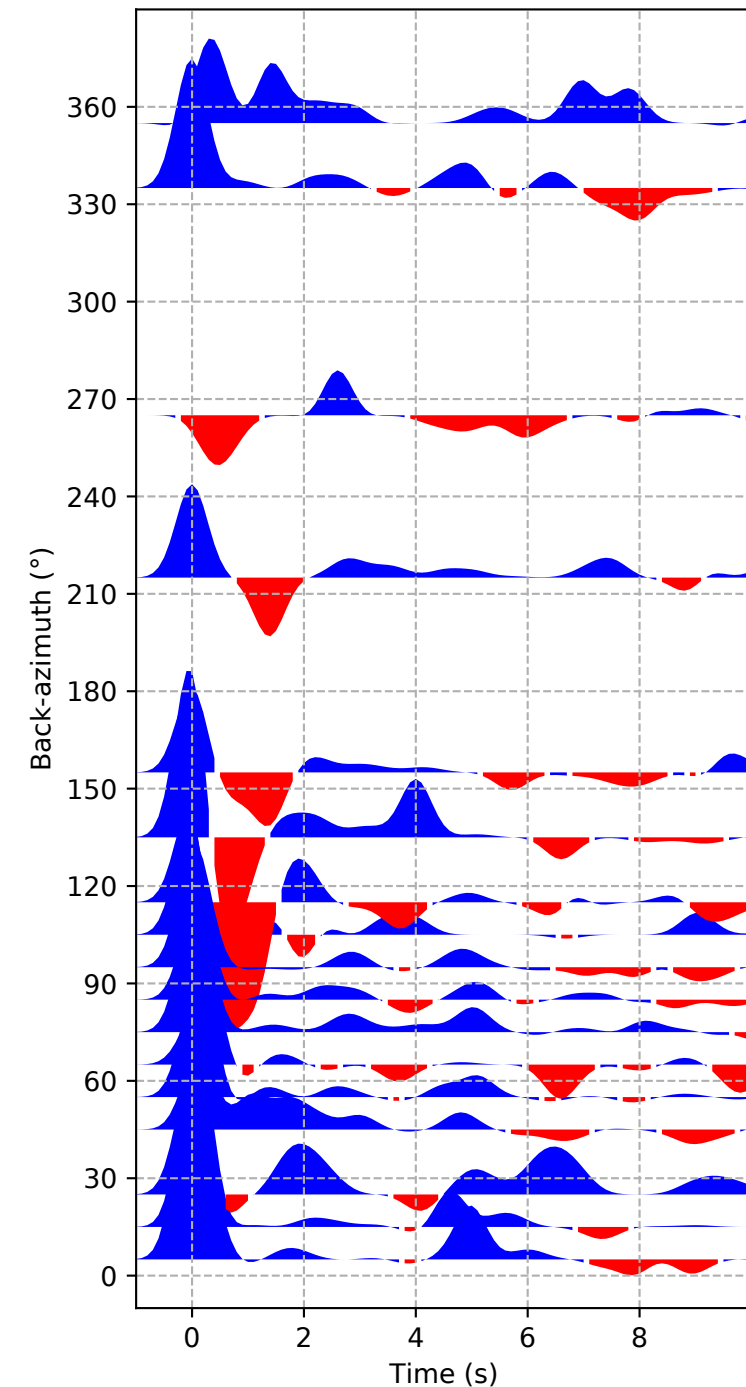


D) Rotated Harmonics components

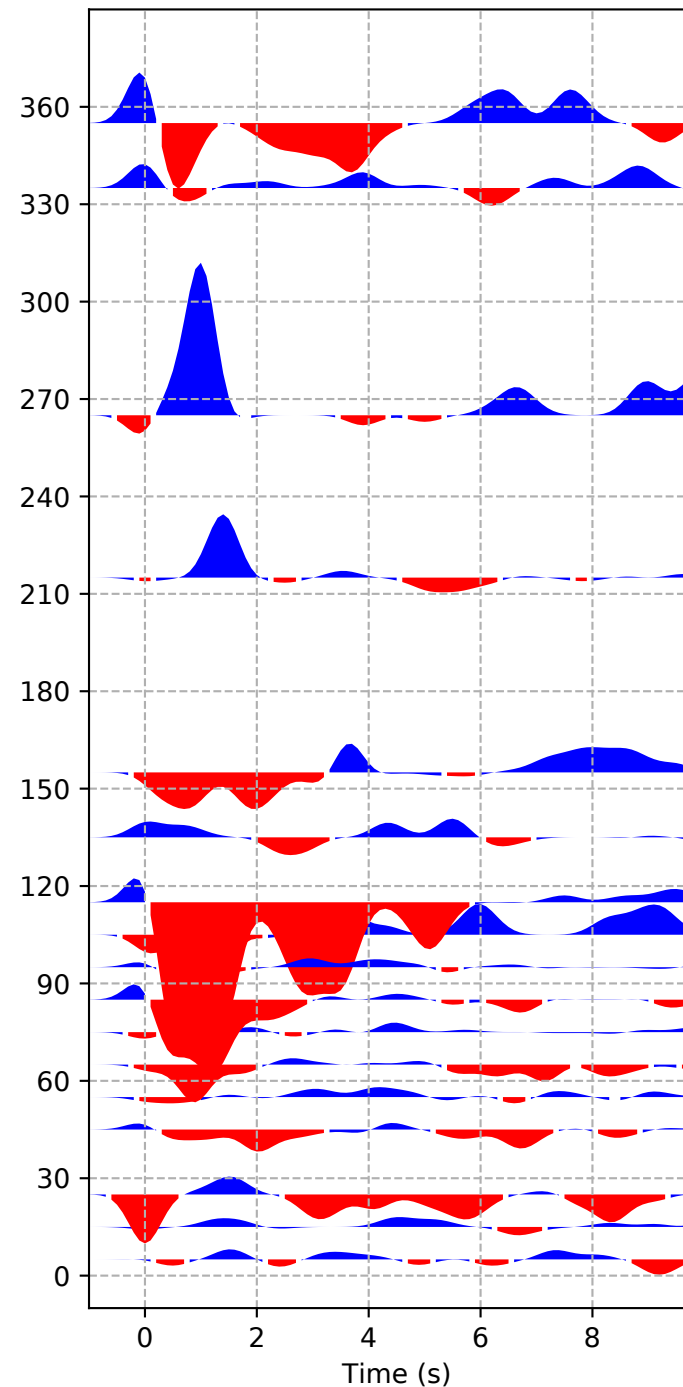


## XV-BARY

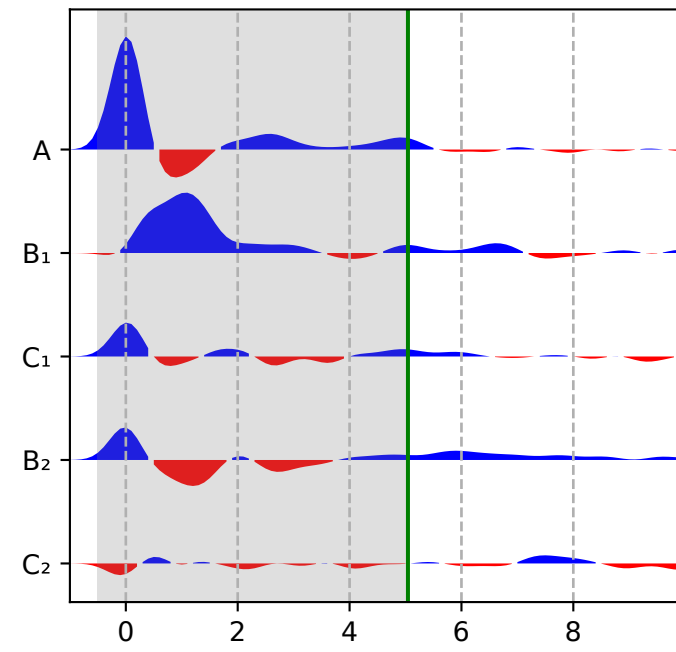
A) Radial



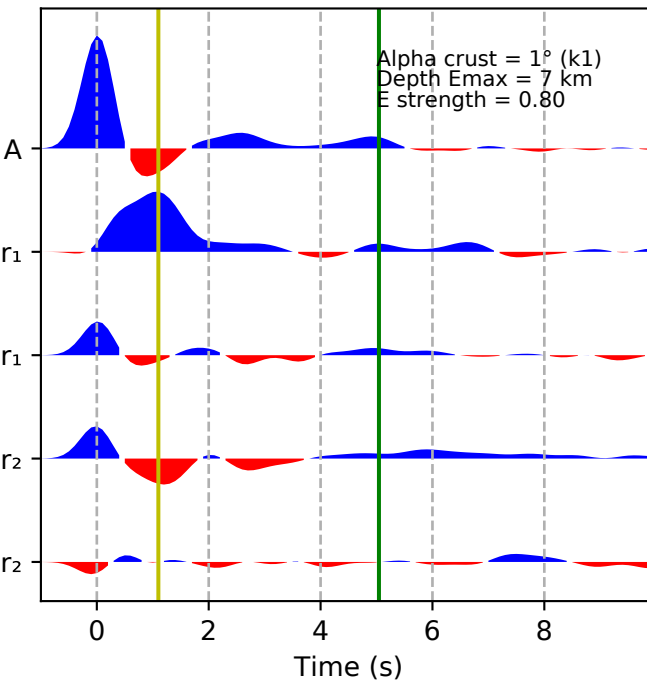
B) Transverse



C) Harmonics components

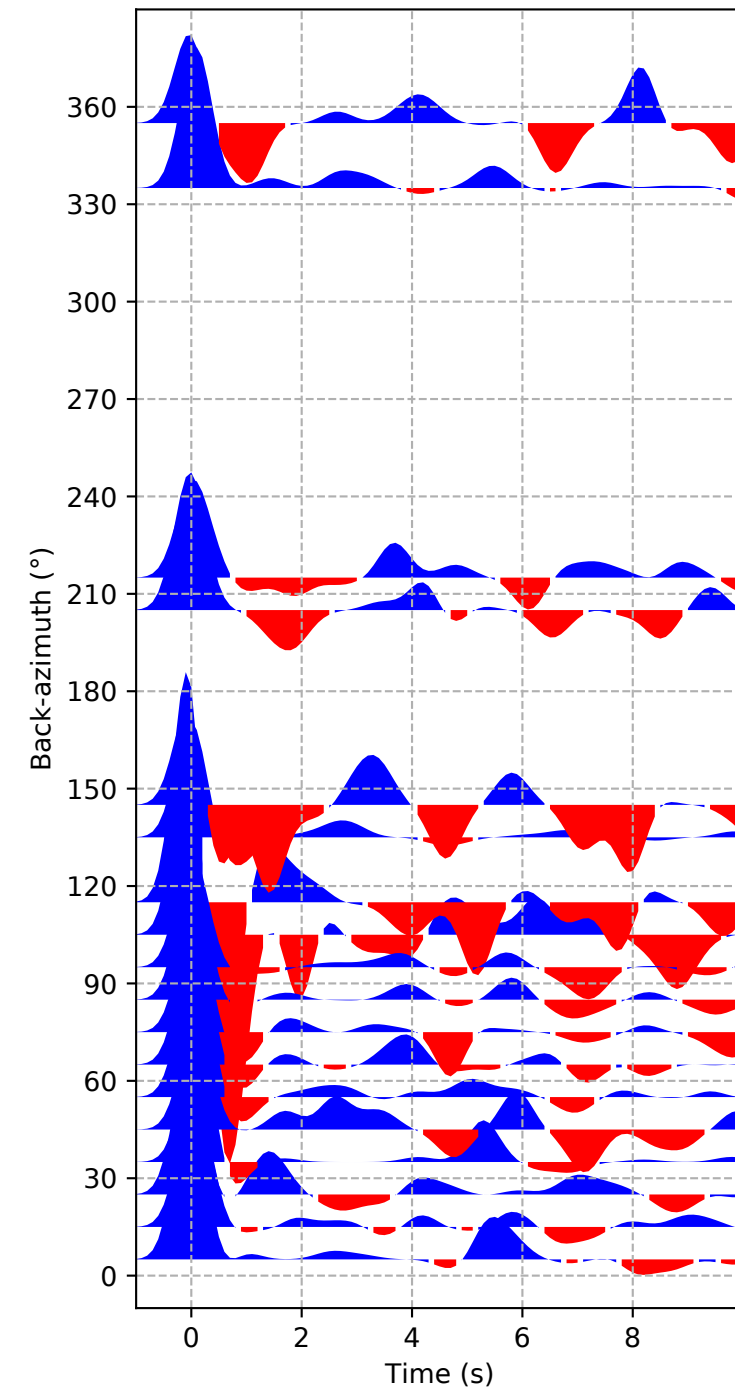


D) Rotated Harmonics components

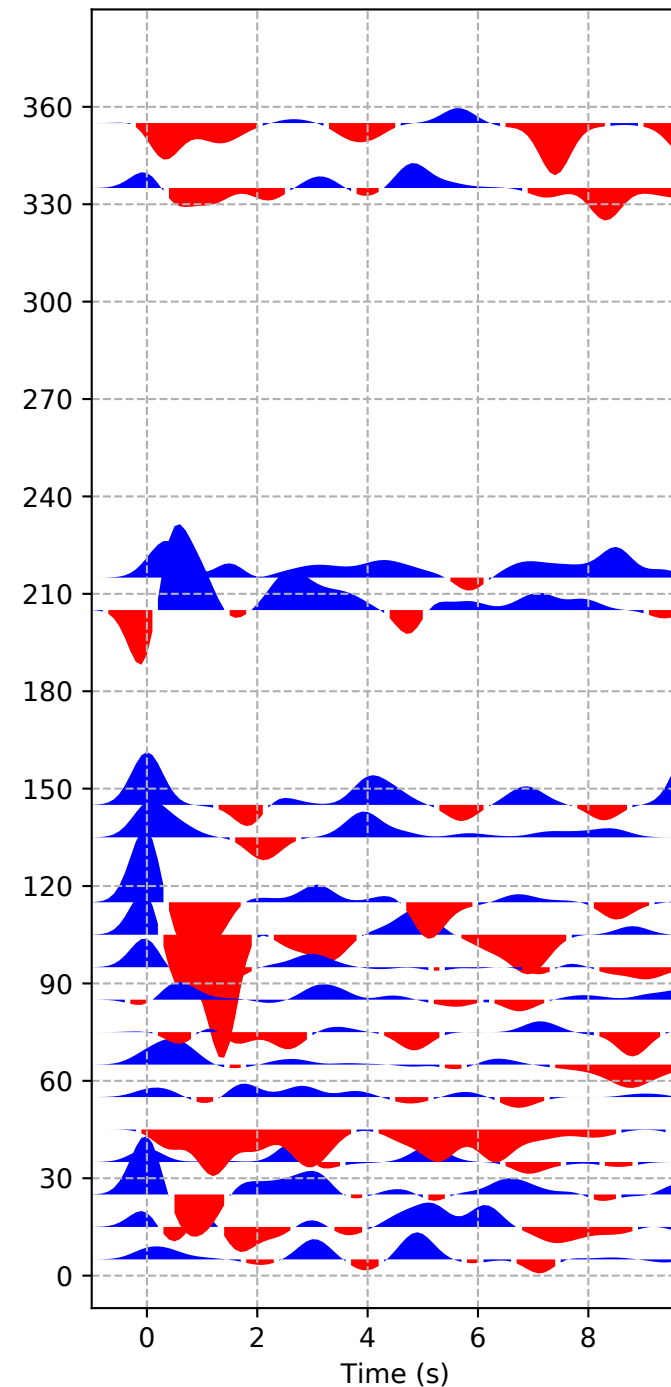


## XV-BATG

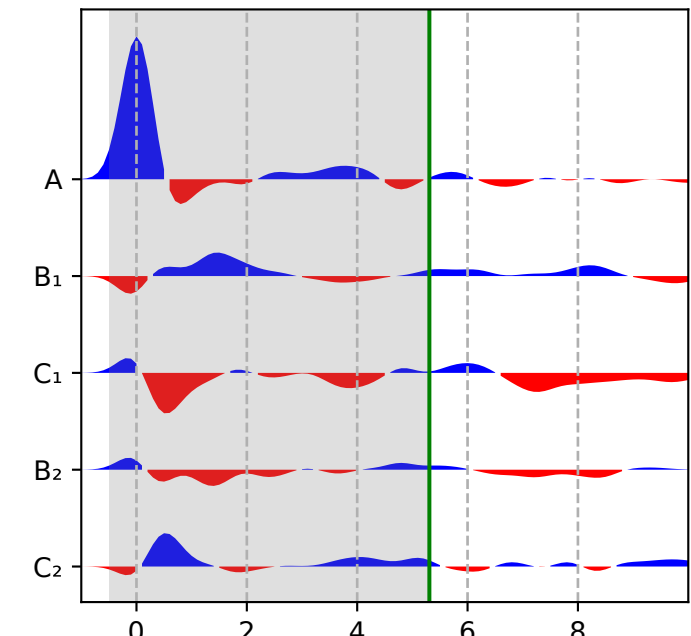
A) Radial



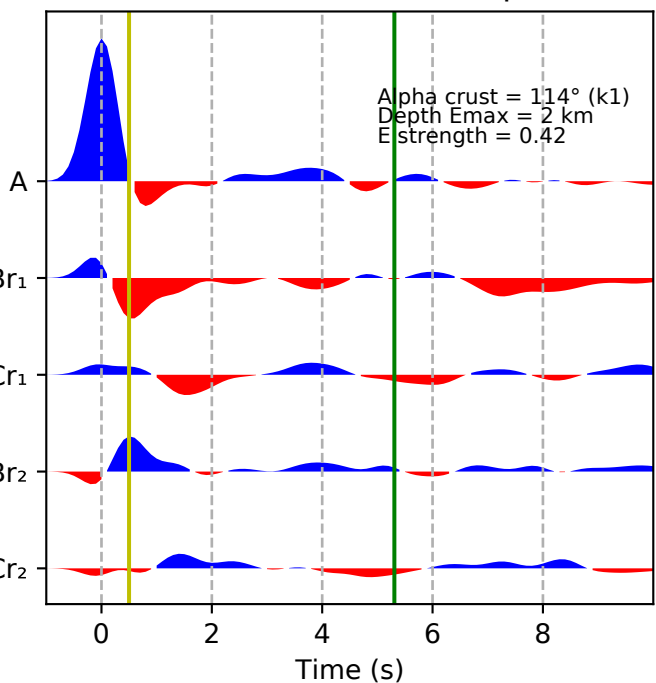
B) Transverse



C) Harmonics components

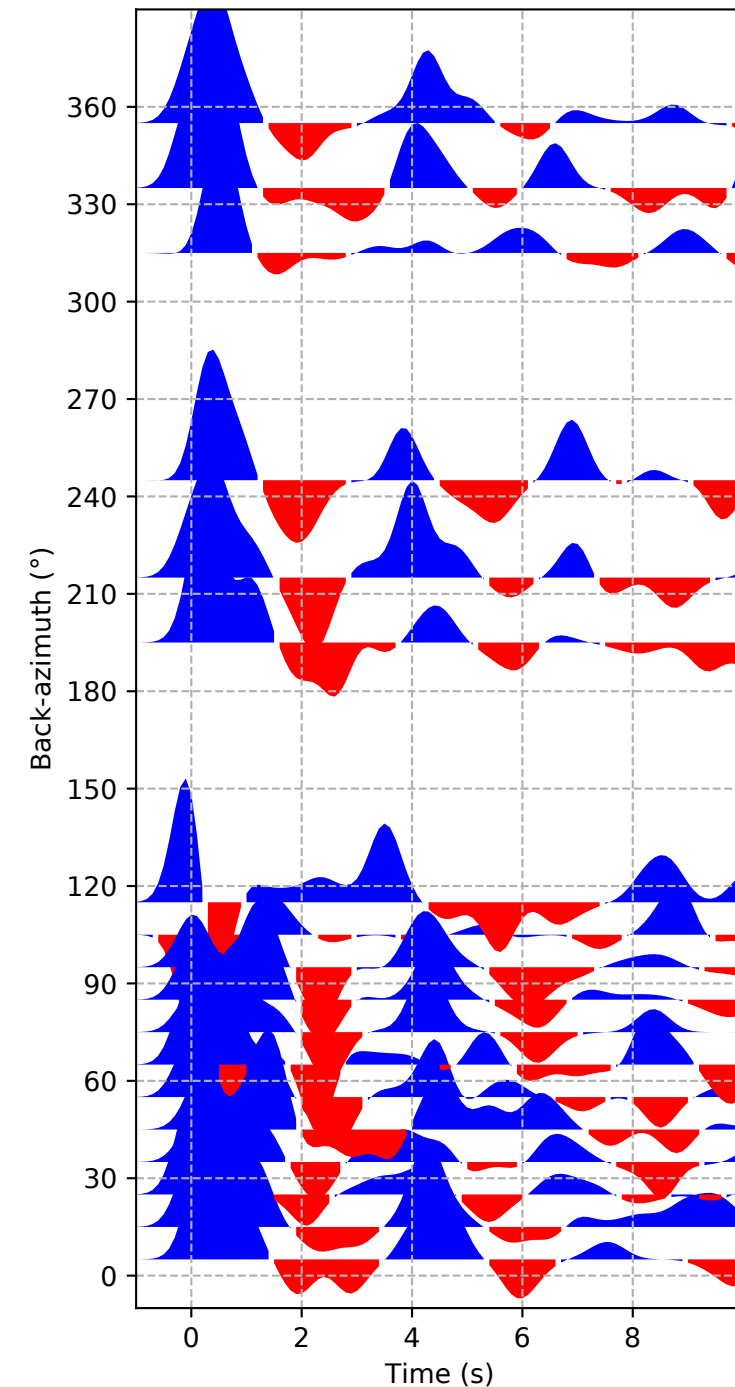


D) Rotated Harmonics components

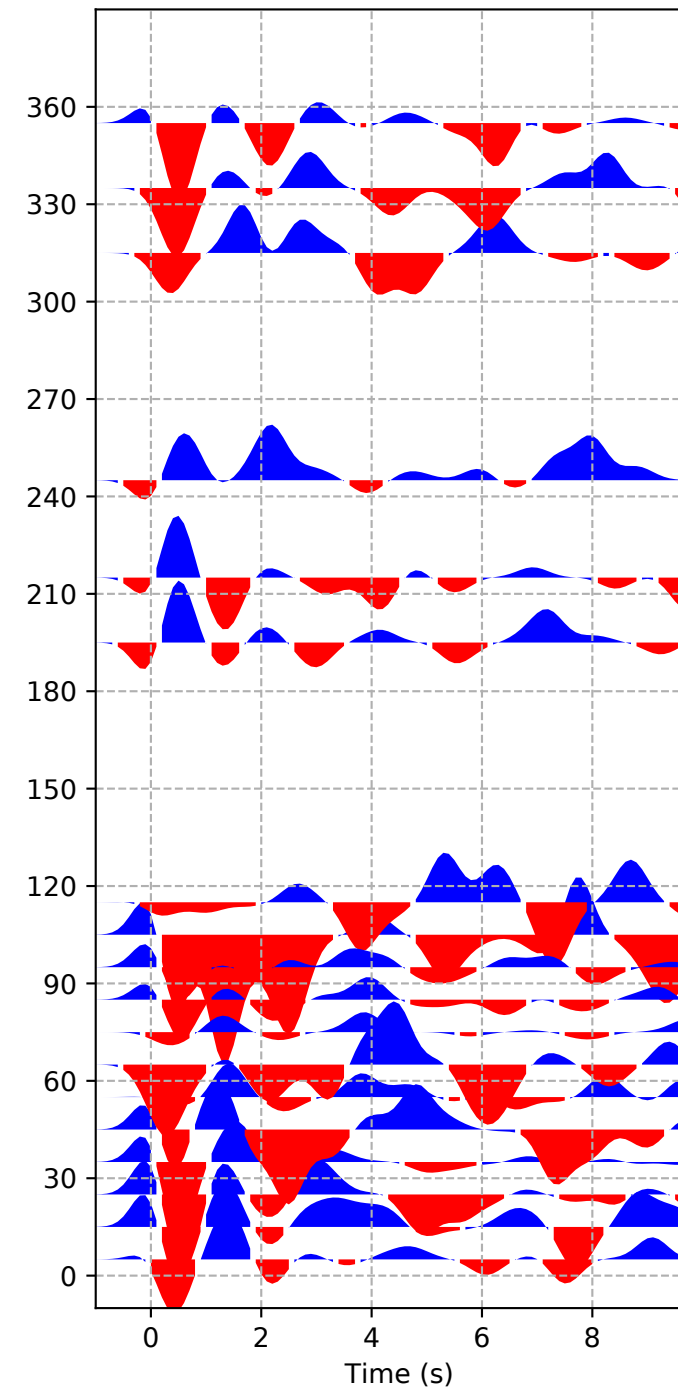


# XV-BERG

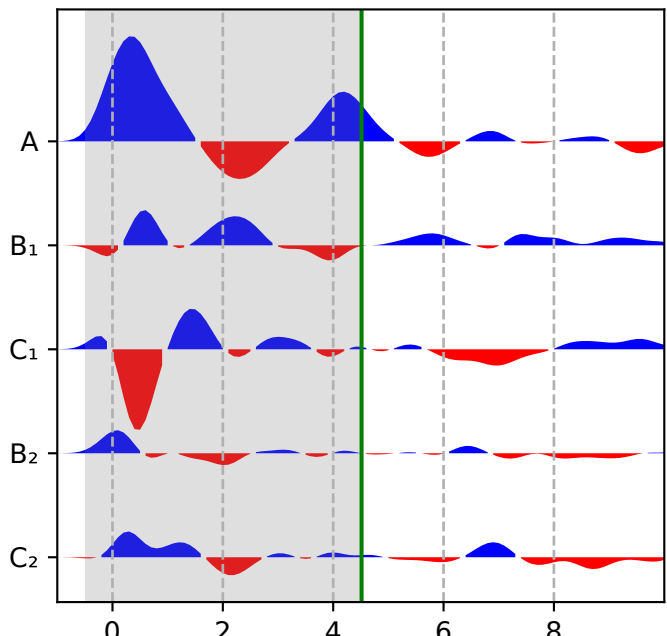
A) Radial



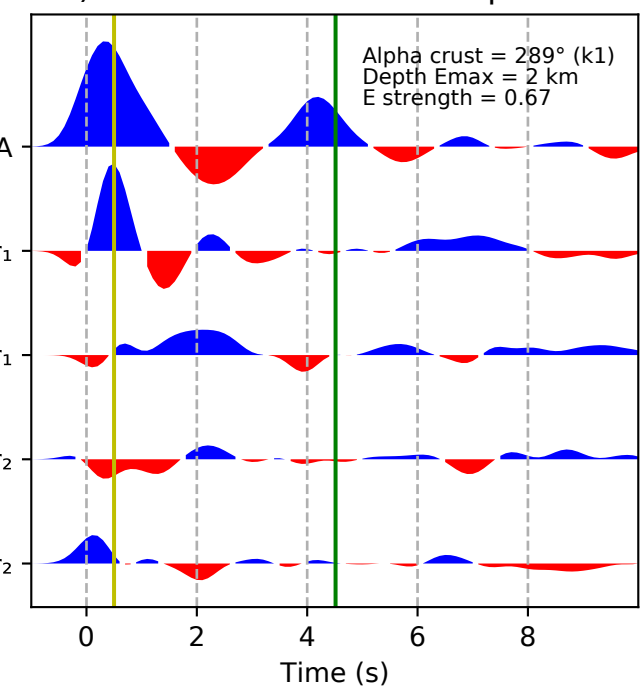
B) Transverse



C) Harmonics components

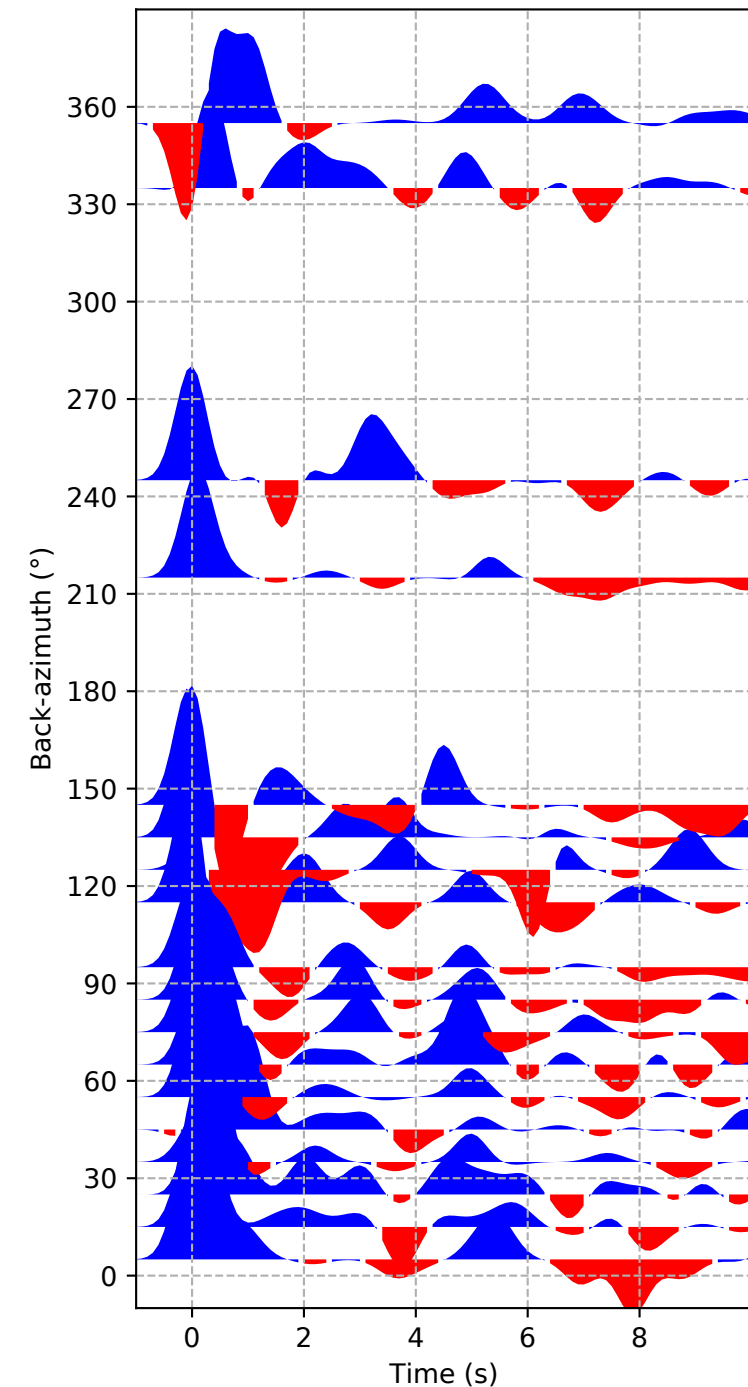


D) Rotated Harmonics components

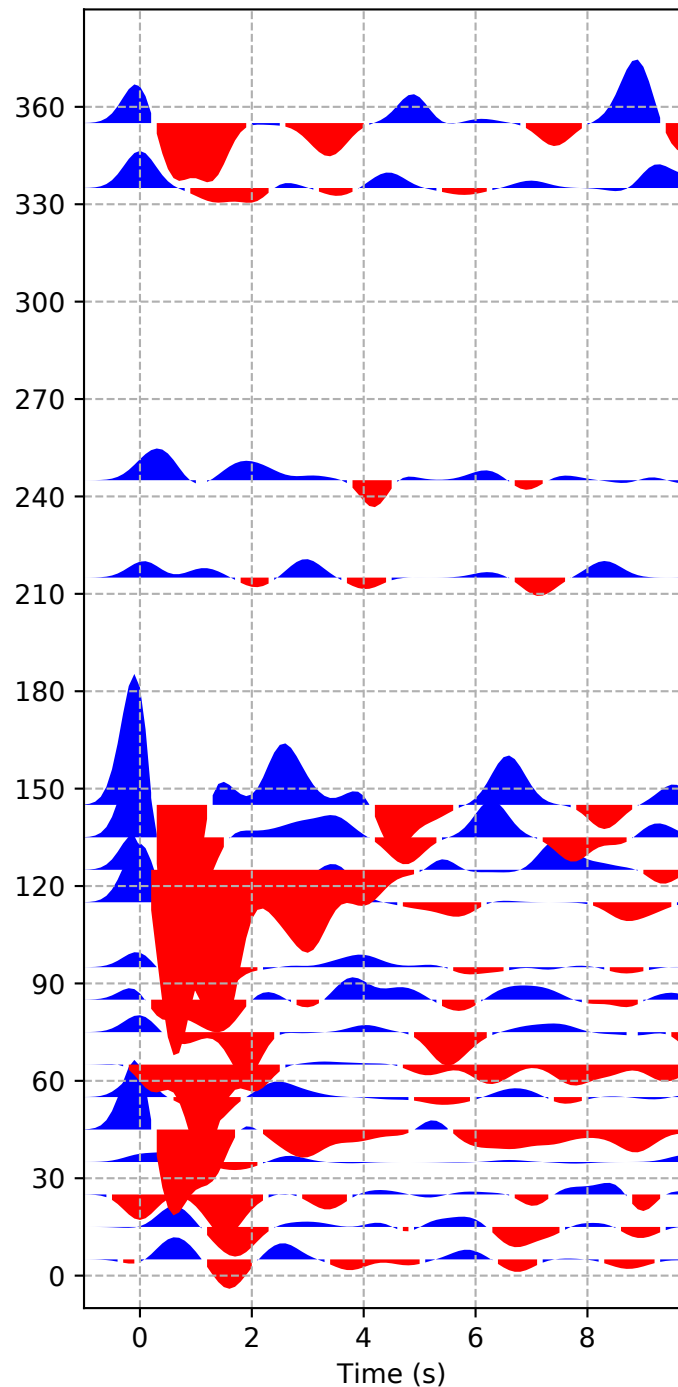


## XV-BITY

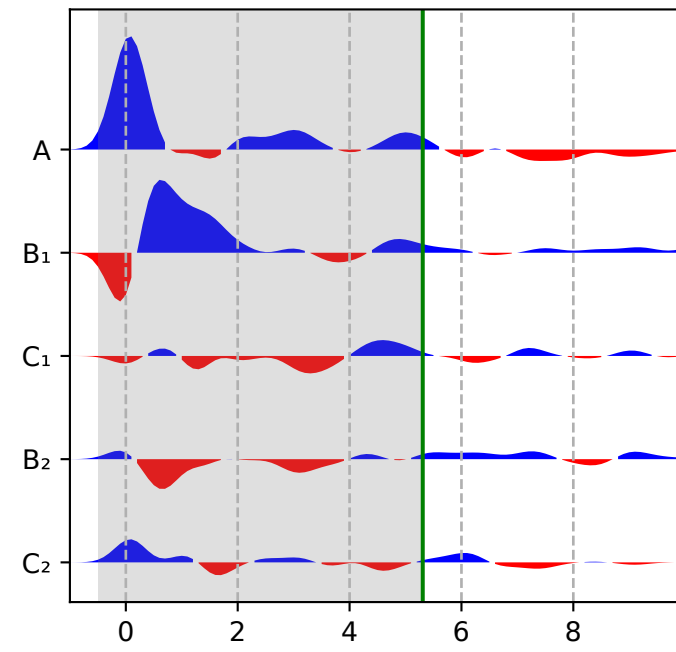
A) Radial



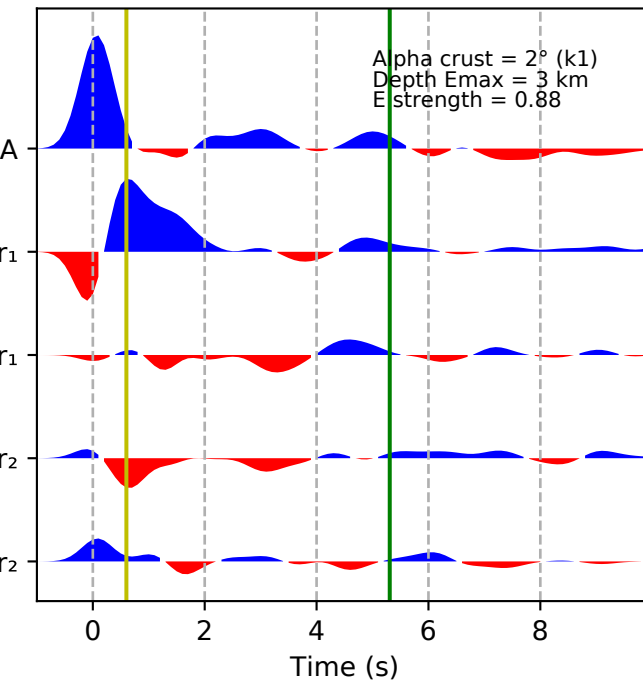
B) Transverse



C) Harmonics components

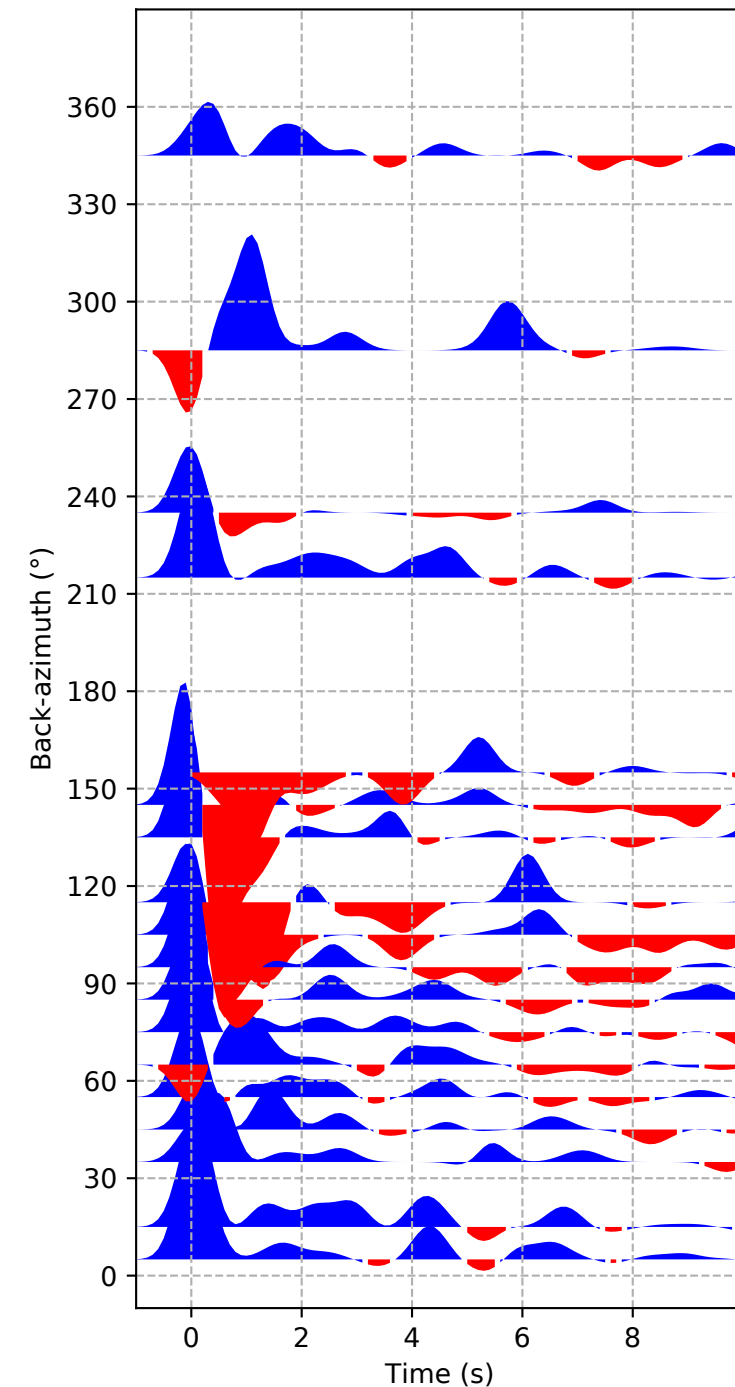


D) Rotated Harmonics components

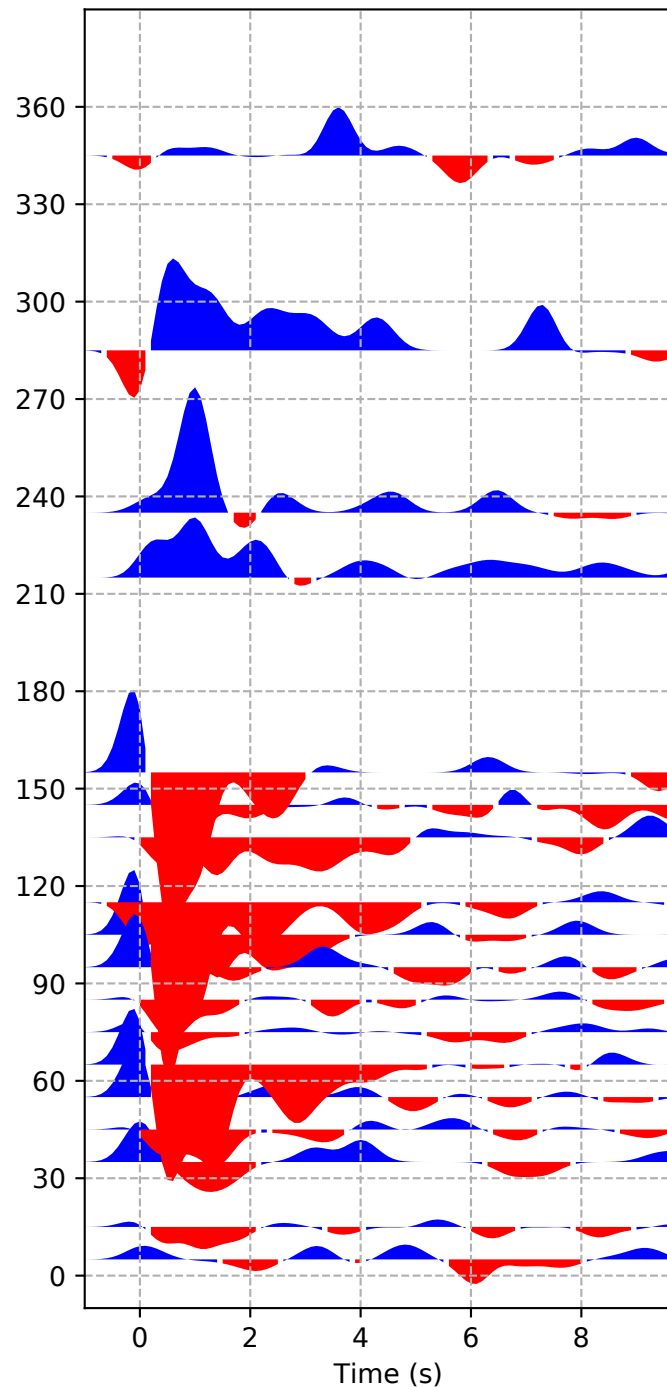


## XV-BKTA

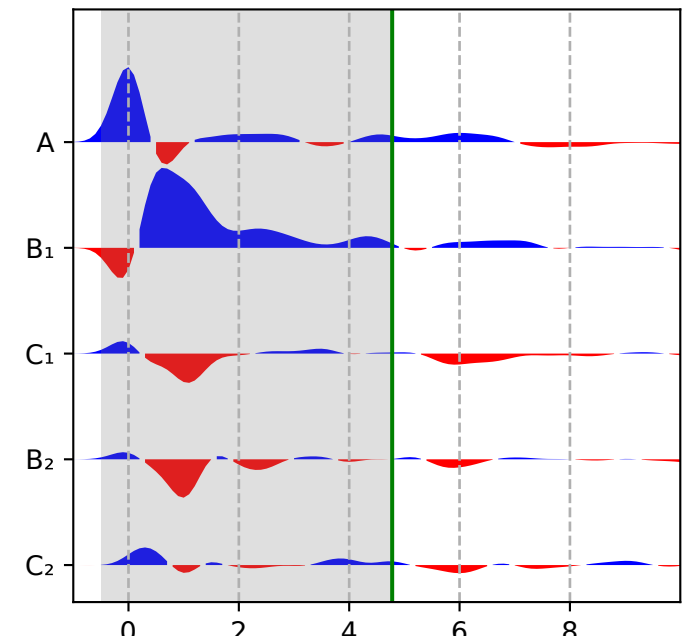
A) Radial



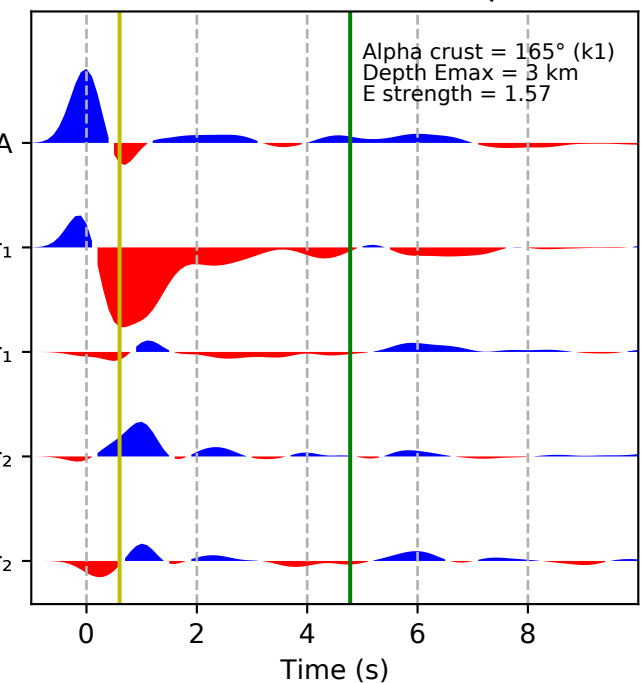
B) Transverse



C) Harmonics components

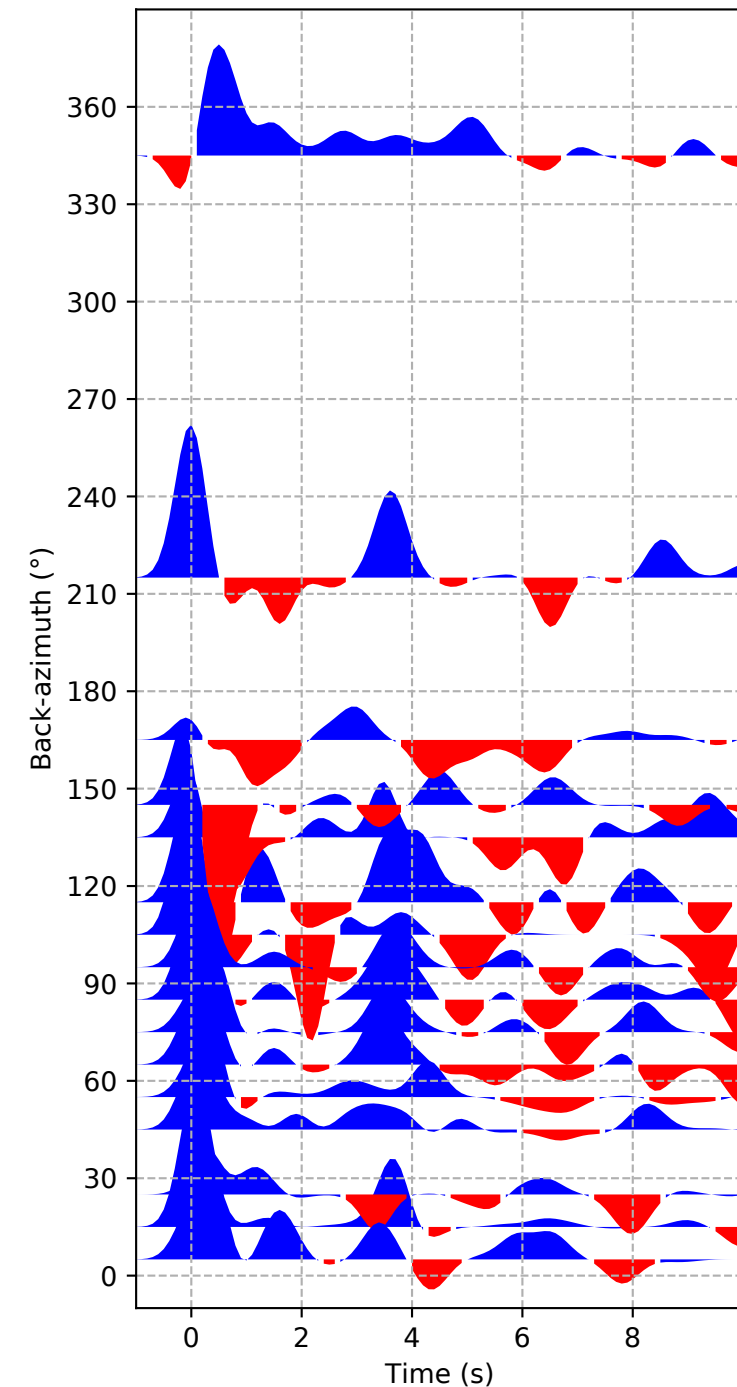


D) Rotated Harmonics components

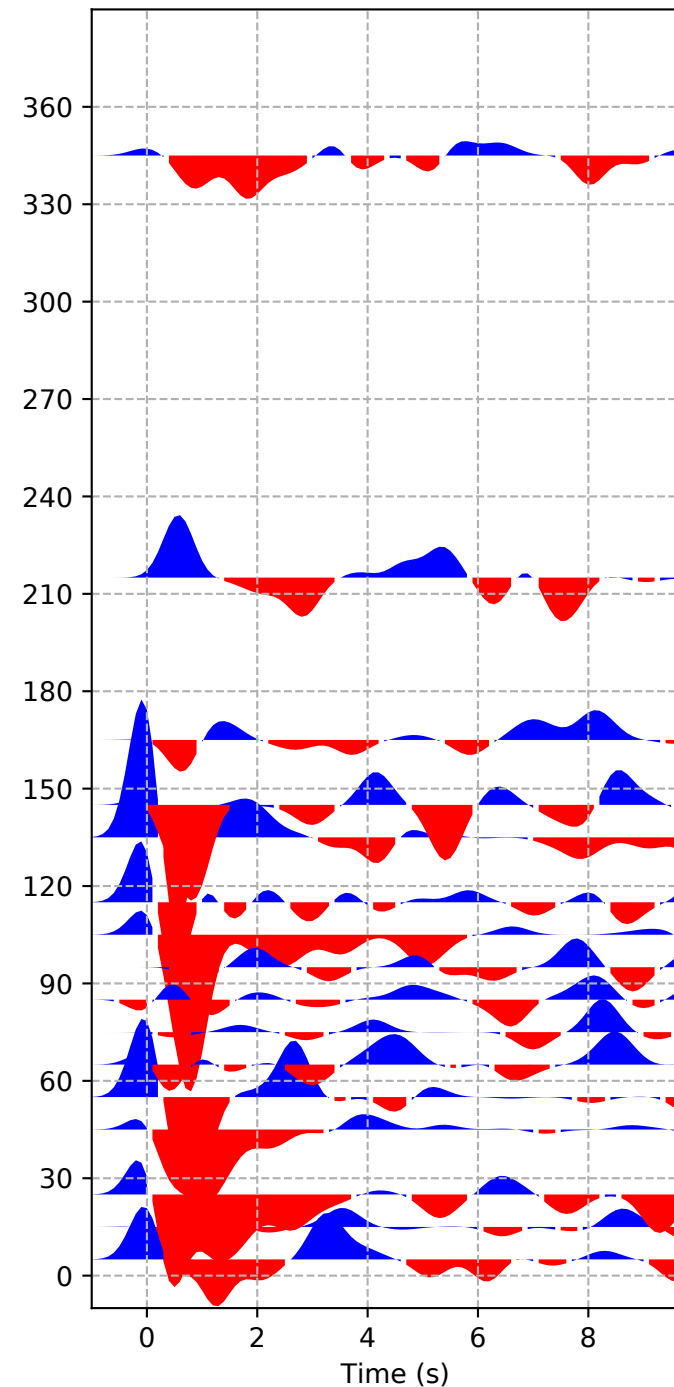


# XV-CPSM

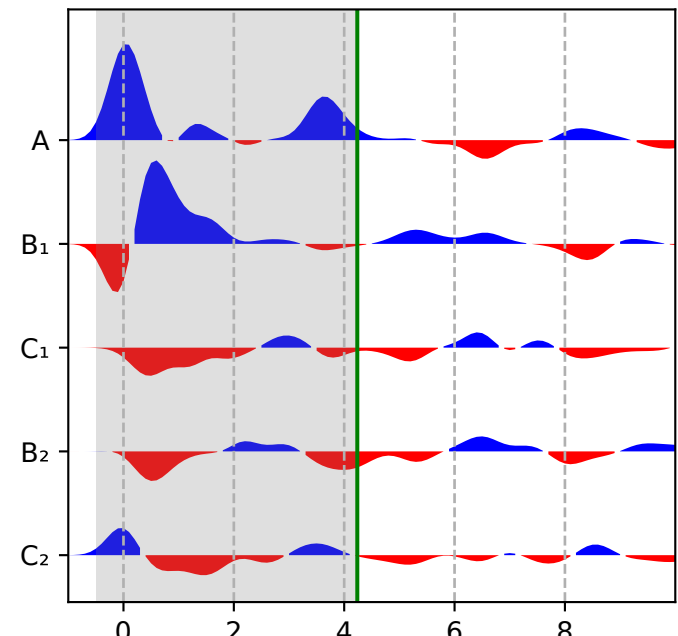
A) Radial



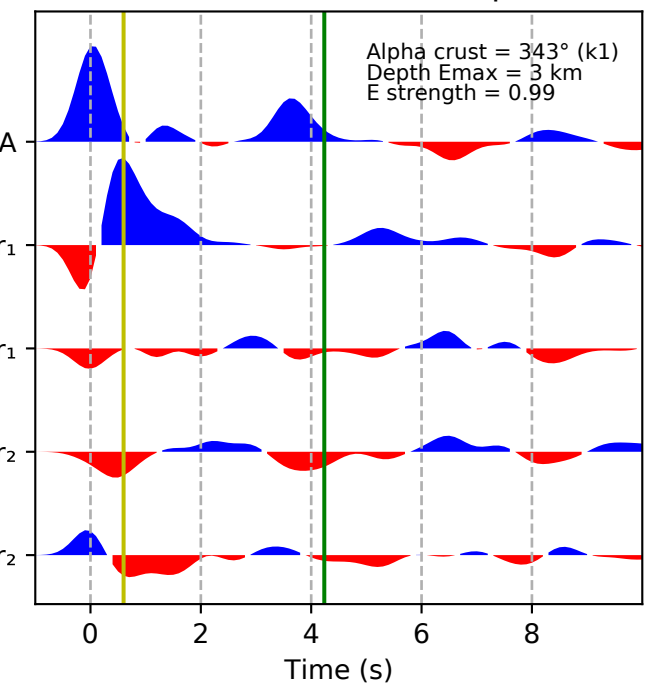
B) Transverse



C) Harmonics components

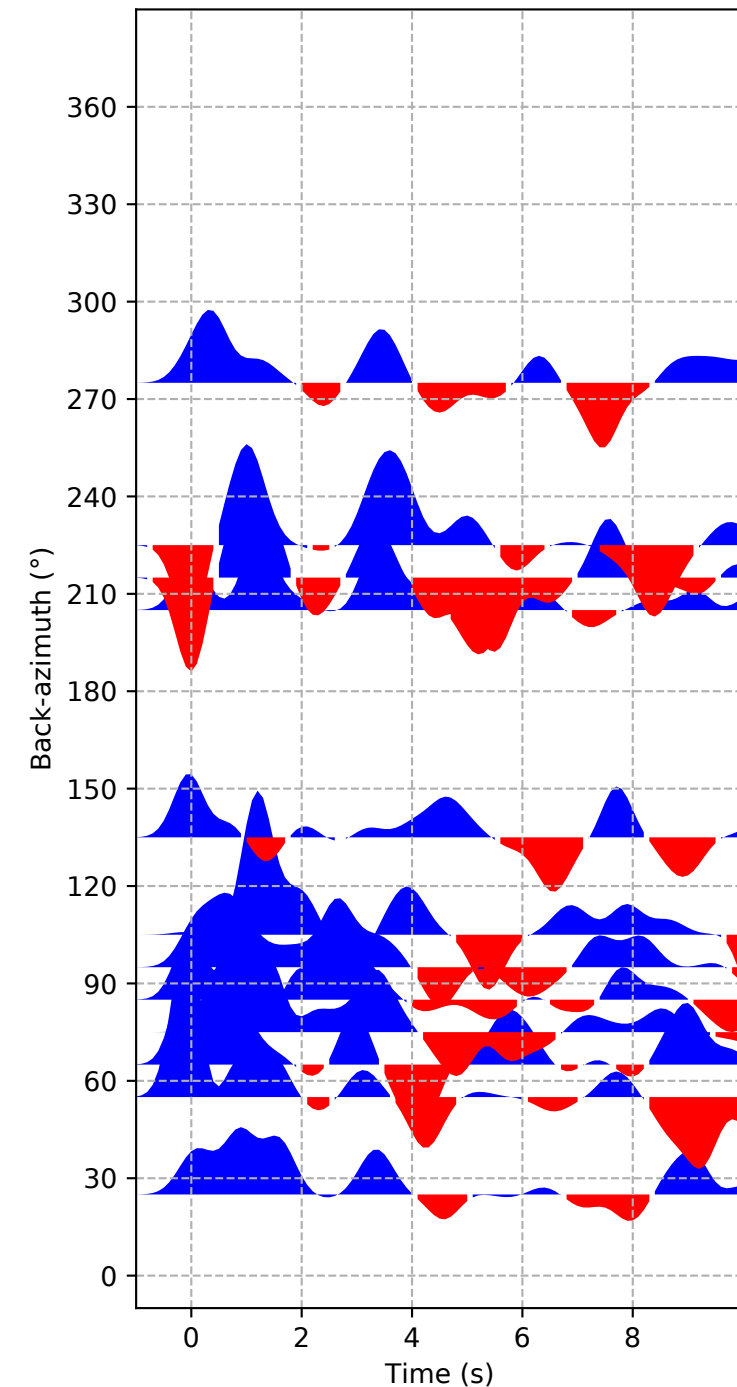


D) Rotated Harmonics components

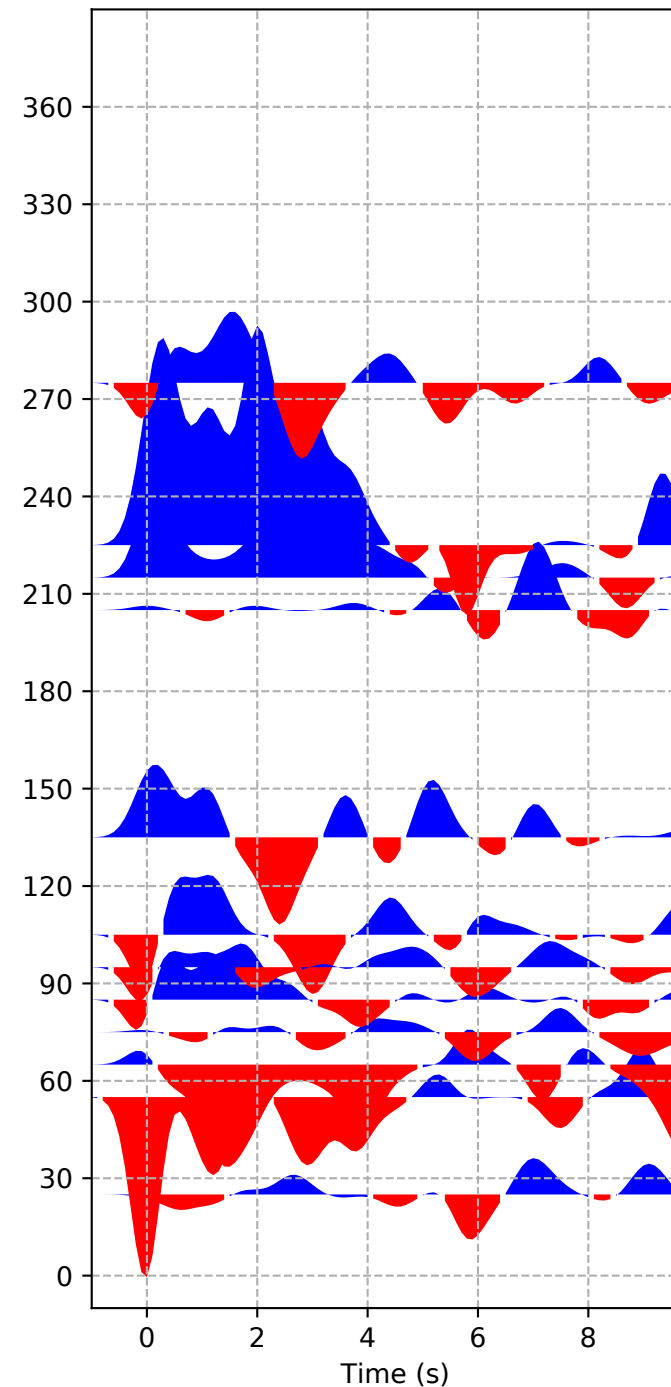


# XV-DGOS

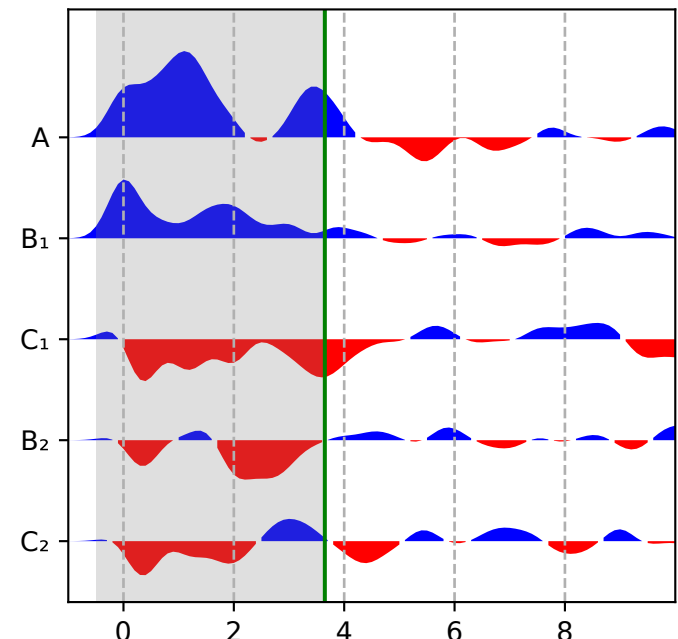
A) Radial



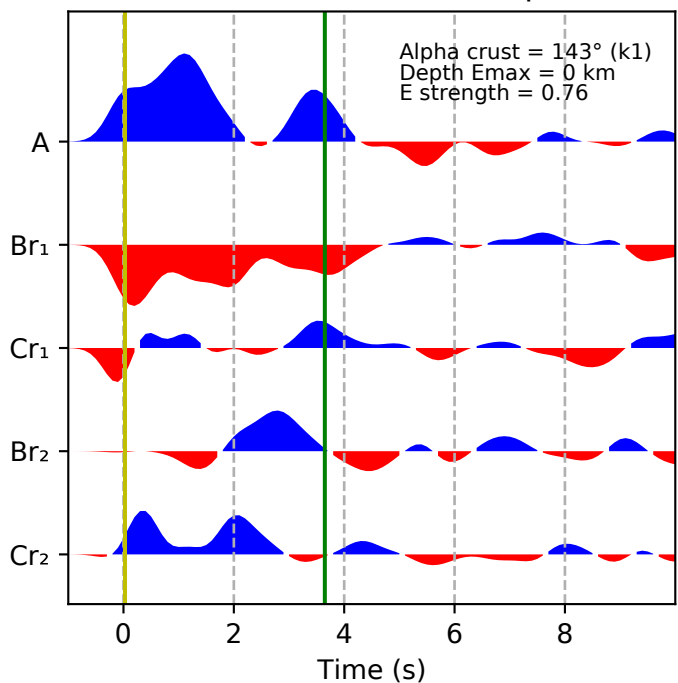
B) Transverse



C) Harmonics components

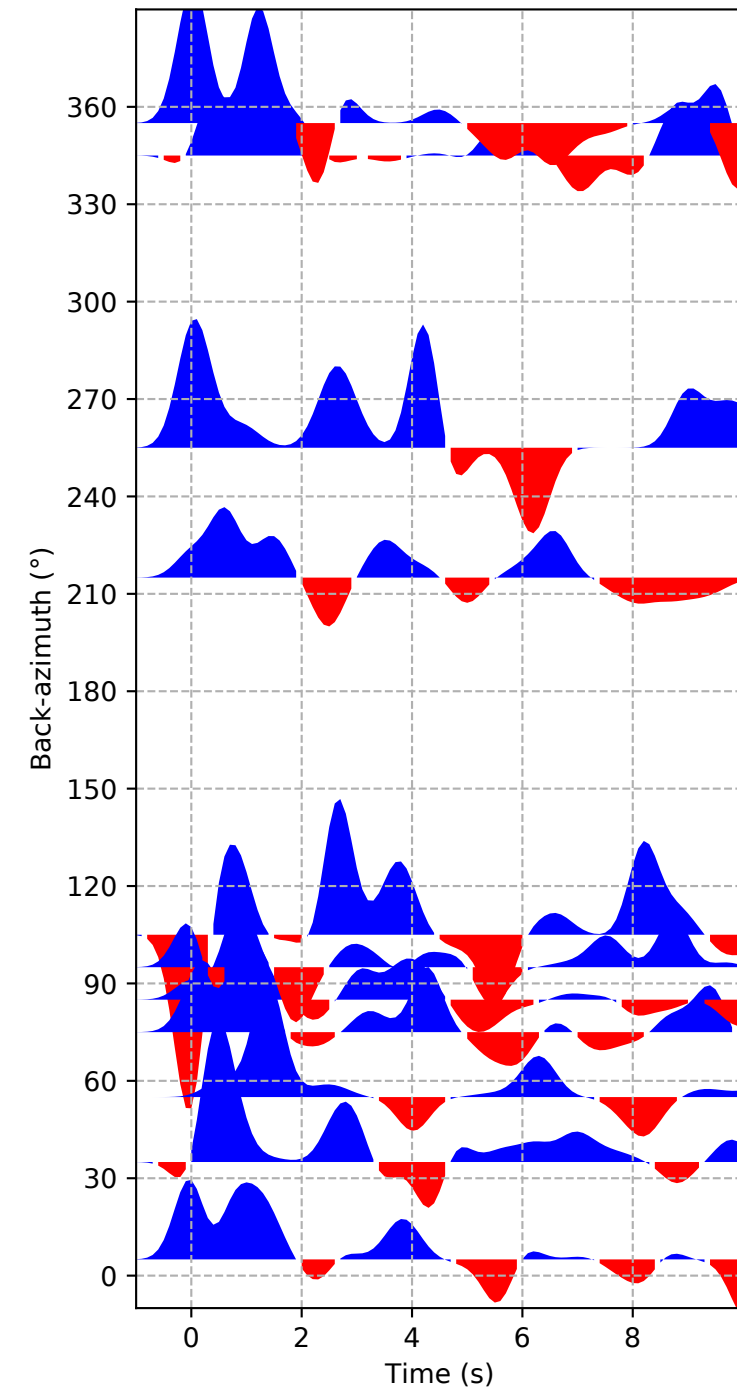


D) Rotated Harmonics components

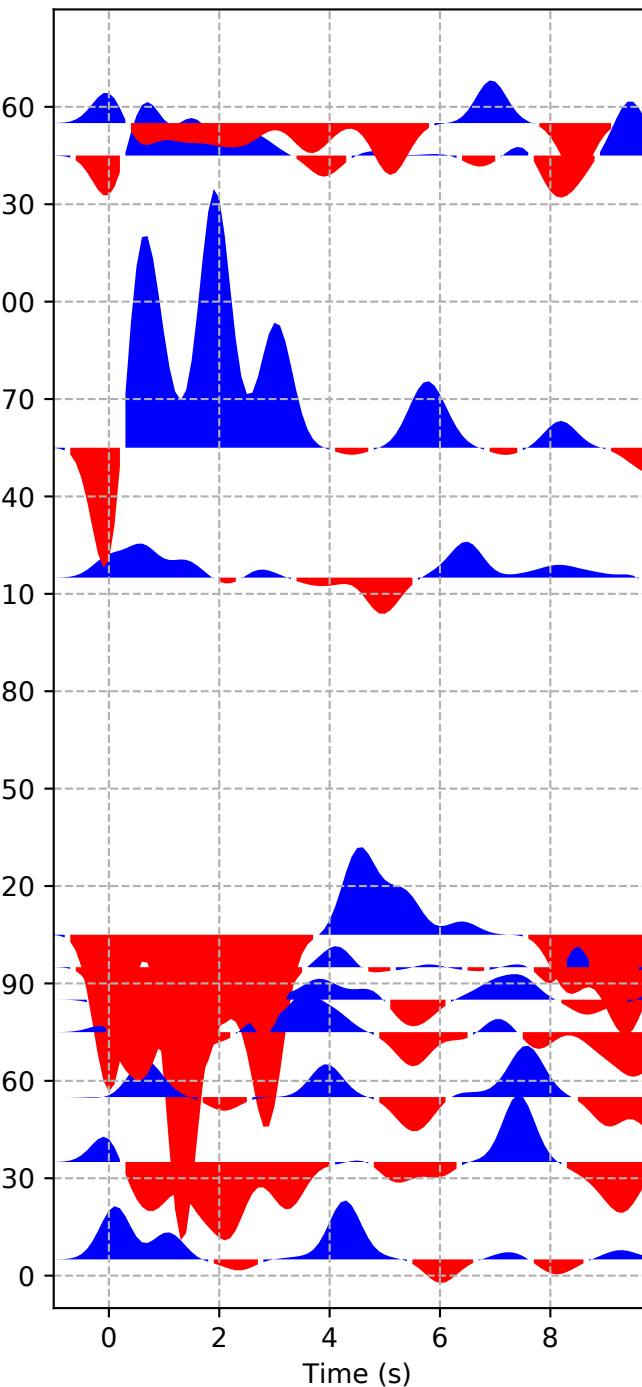


## XV-KIRI

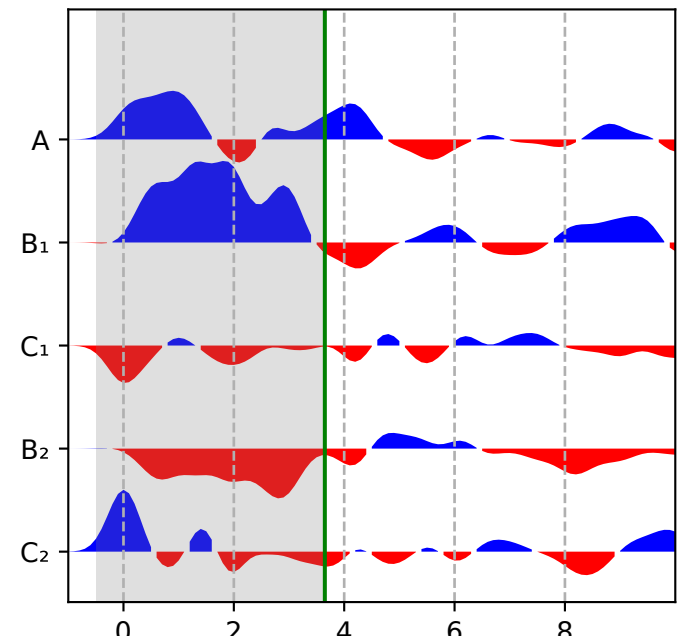
A) Radial



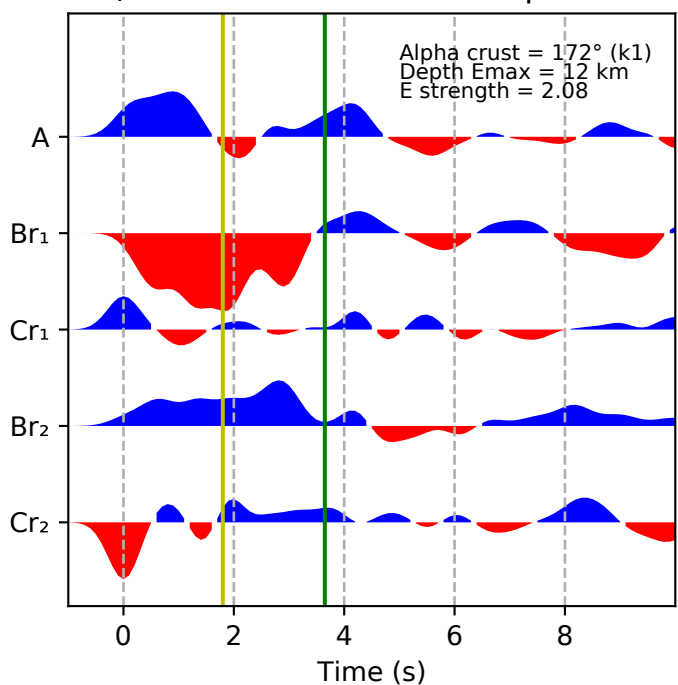
B) Transverse



C) Harmonics components

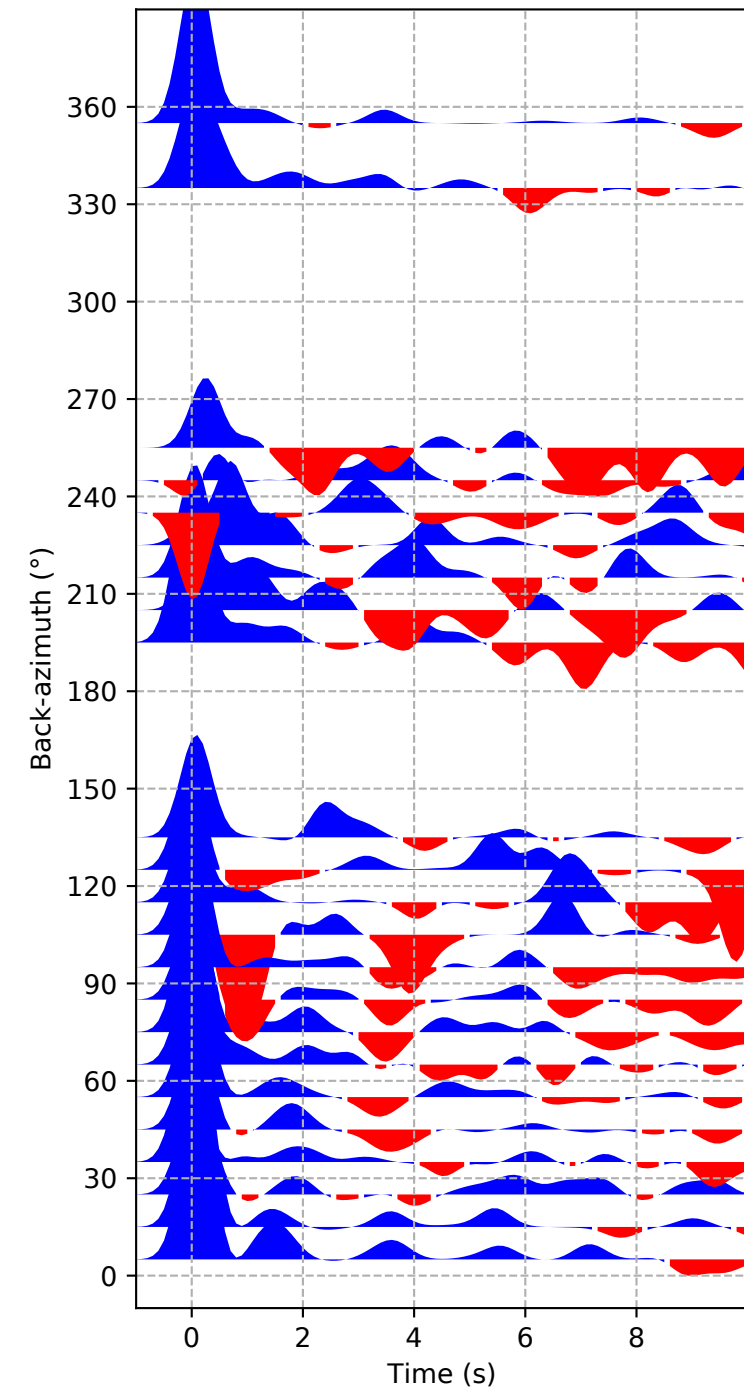


D) Rotated Harmonics components

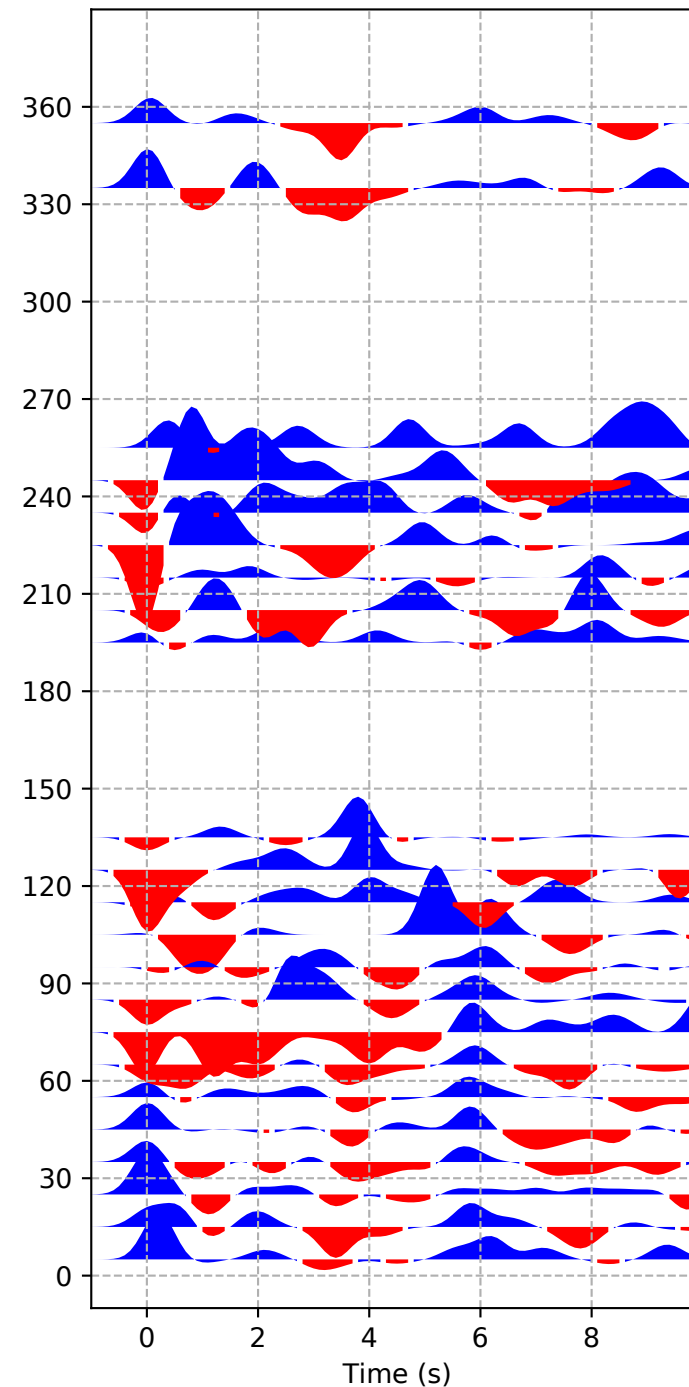


## XV-LAHA

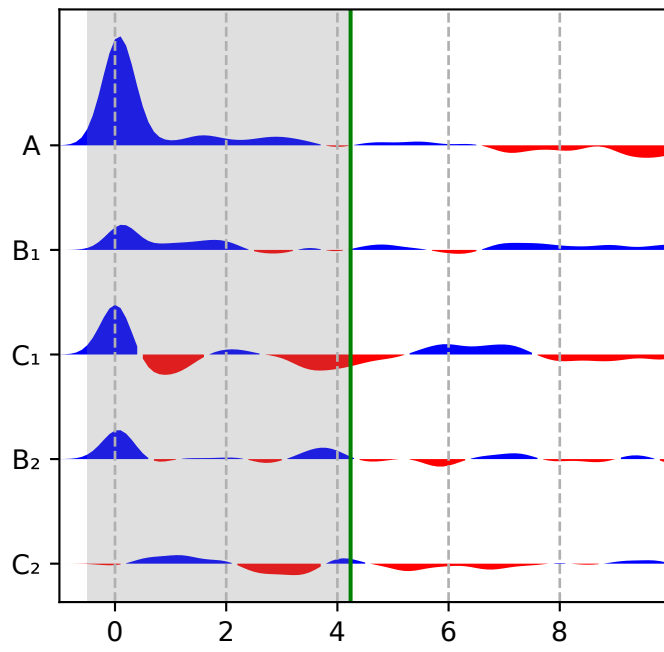
A) Radial



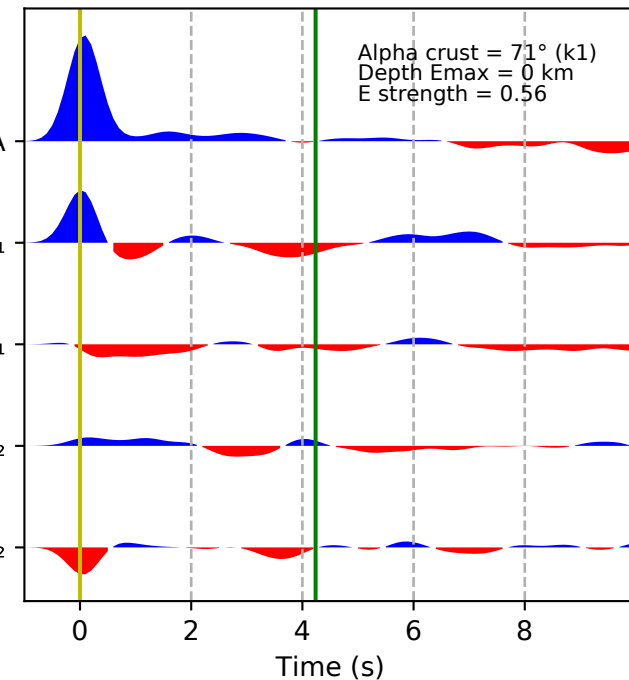
B) Transverse



C) Harmonics components

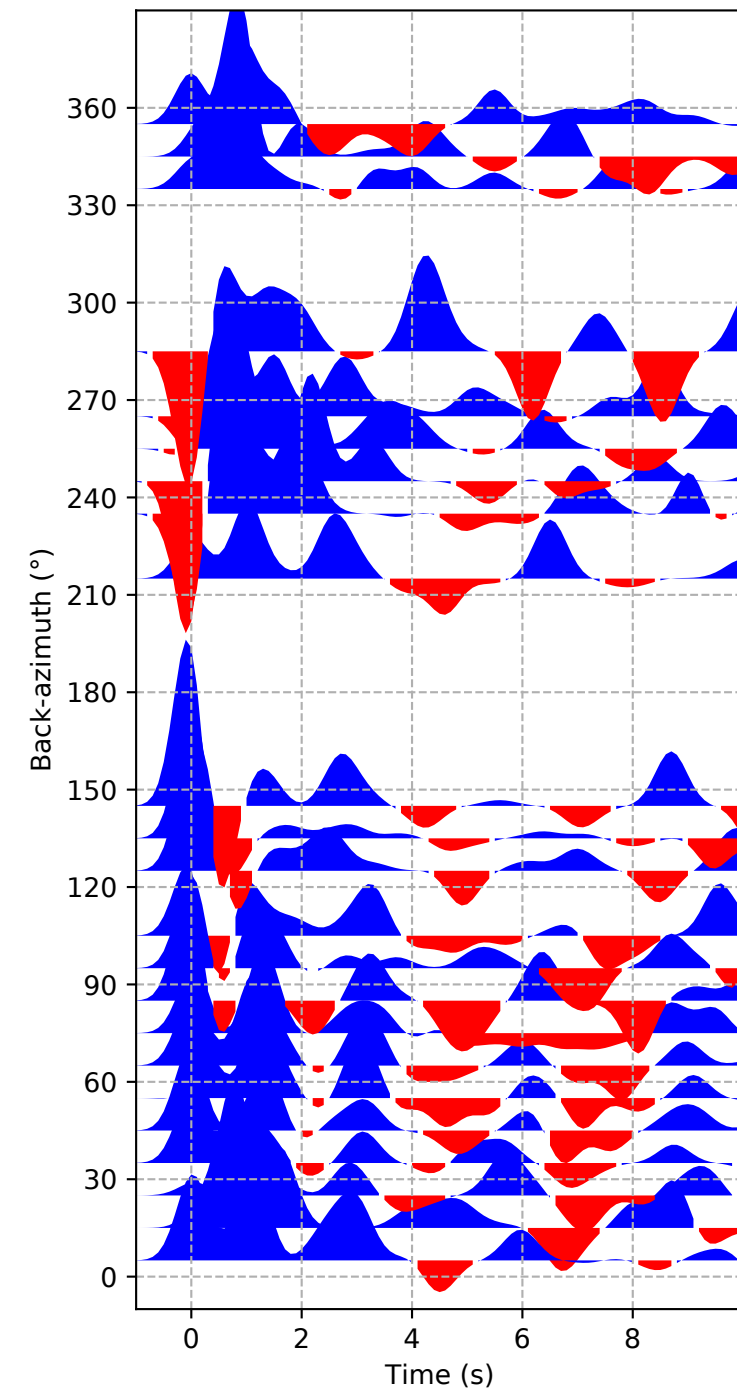


D) Rotated Harmonics components

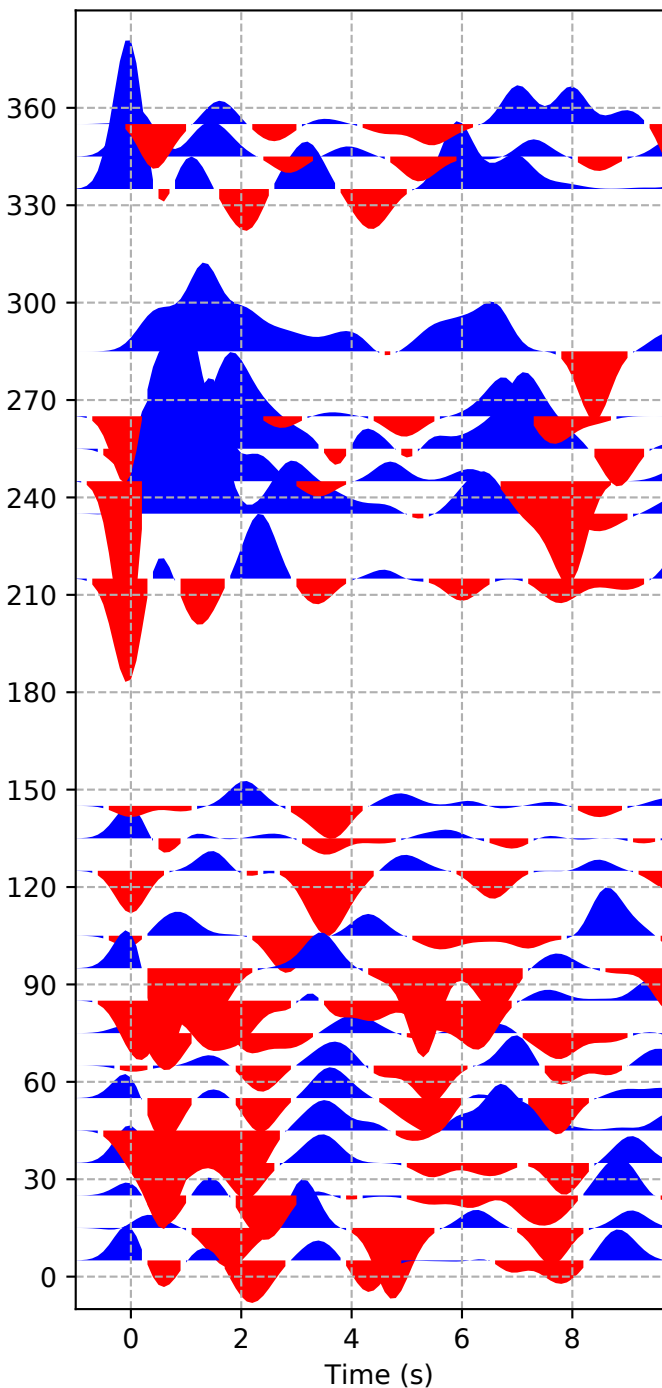


### XV-LONA

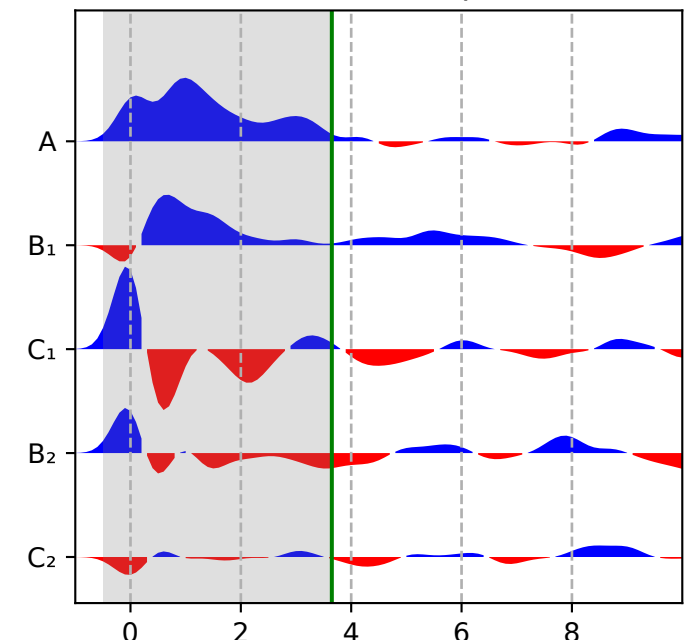
A) Radial



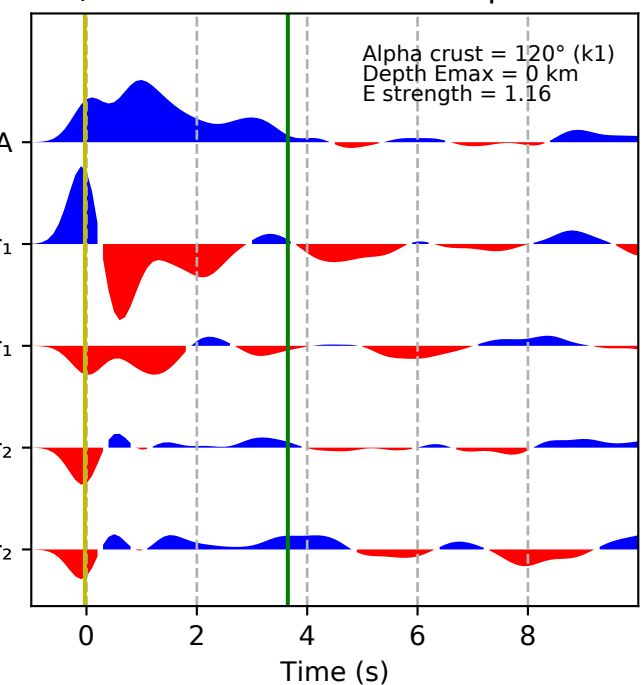
B) Transverse



C) Harmonics components

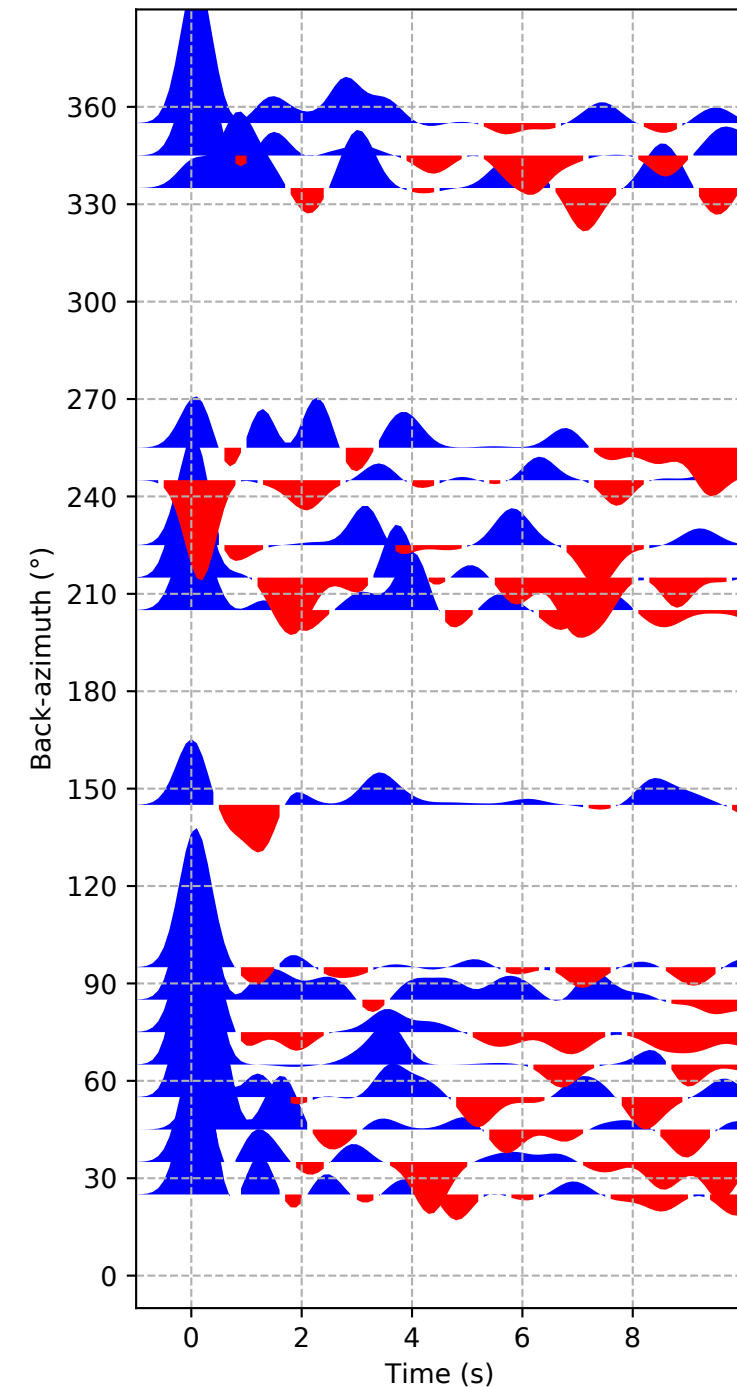


D) Rotated Harmonics components

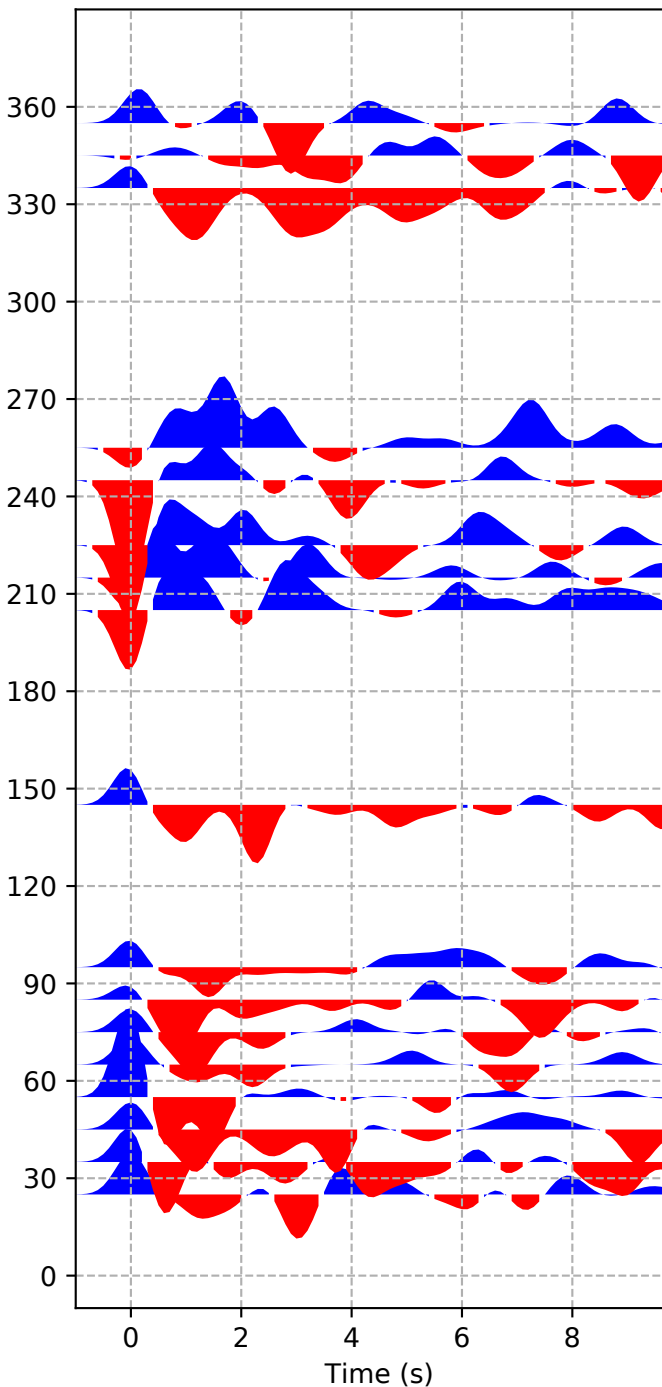


# XV-MAGY

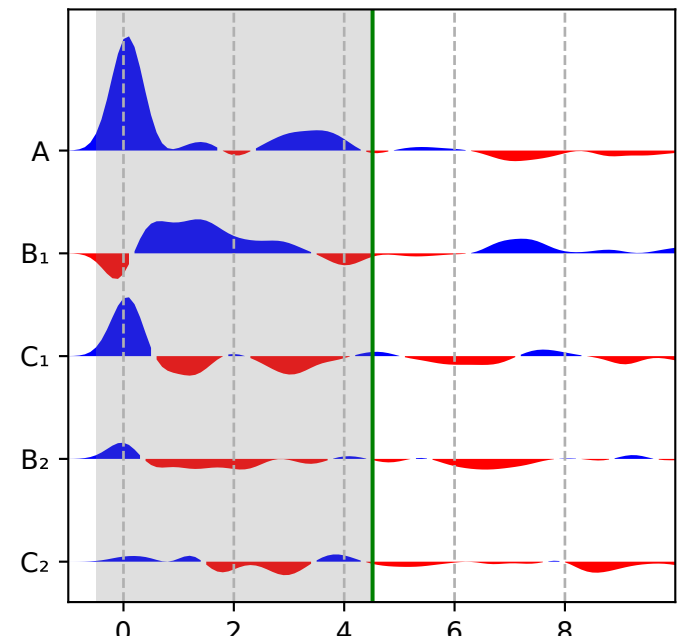
A) Radial



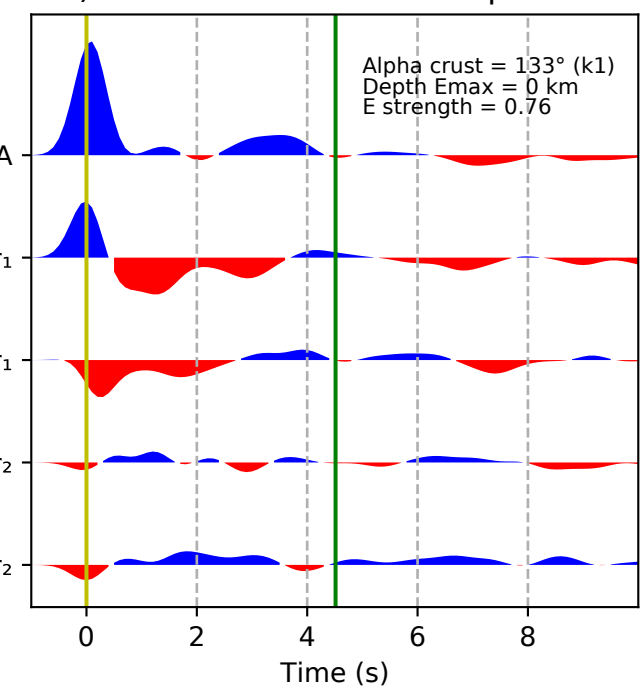
B) Transverse



C) Harmonics components

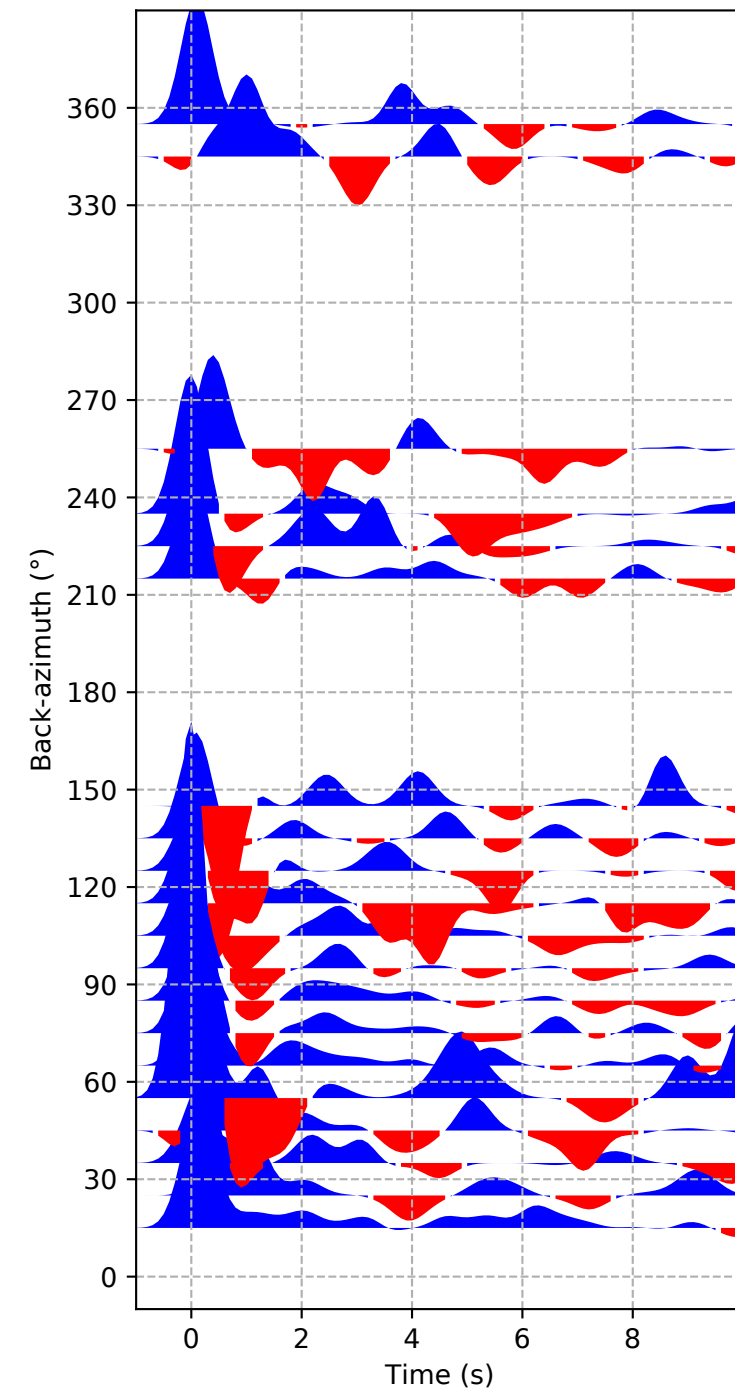


D) Rotated Harmonics components

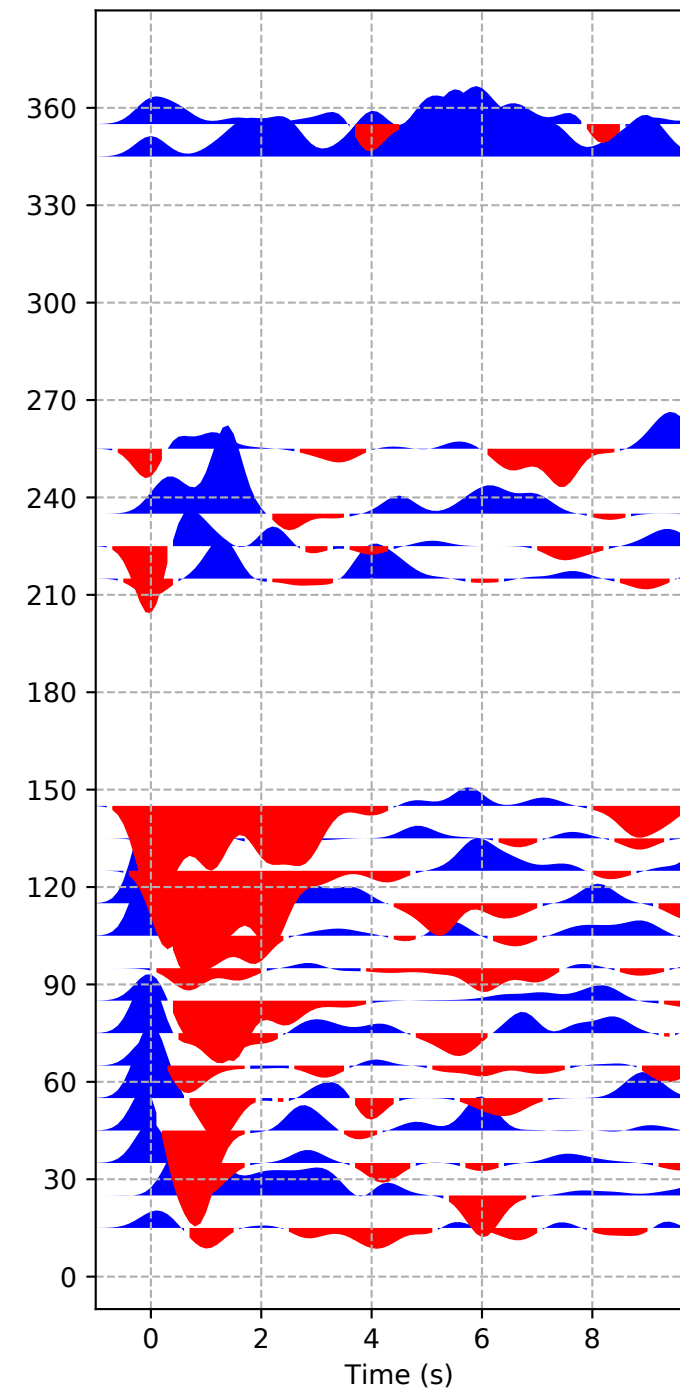


# XV-MAHA

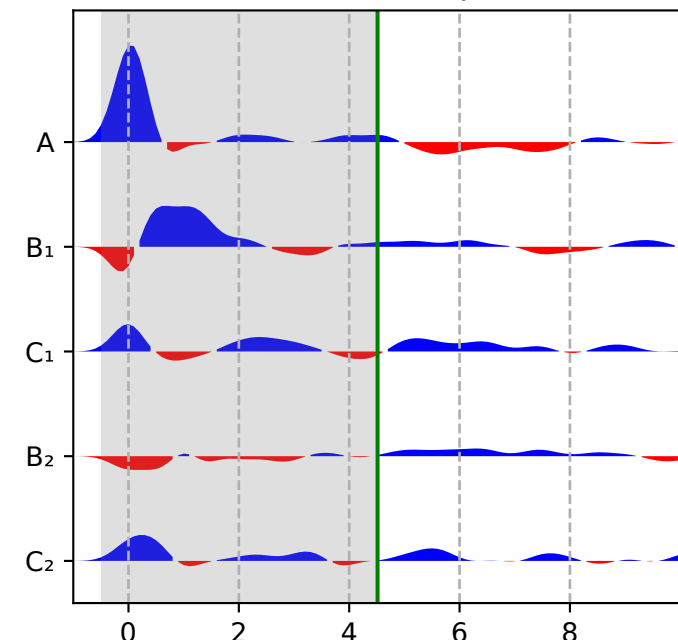
A) Radial



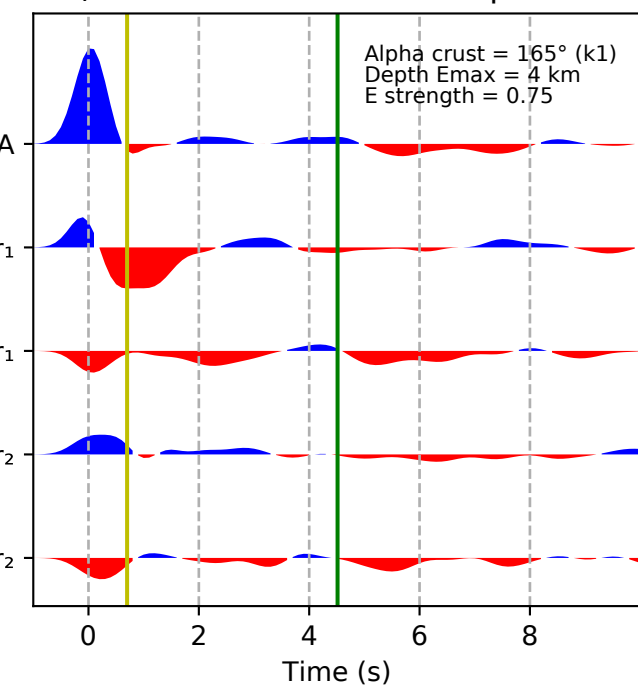
B) Transverse



C) Harmonics components

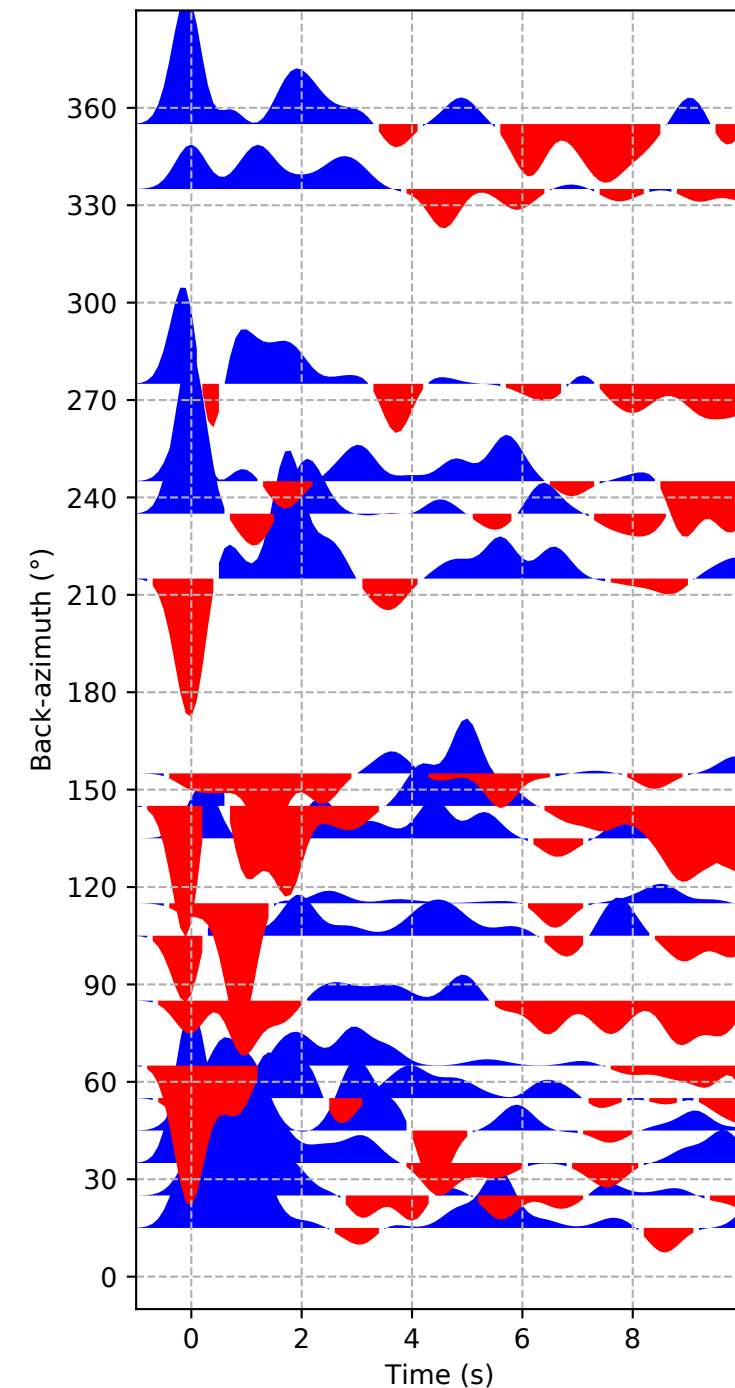


D) Rotated Harmonics components

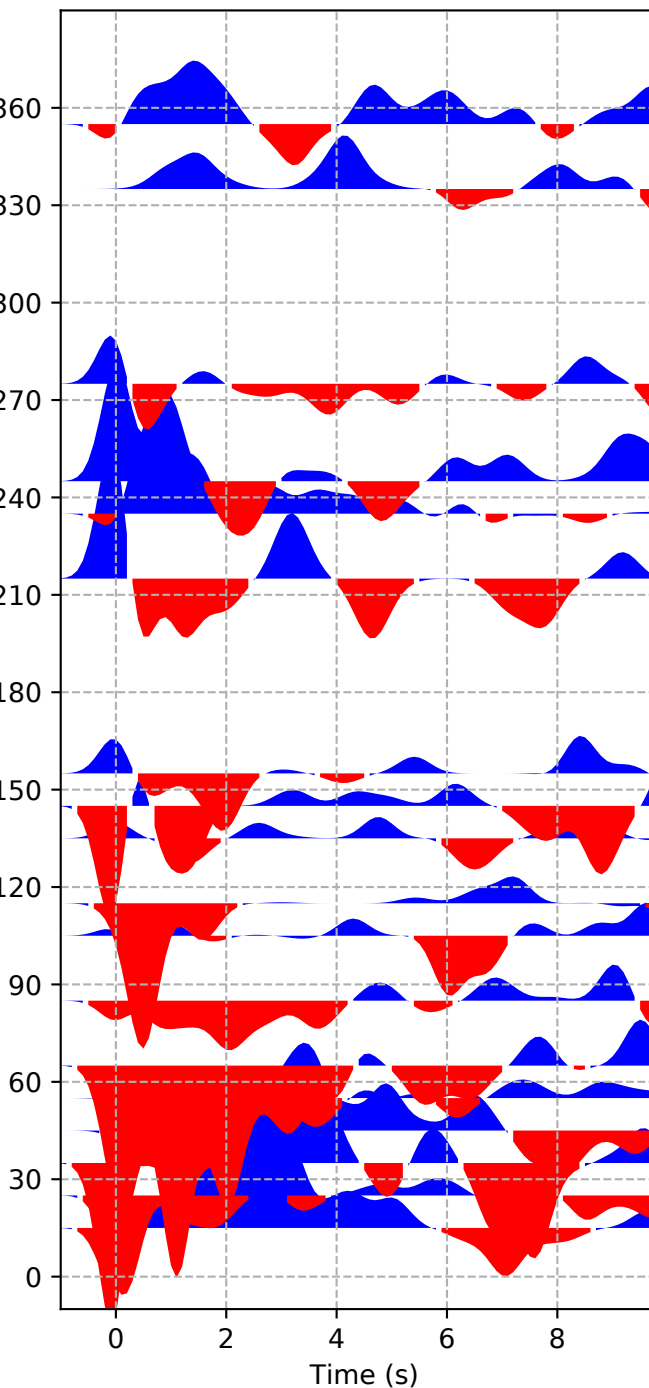


## XV-MAJA

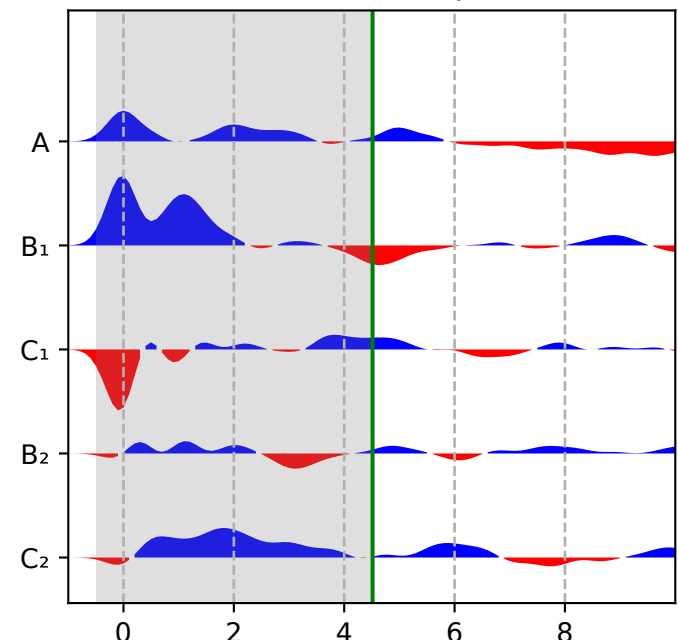
A) Radial



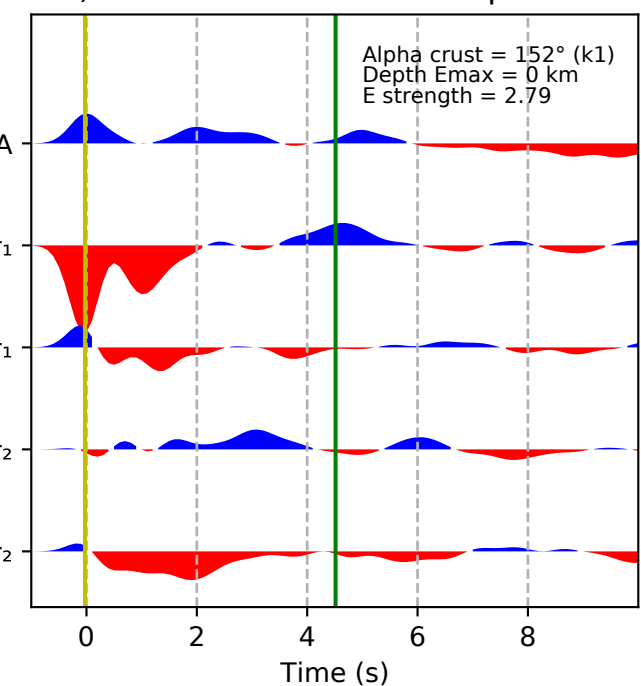
B) Transverse



C) Harmonics components

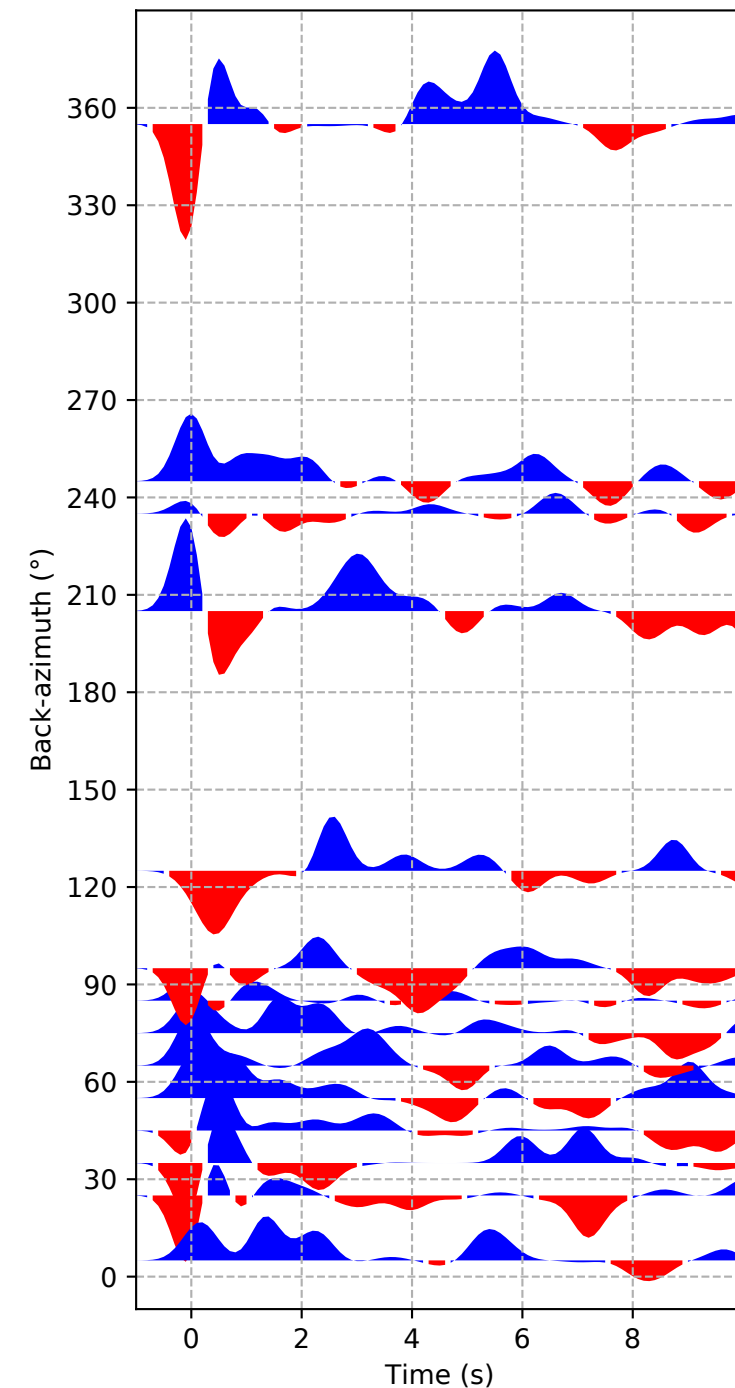


D) Rotated Harmonics components

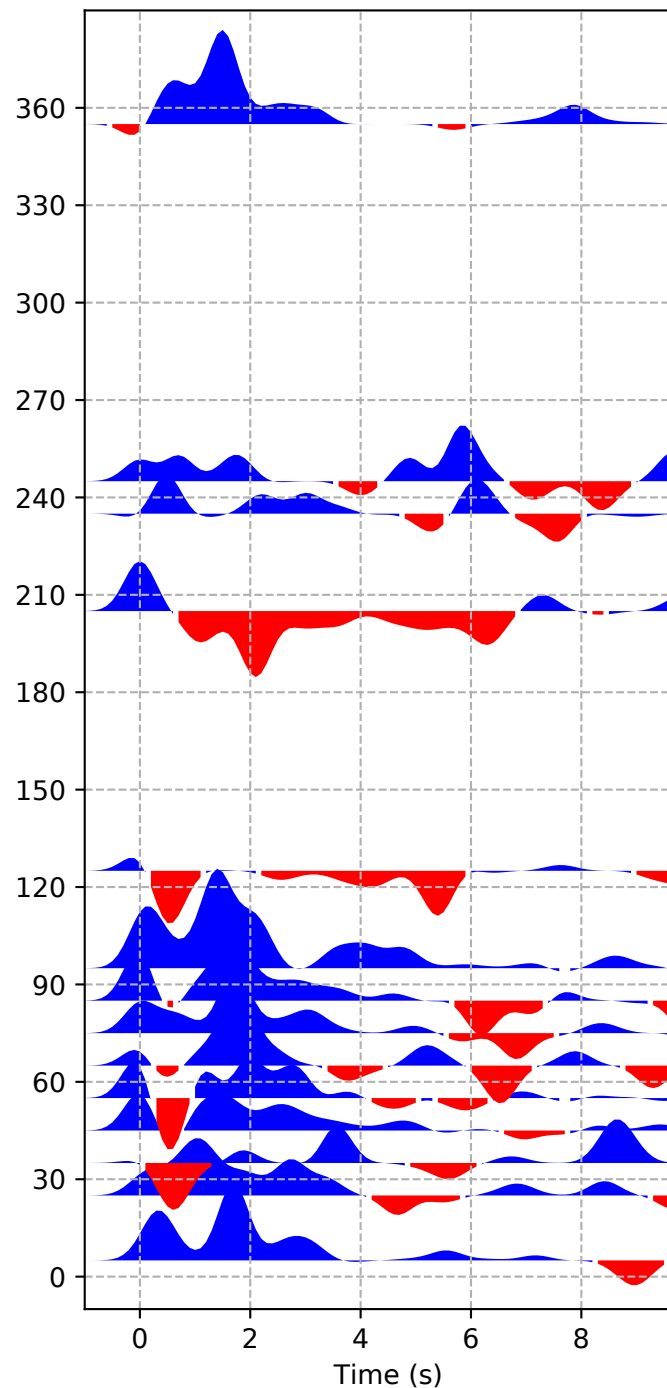


# XV-MAPH

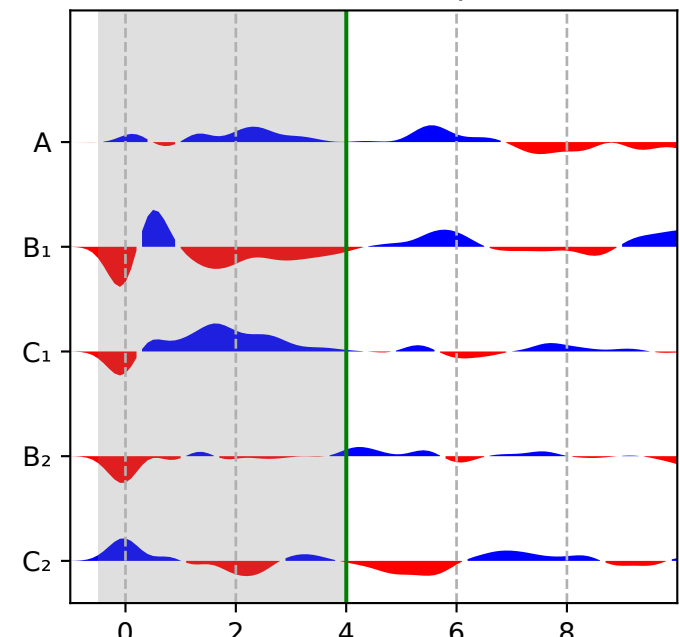
A) Radial



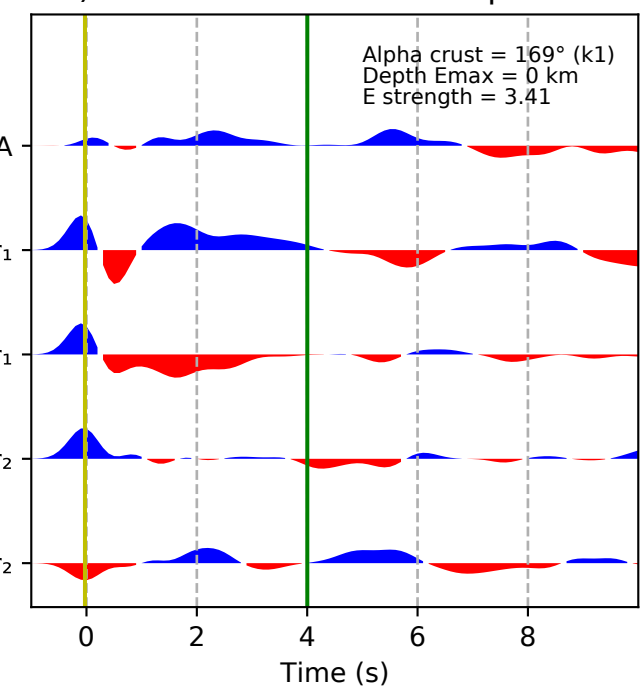
B) Transverse



C) Harmonics components

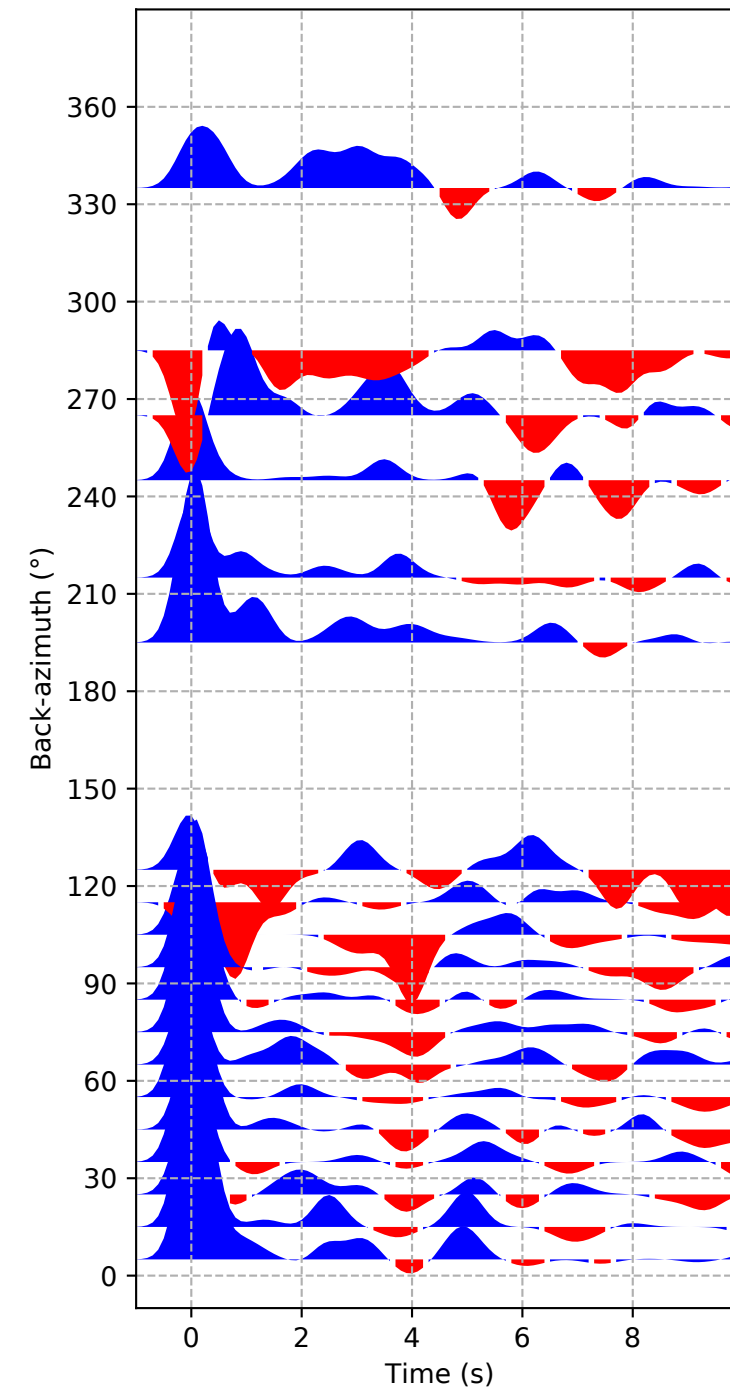


D) Rotated Harmonics components

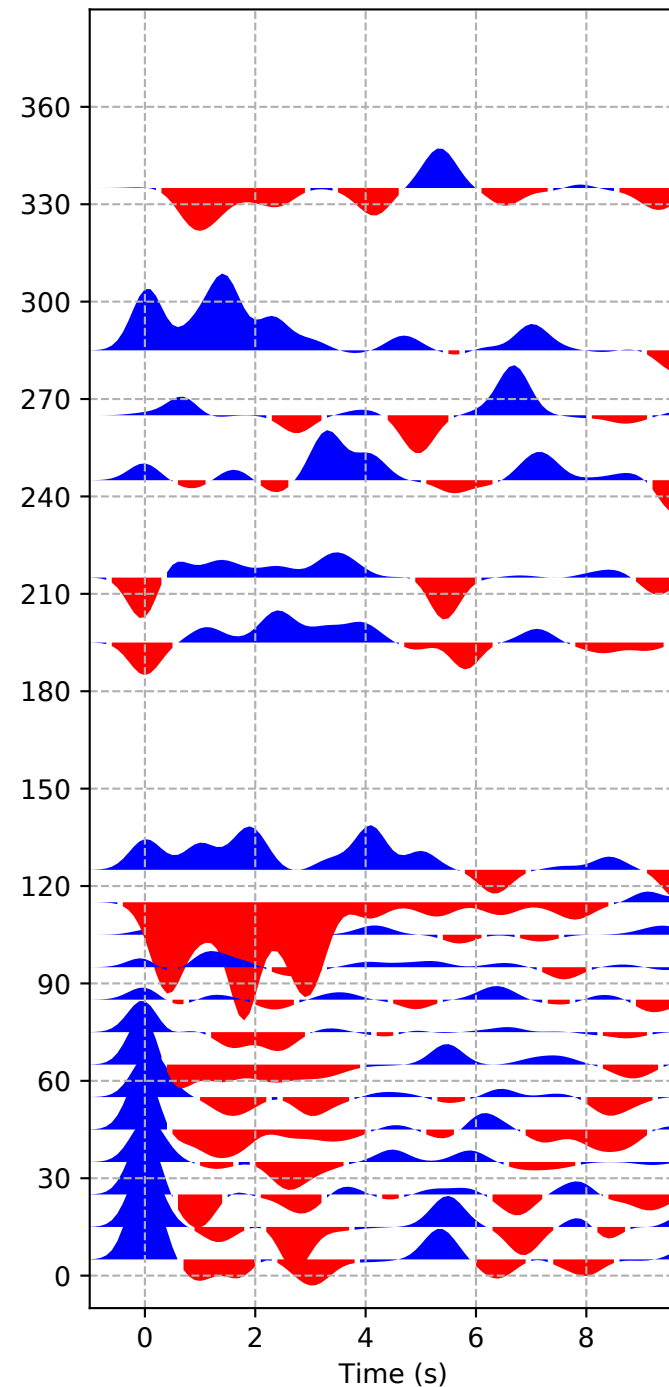


# XV-MKVA

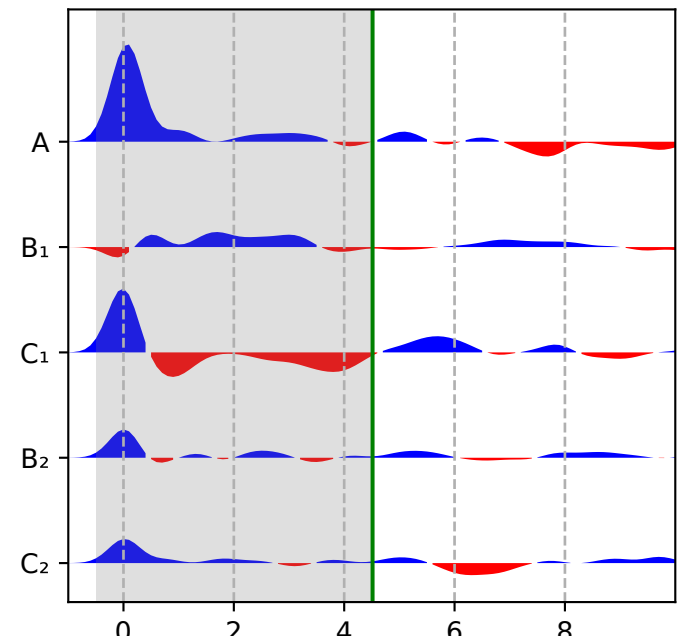
A) Radial



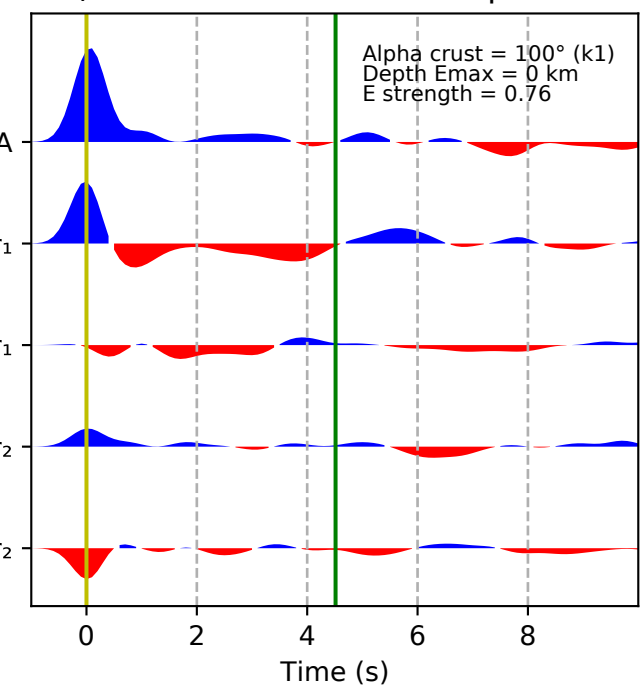
B) Transverse



C) Harmonics components

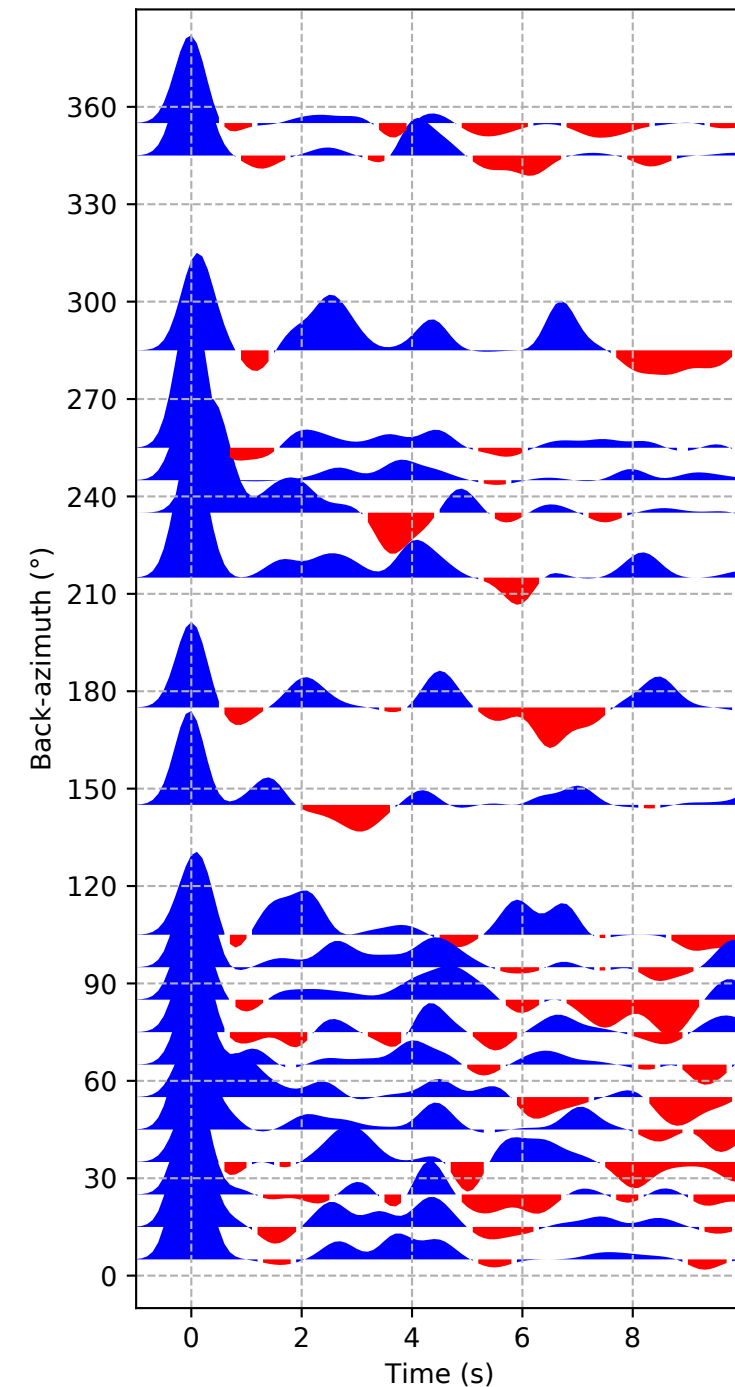


D) Rotated Harmonics components

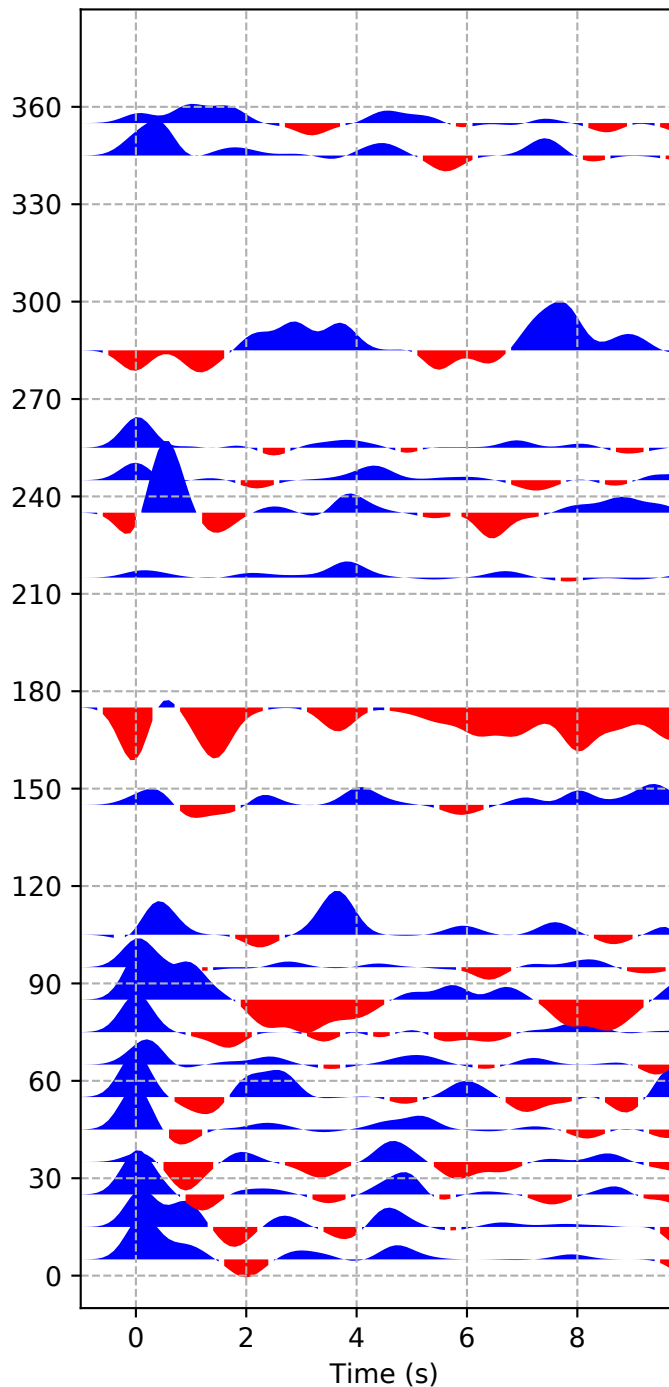


# XV-MOCU

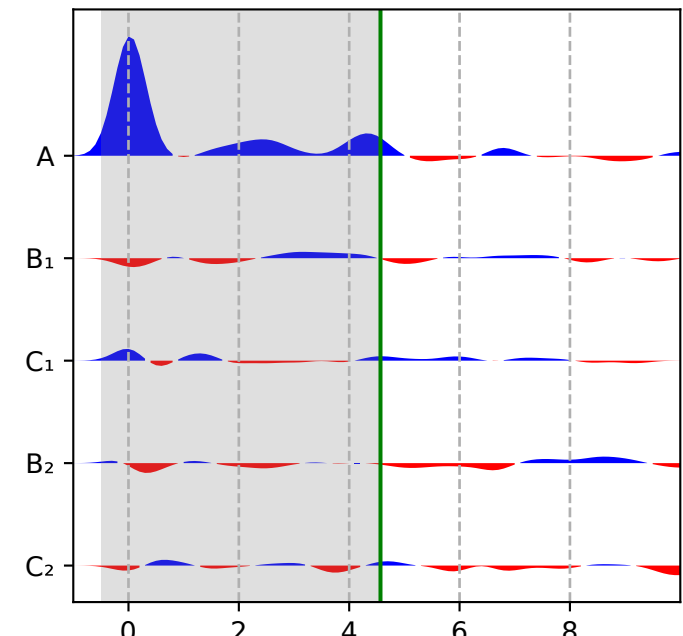
A) Radial



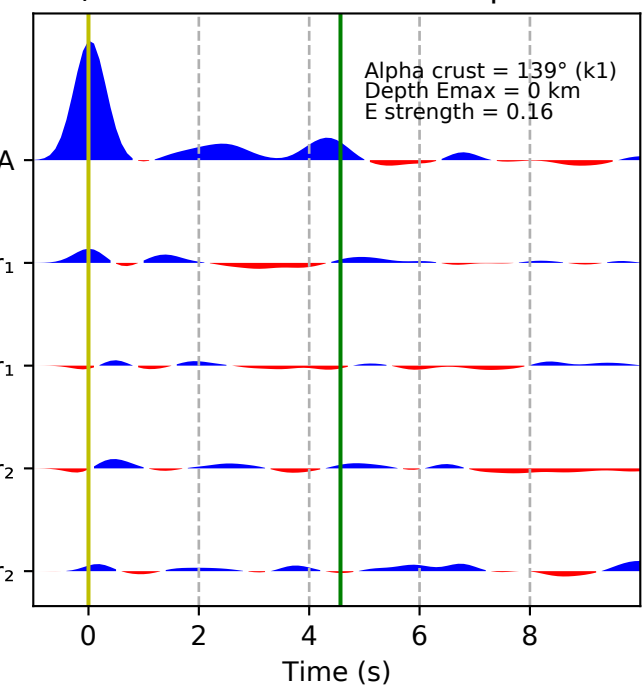
B) Transverse



C) Harmonics components

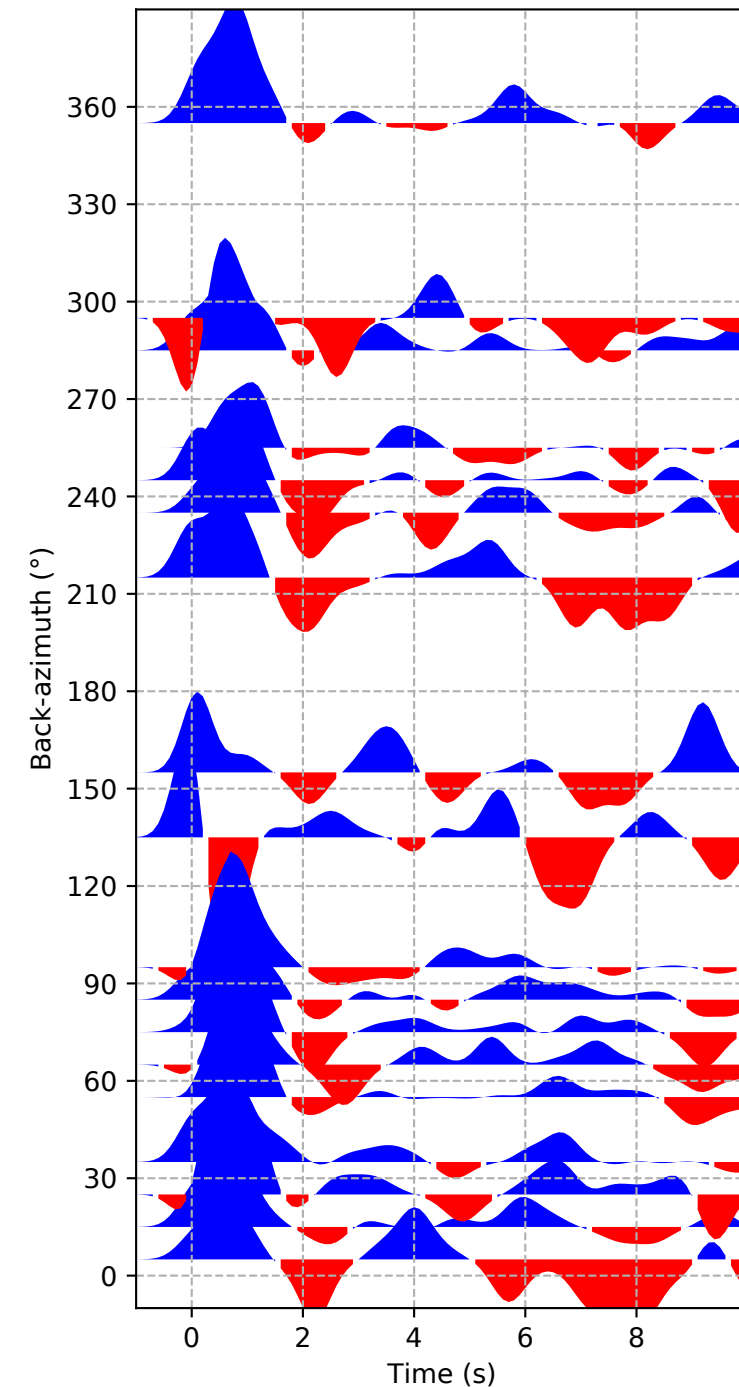


D) Rotated Harmonics components

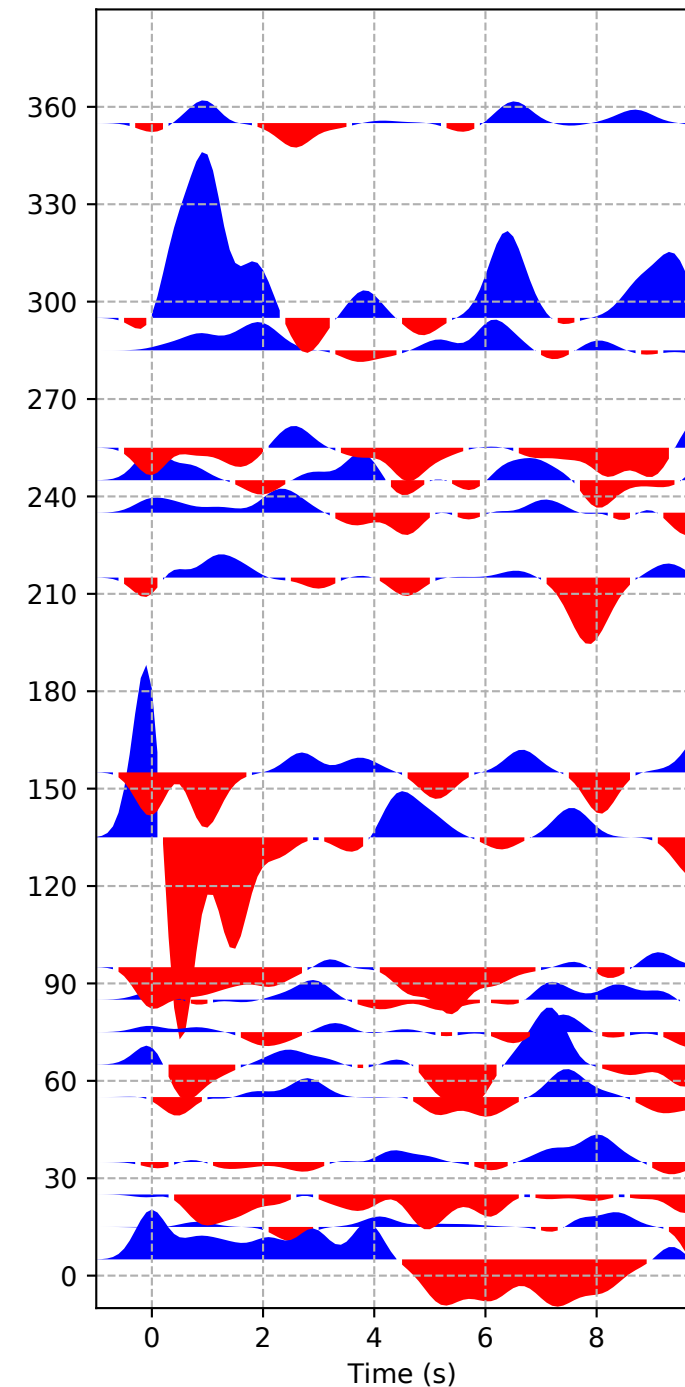


# XV-MSG

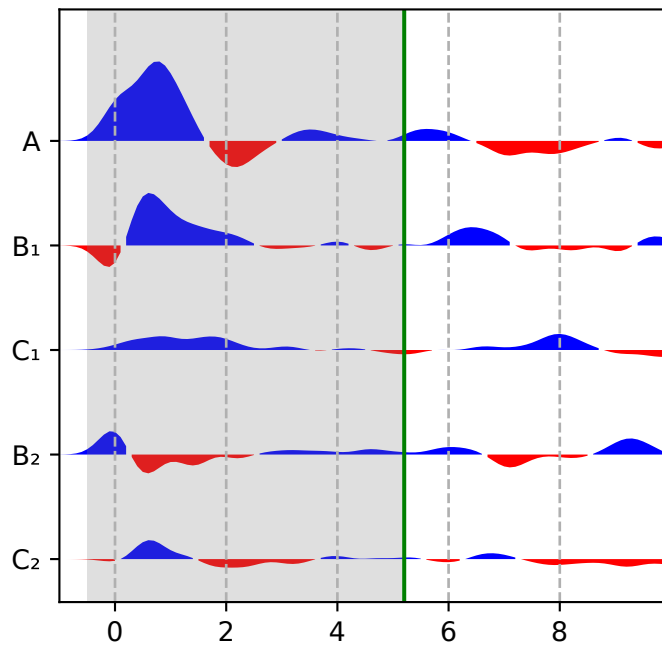
A) Radial



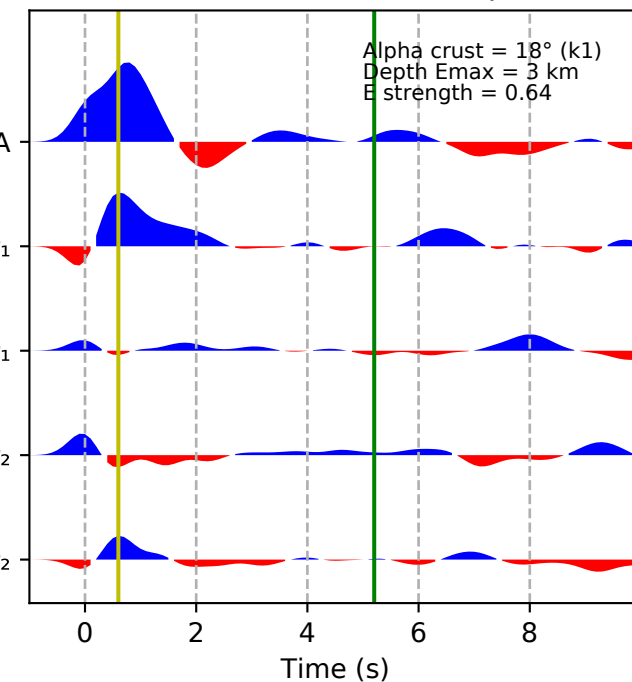
B) Transverse



C) Harmonics components

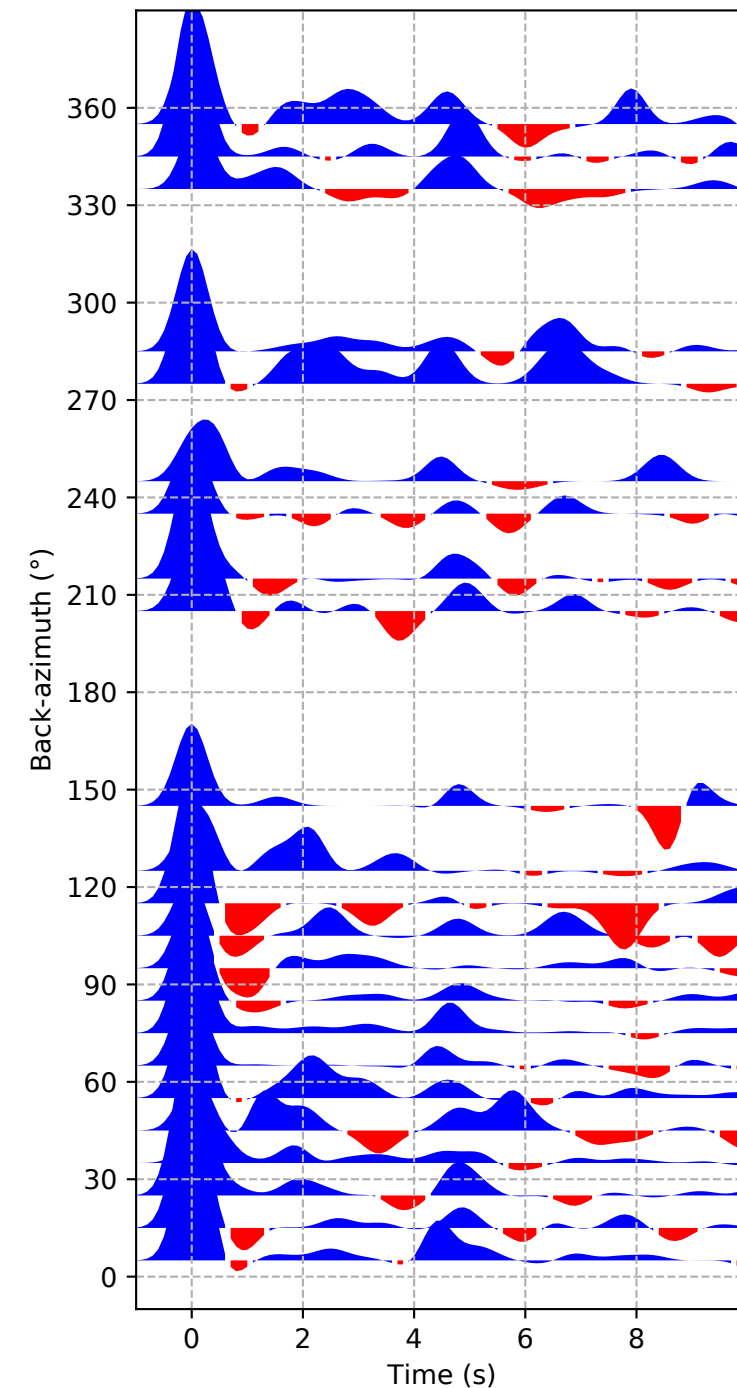


D) Rotated Harmonics components

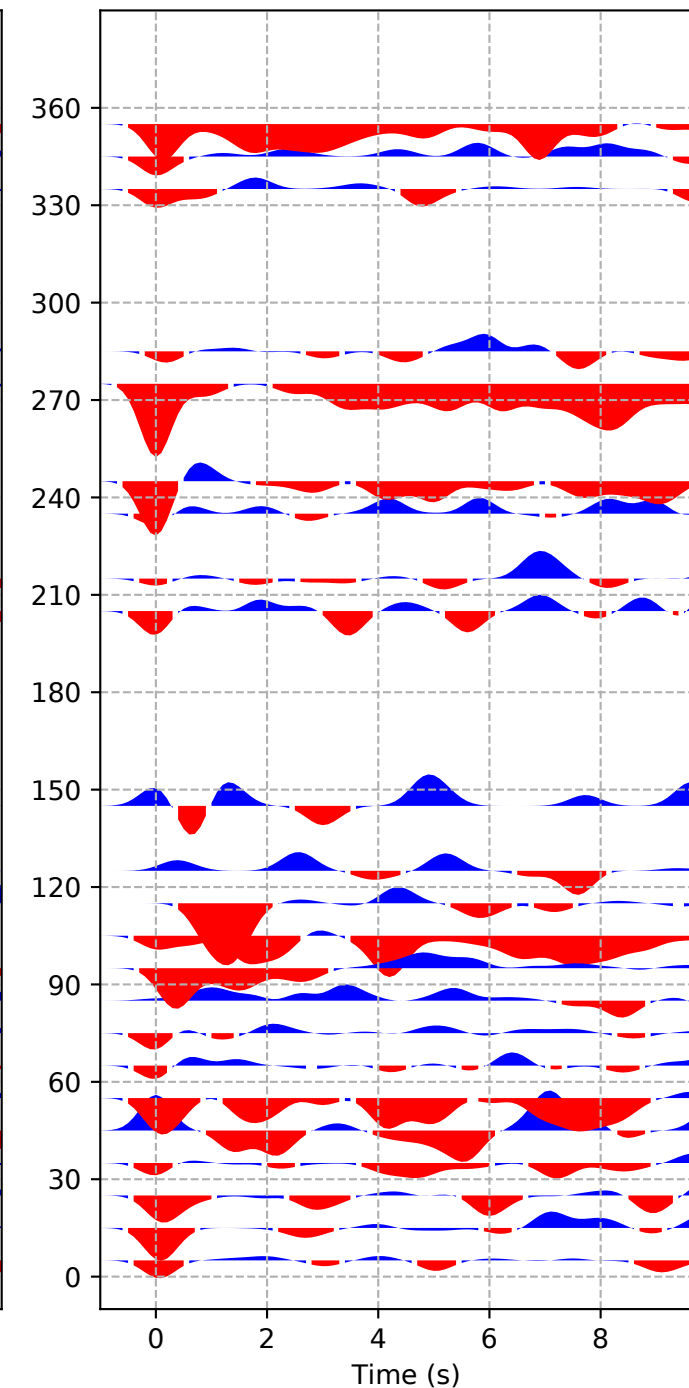


# XV-NAPU

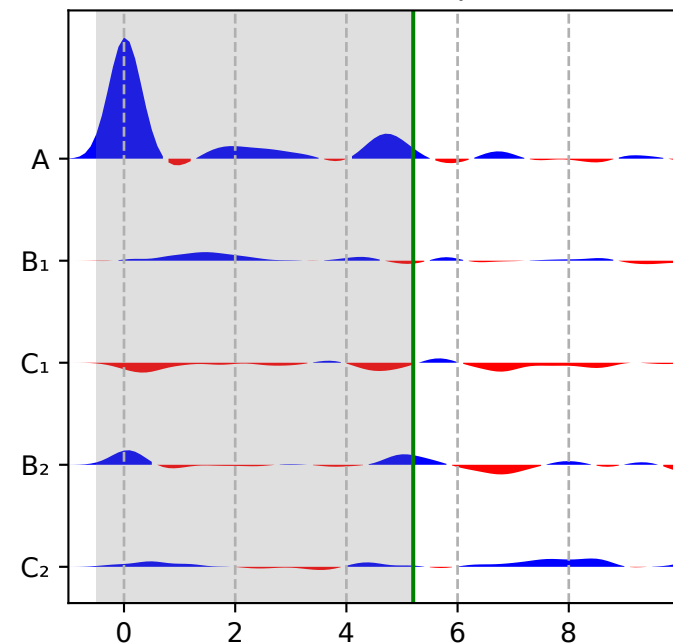
A) Radial



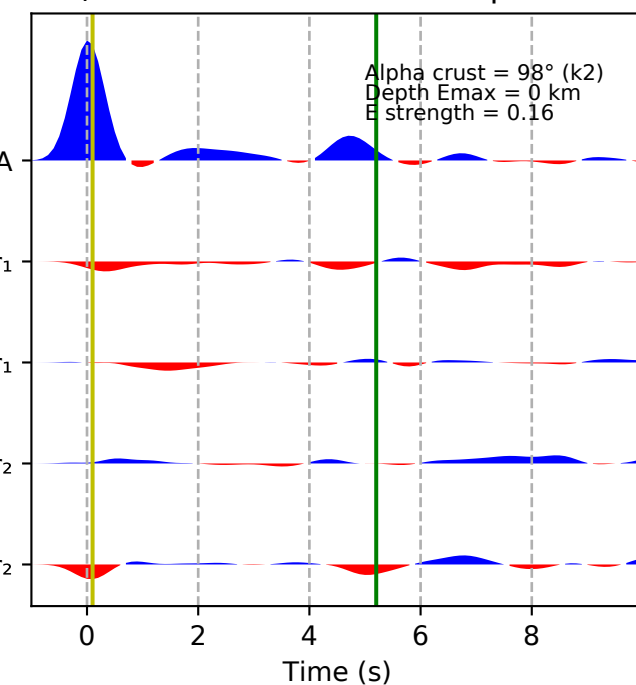
B) Transverse



C) Harmonics components

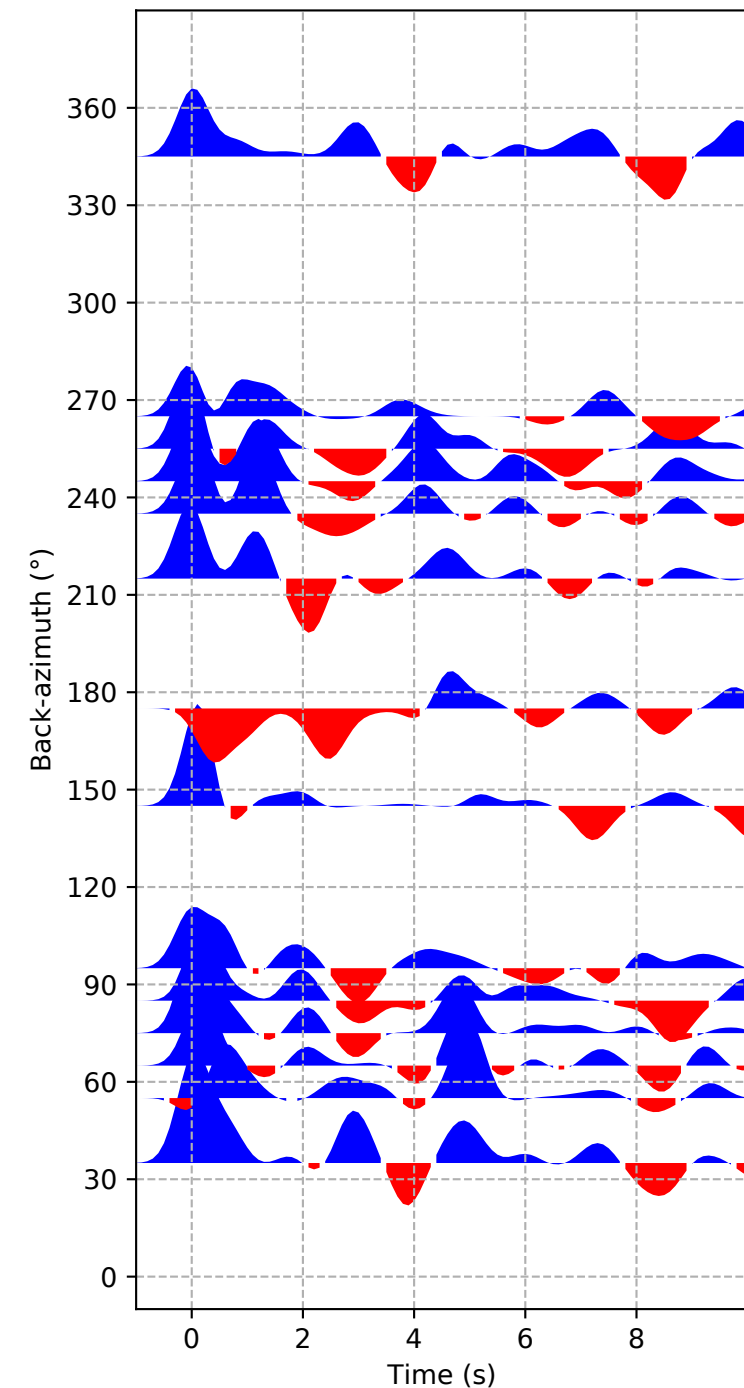


D) Rotated Harmonics components

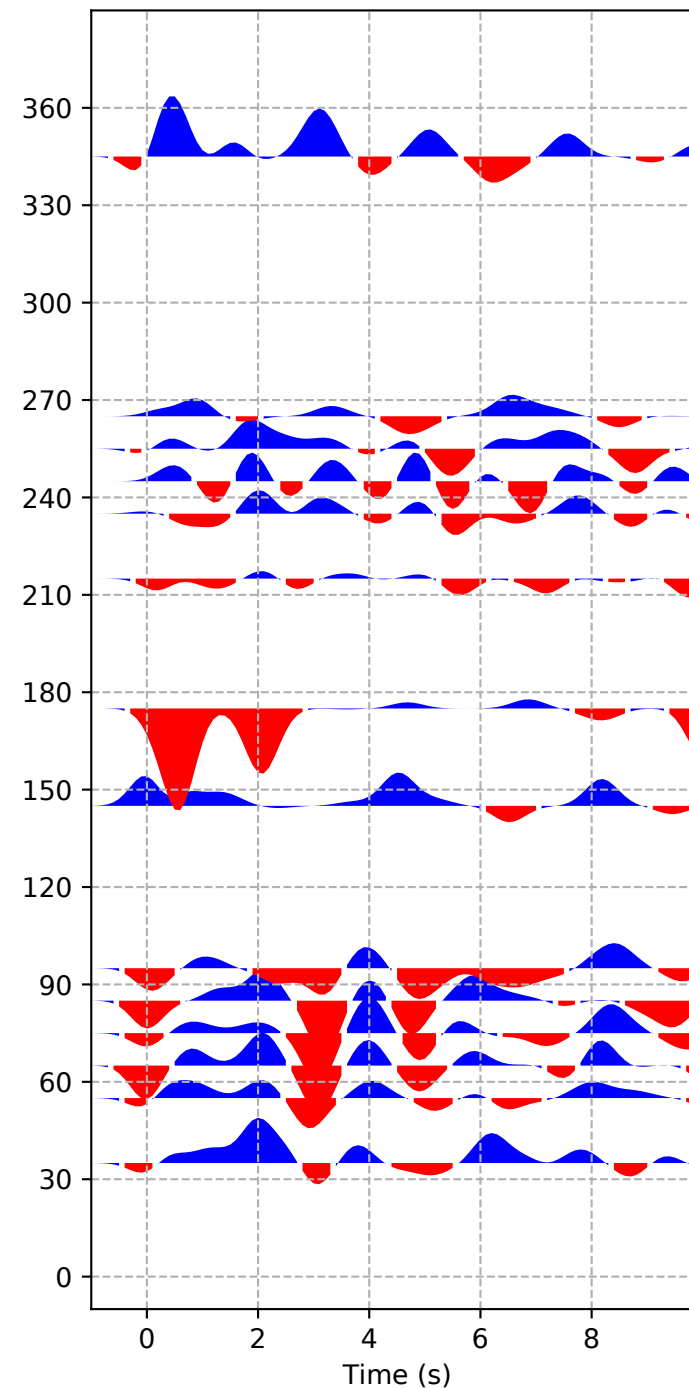


## XV-TETE

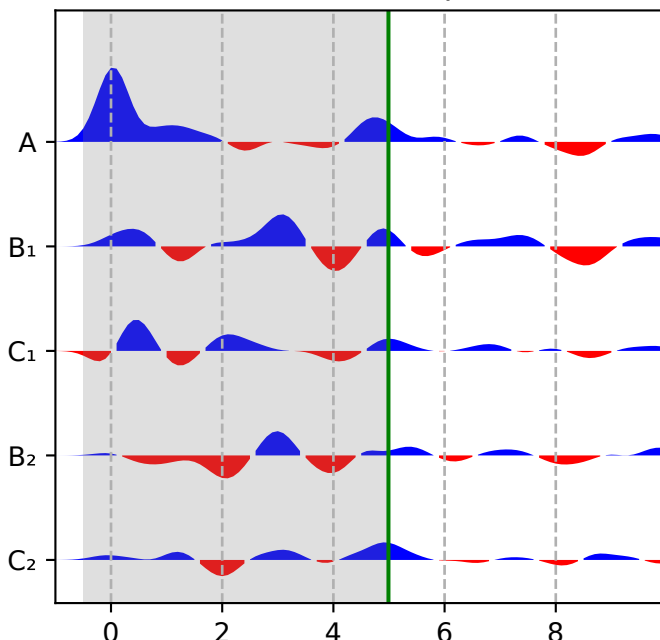
A) Radial



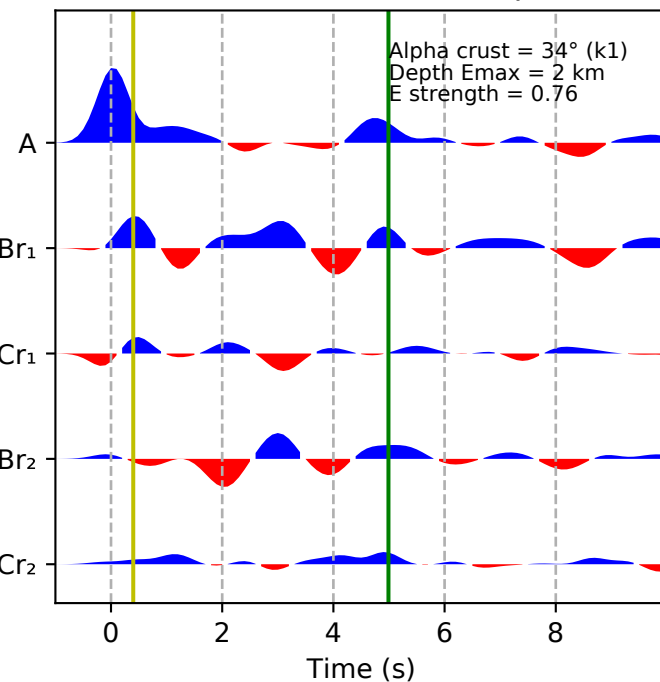
B) Transverse



C) Harmonics components

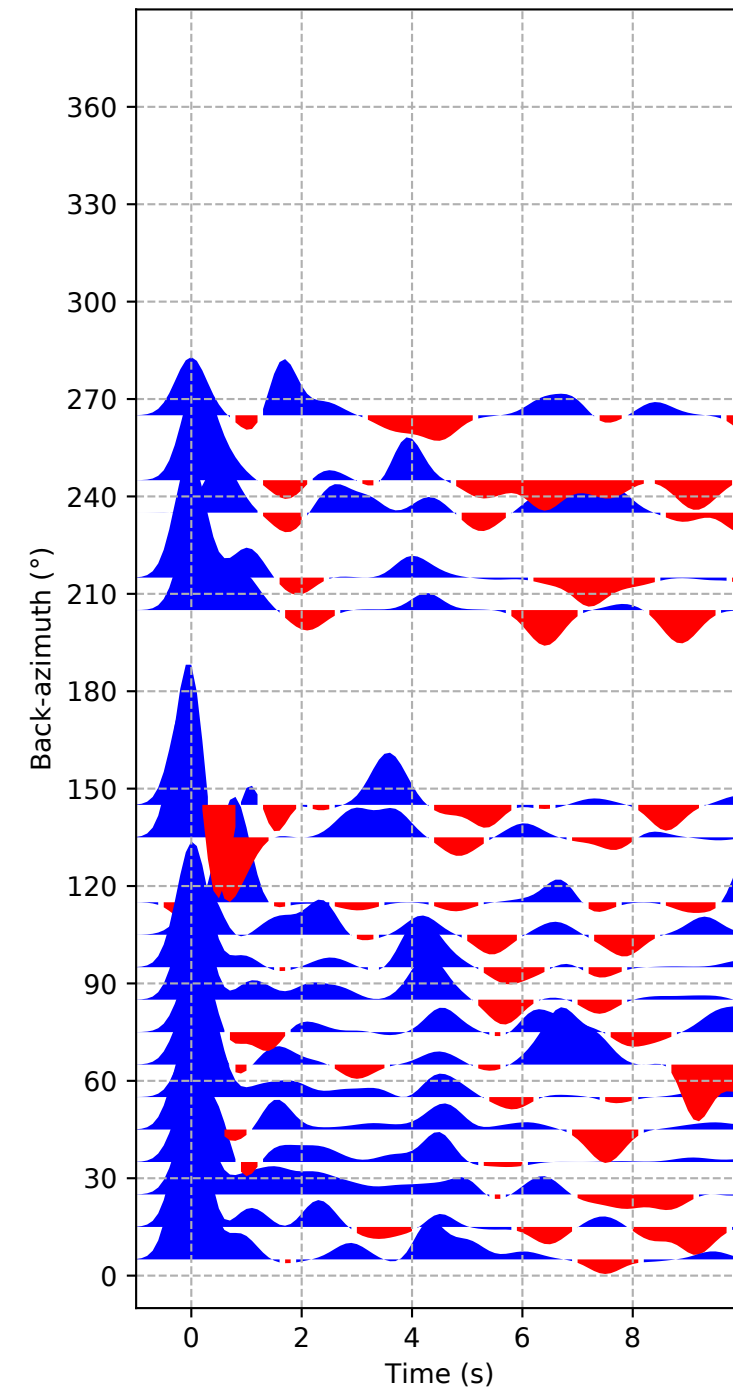


D) Rotated Harmonics components

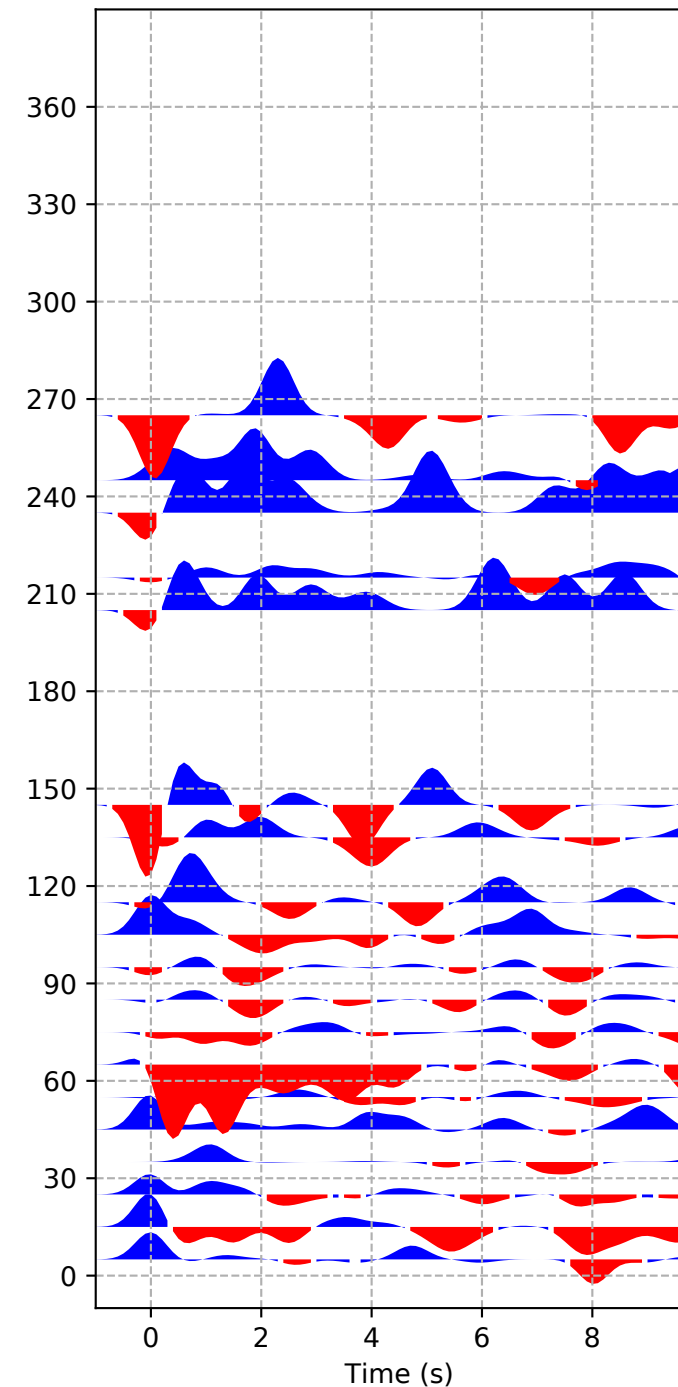


## XV-VINA

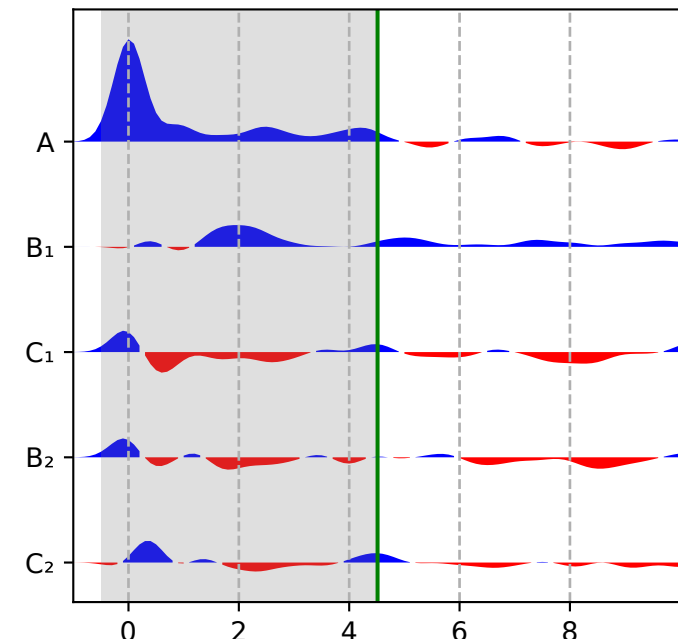
A) Radial



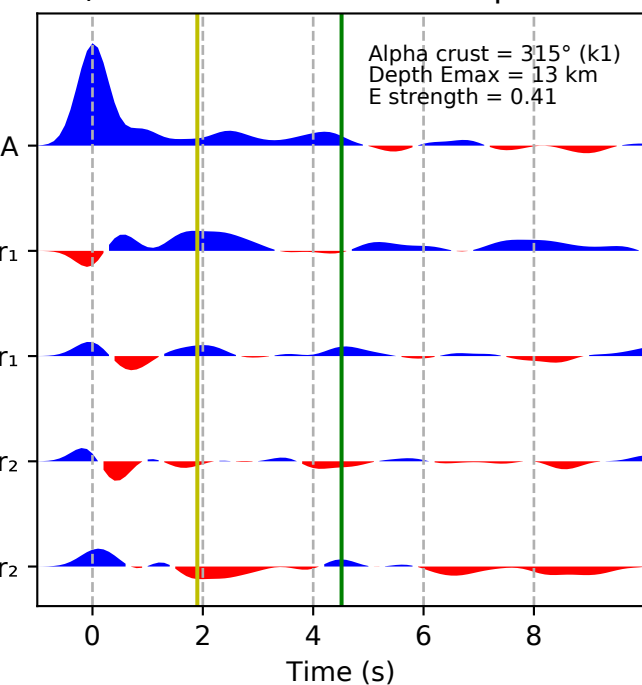
B) Transverse



C) Harmonics components

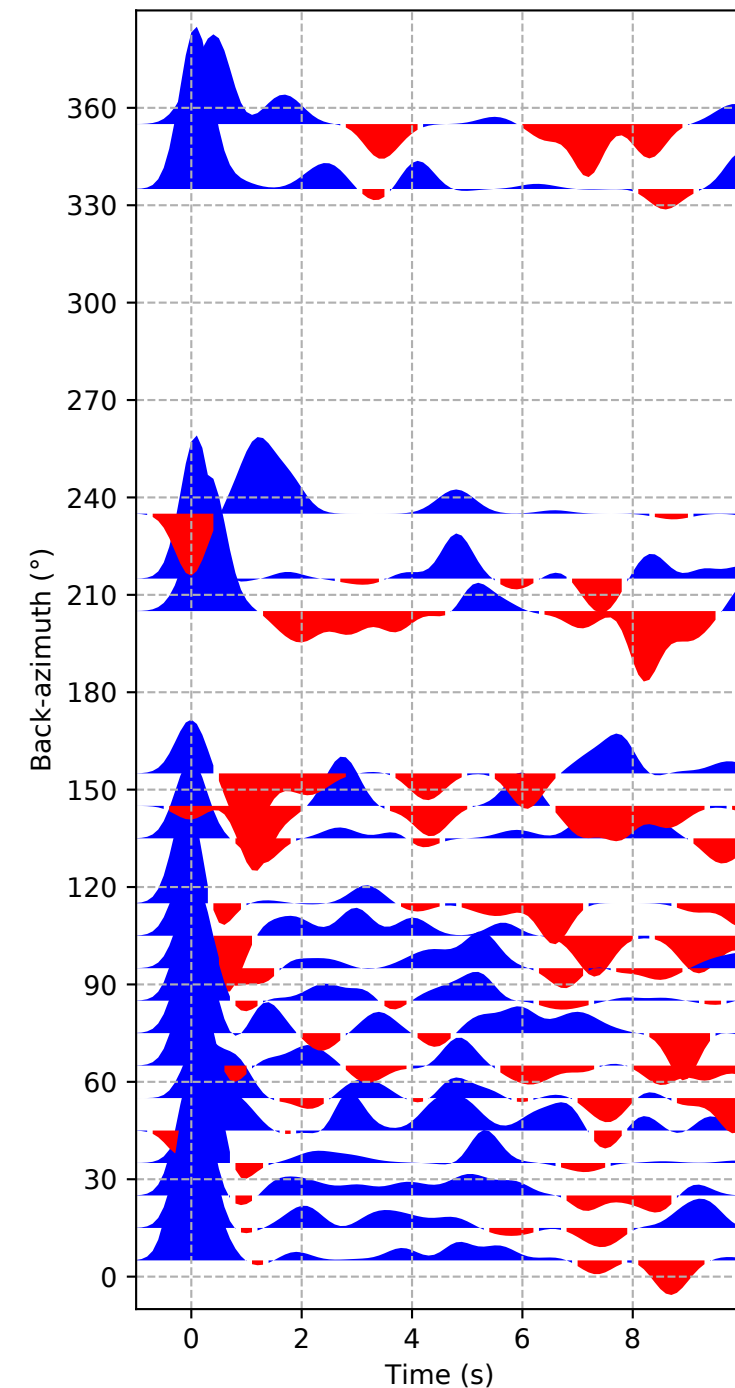


D) Rotated Harmonics components

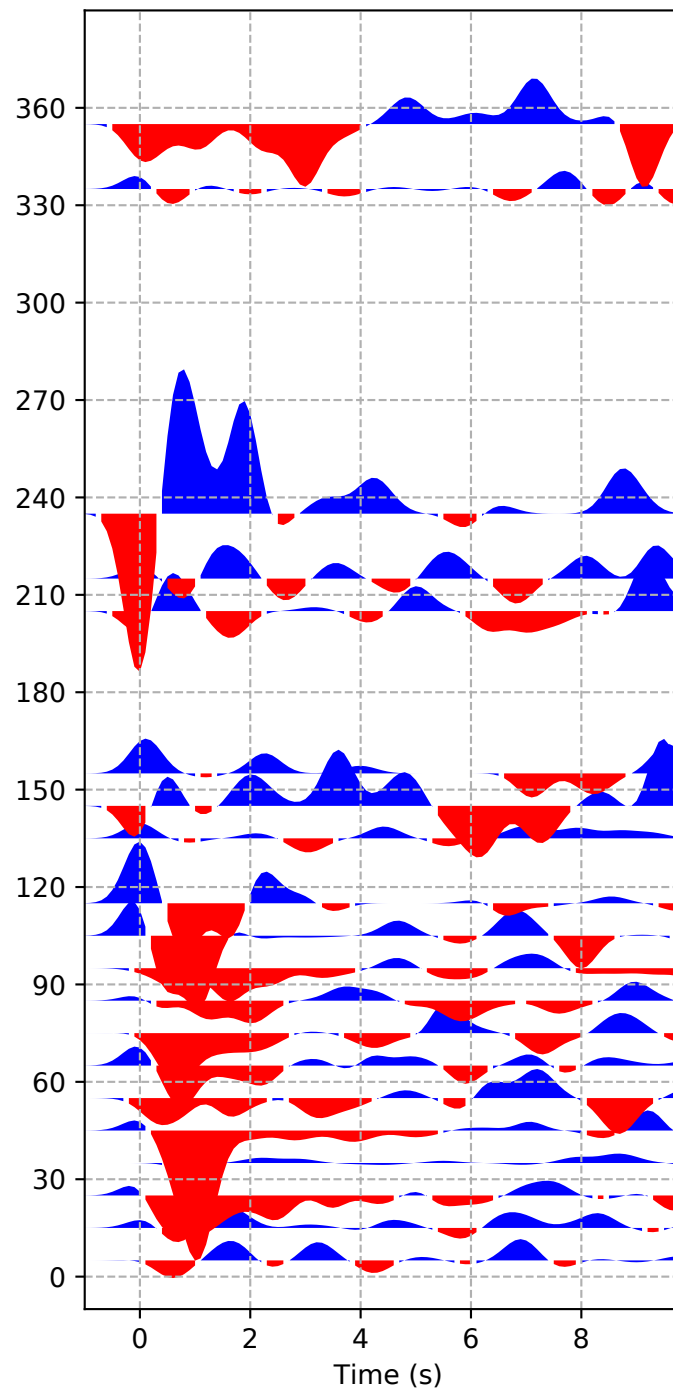


## XV-ZAKA

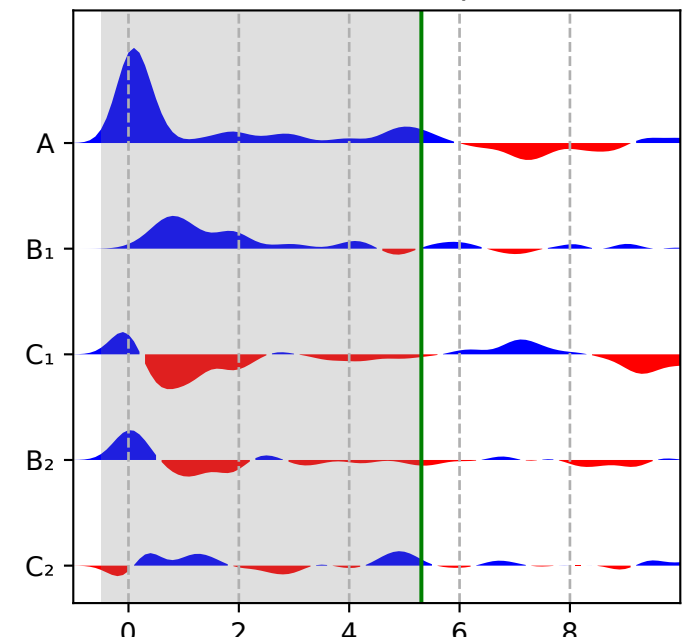
A) Radial



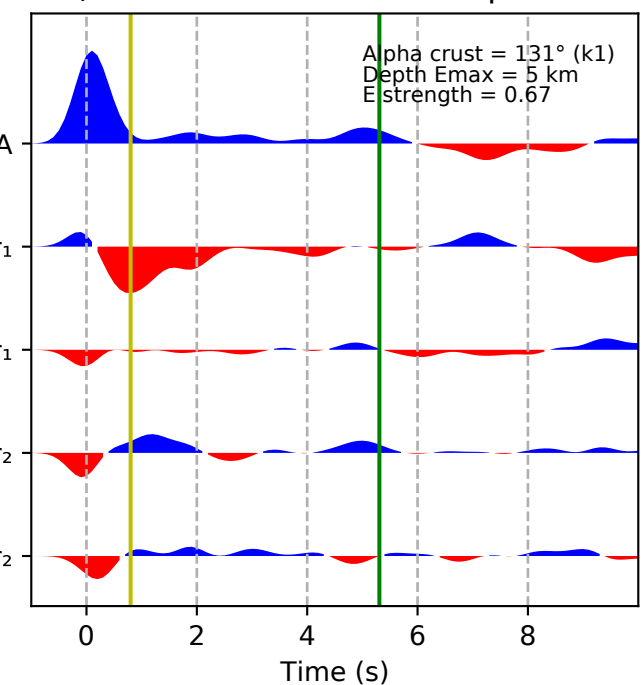
B) Transverse



C) Harmonics components

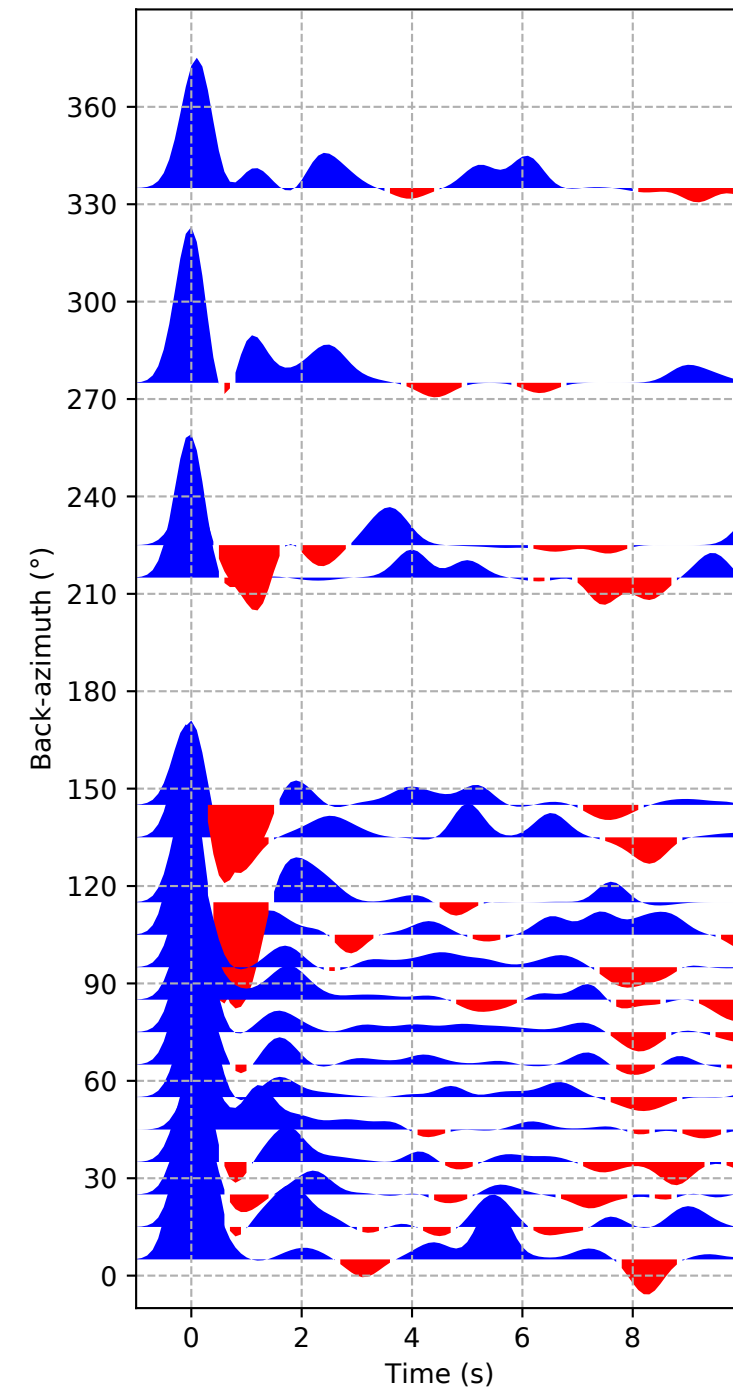


D) Rotated Harmonics components

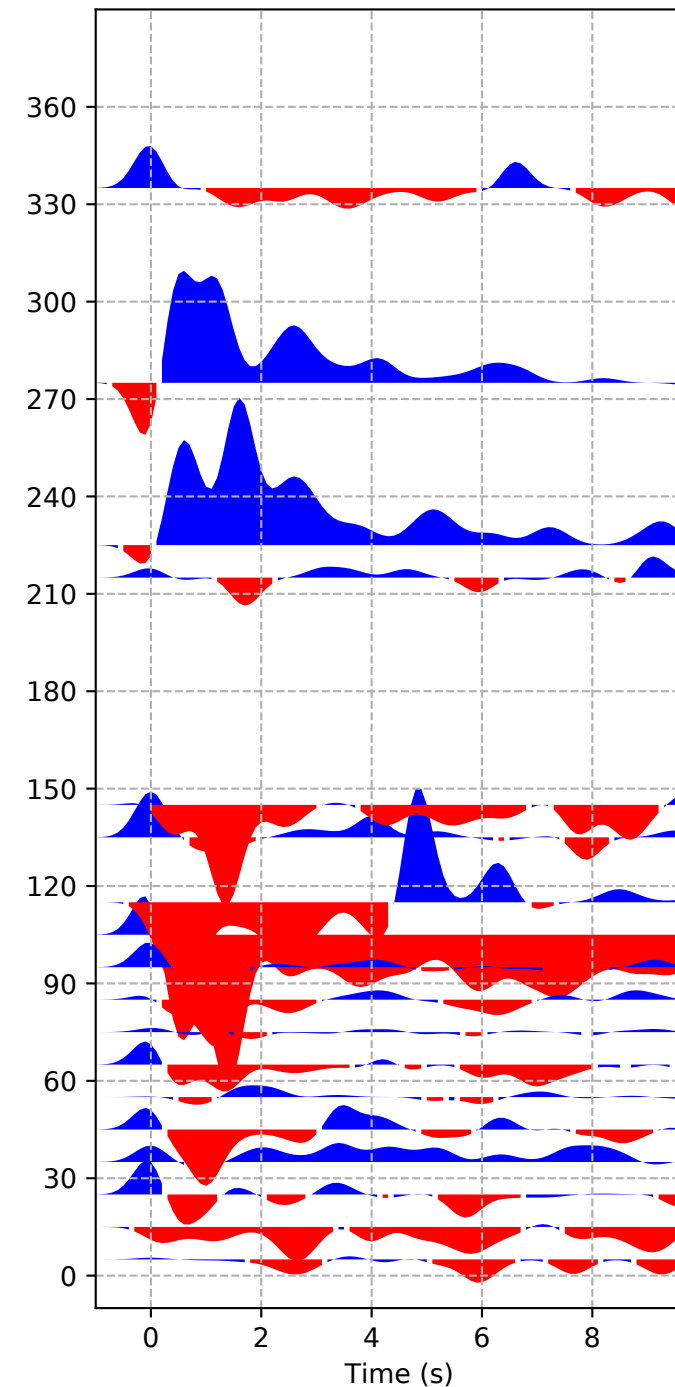


# XV-ZOBE

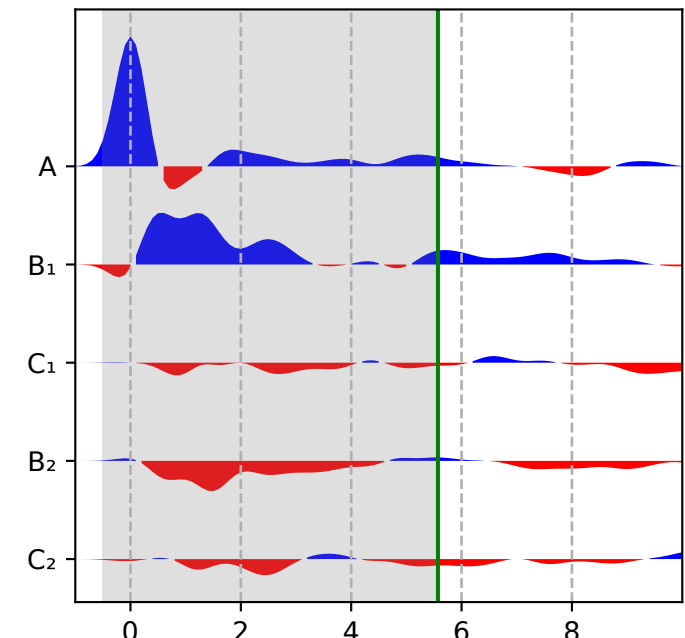
A) Radial



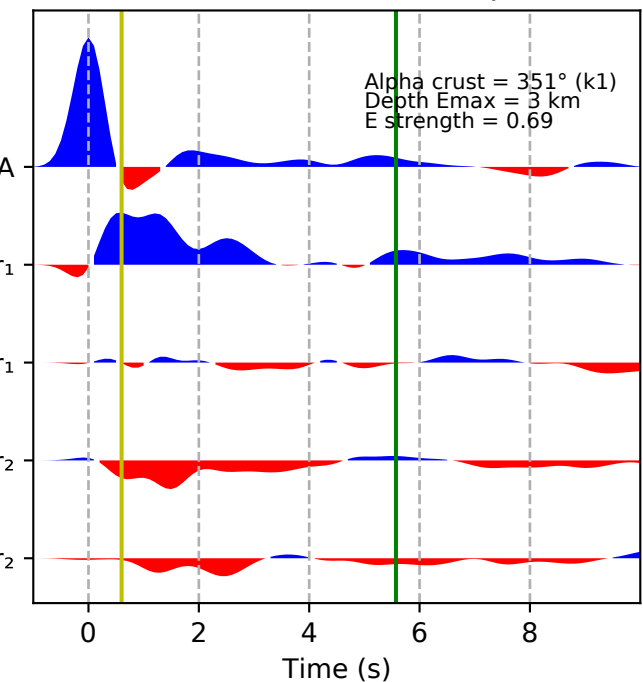
B) Transverse



C) Harmonics components

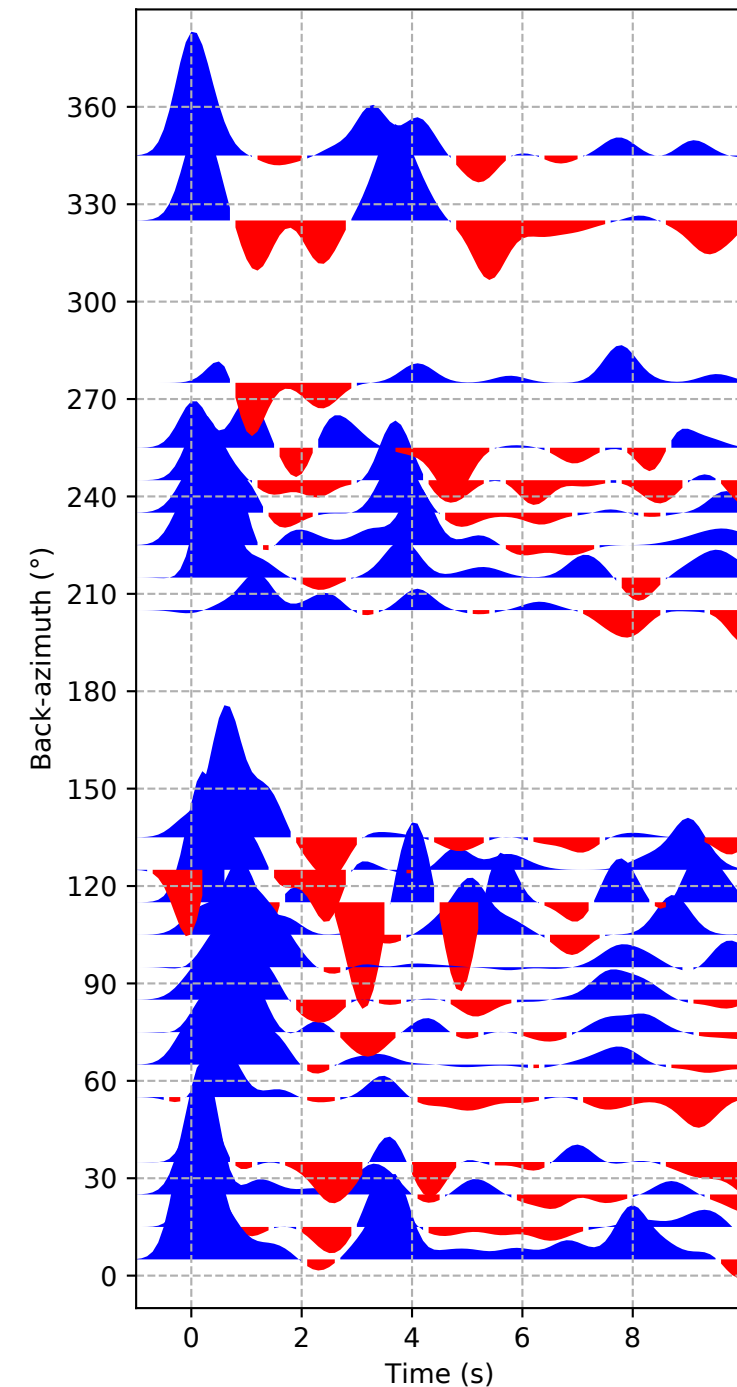


D) Rotated Harmonics components

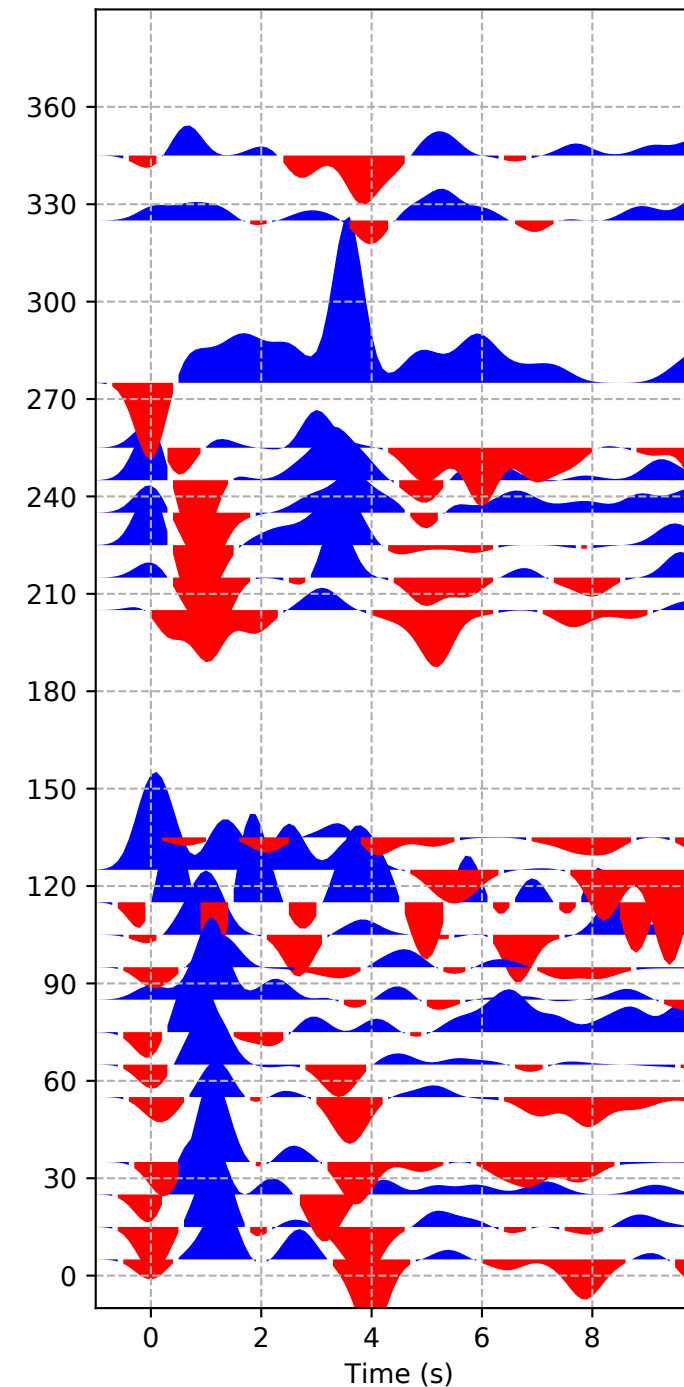


## YH-CHAL

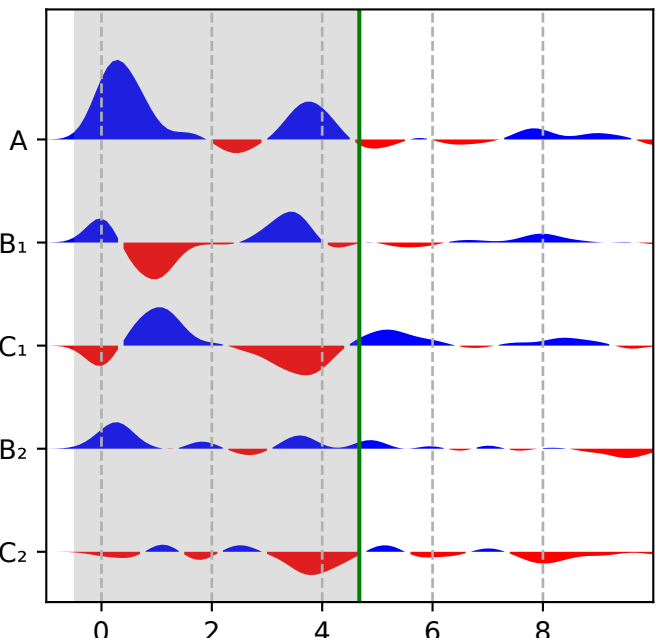
A) Radial



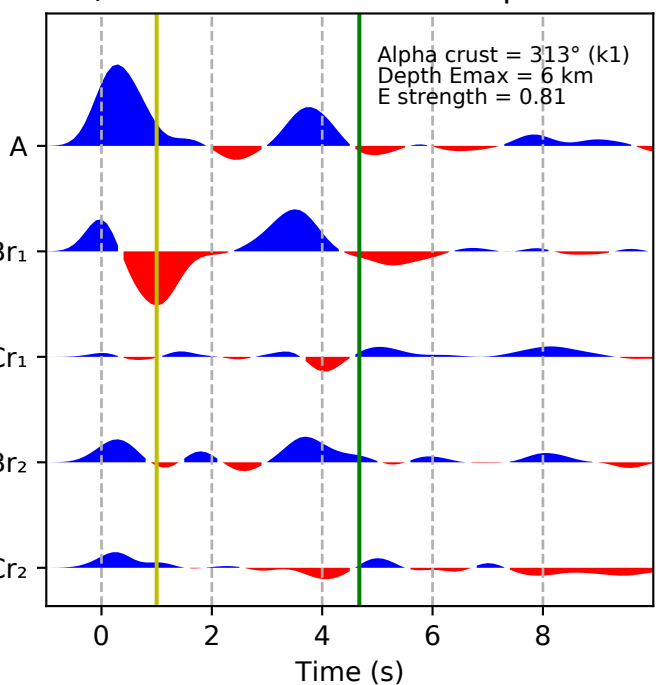
B) Transverse



C) Harmonics components



D) Rotated Harmonics components

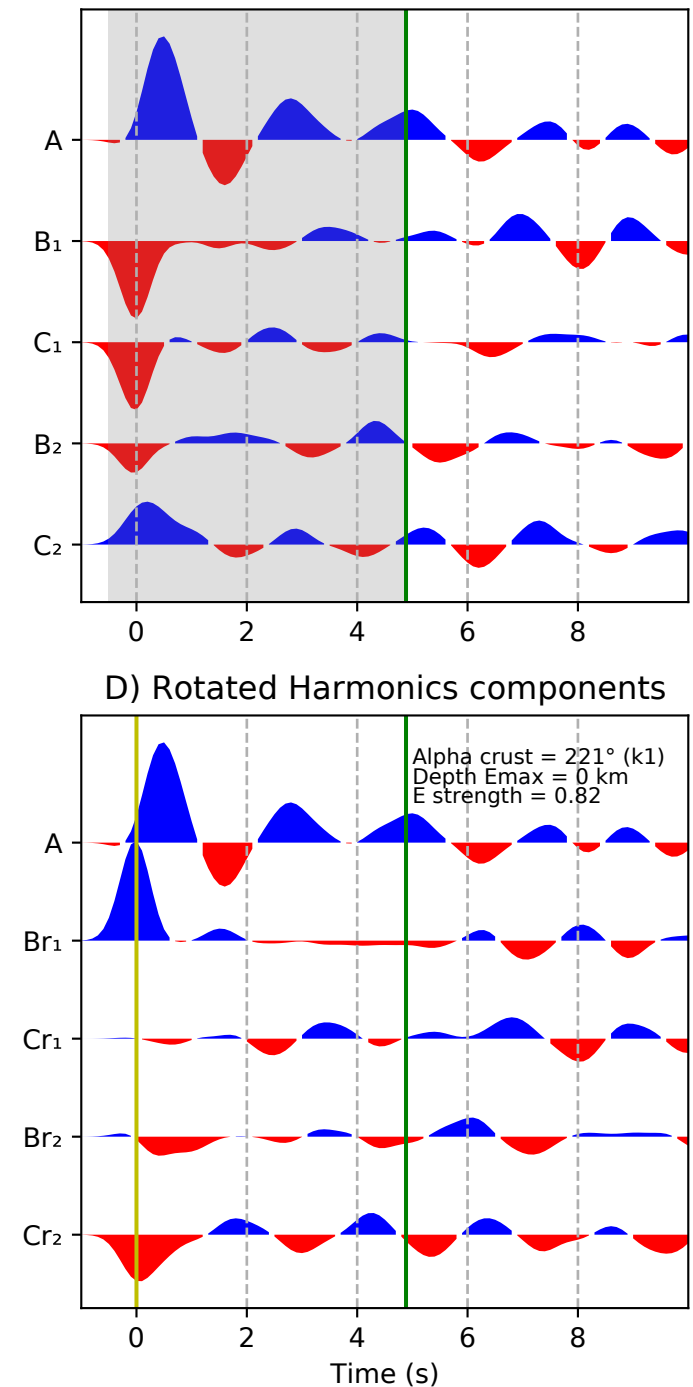
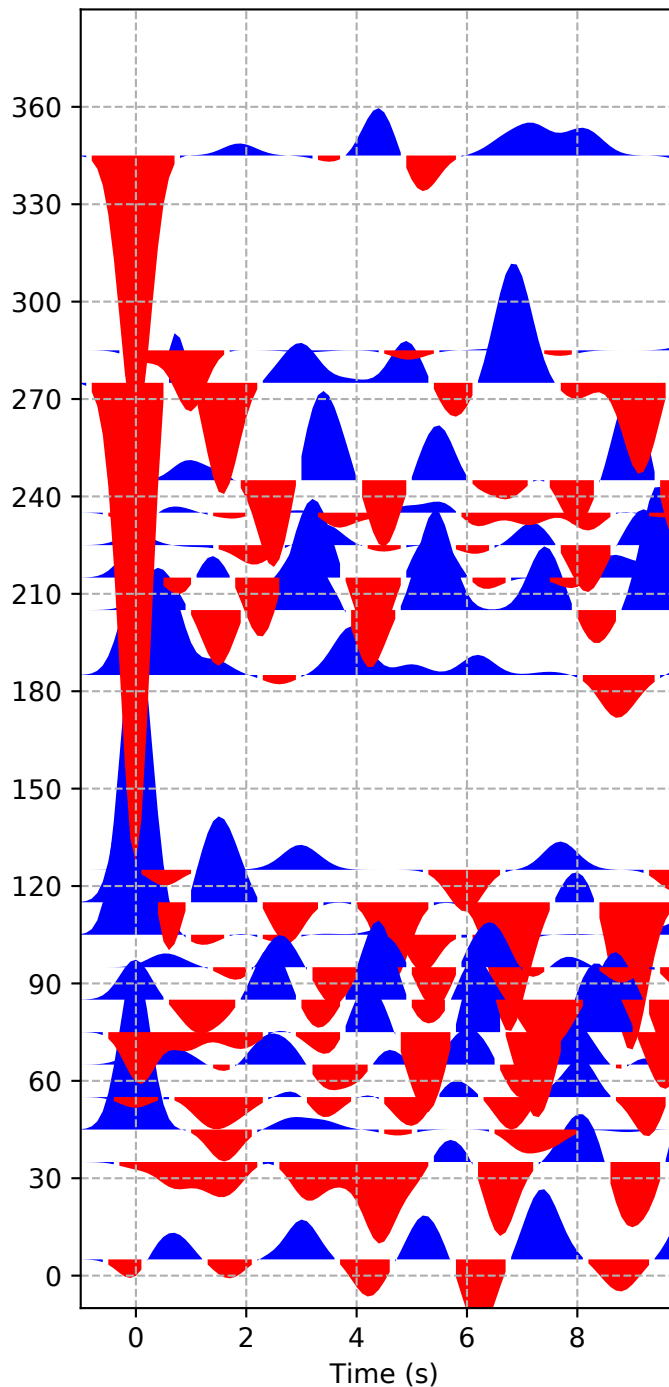
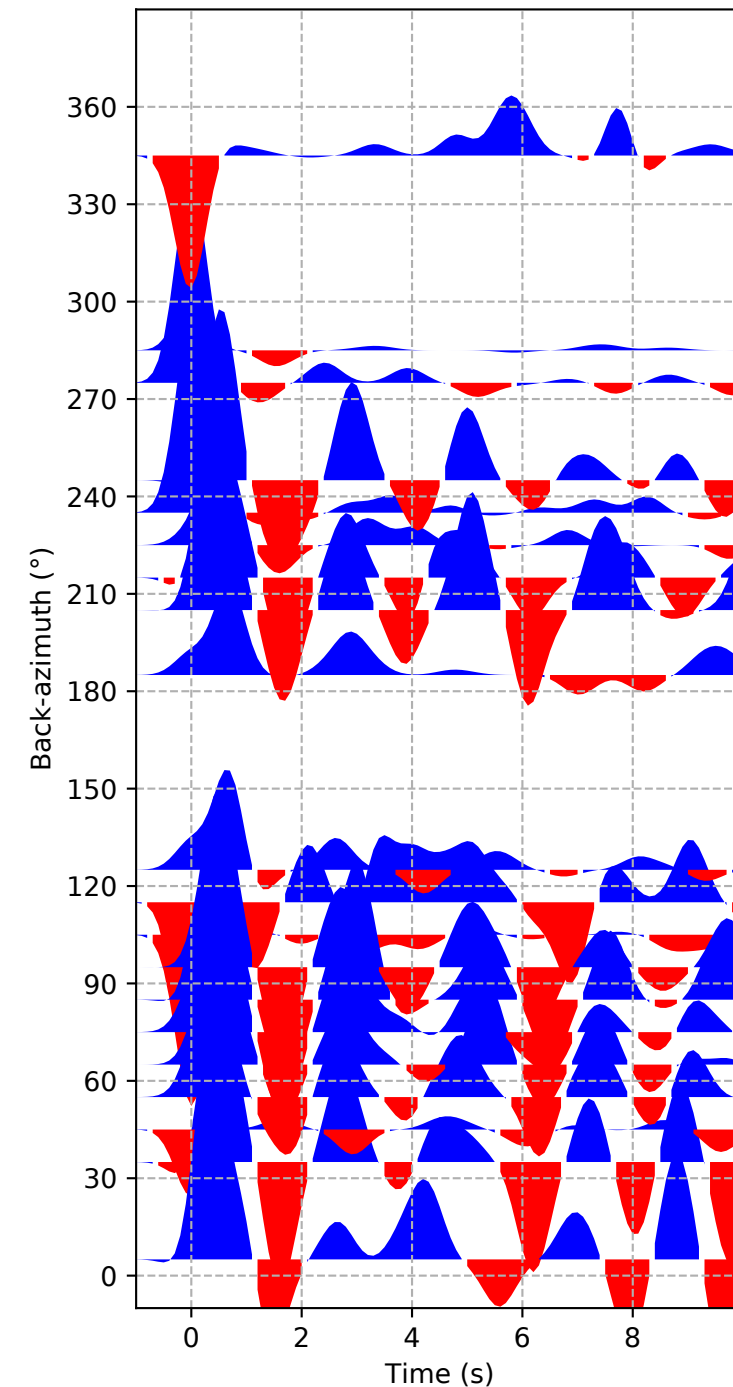


## YH-IFAK

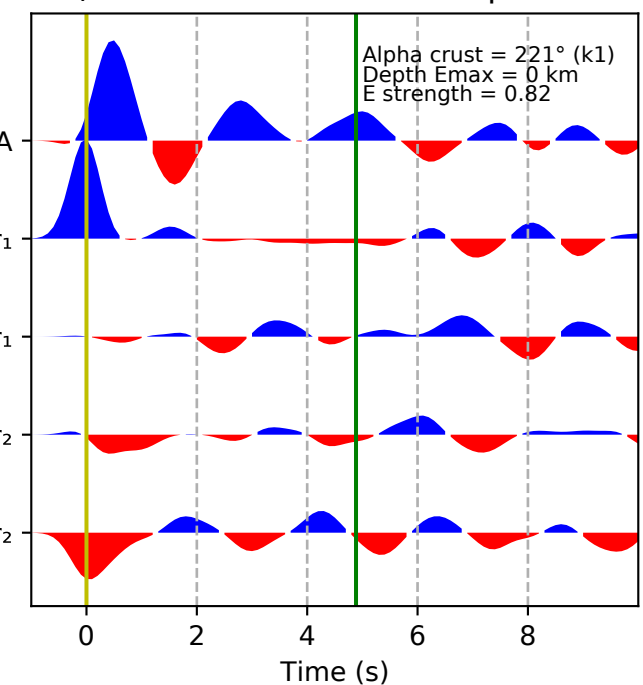
## B) Transverse

## C) Harmonics components

## A) Radial



## D) Rotated Harmonics components

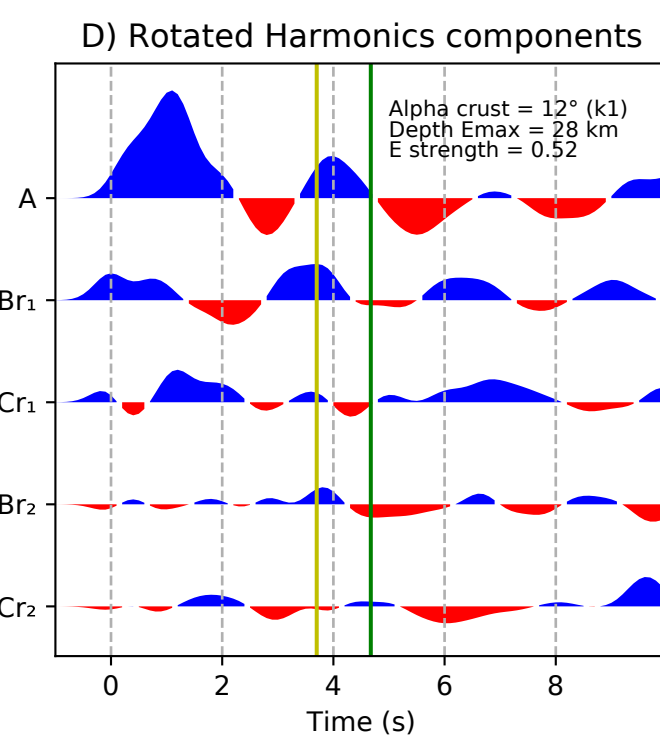
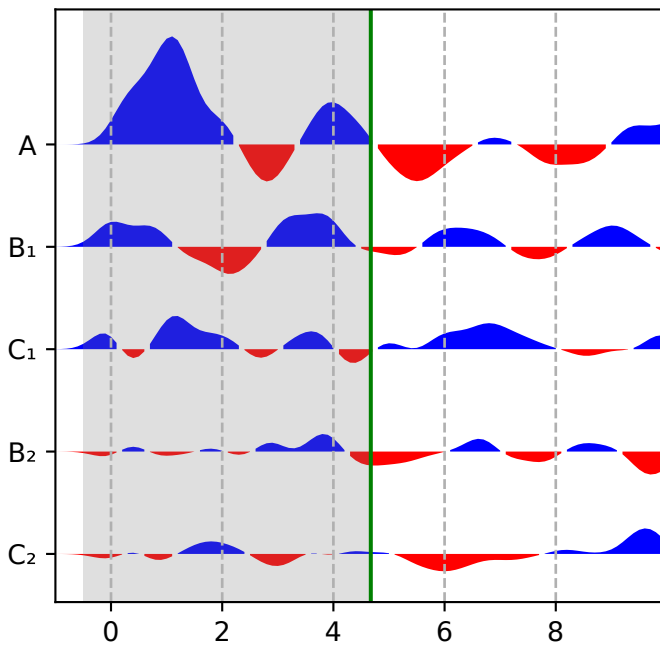
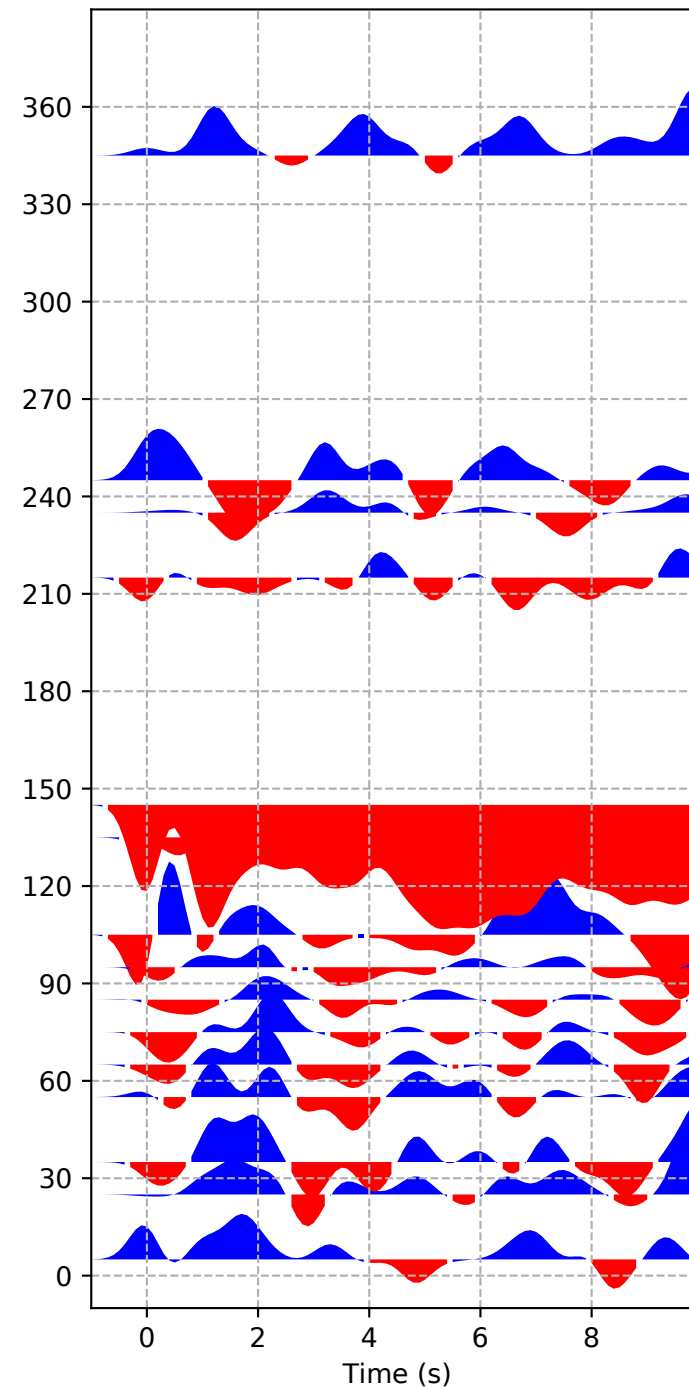
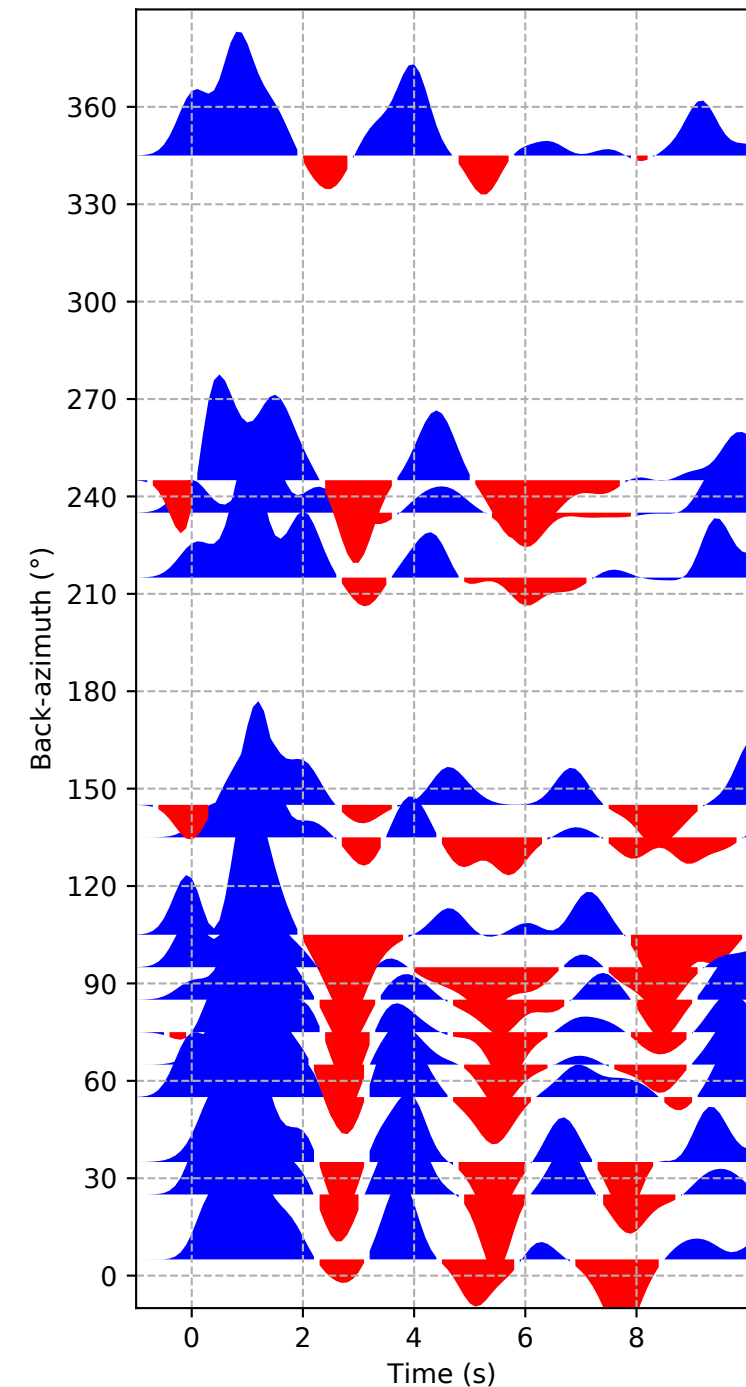


YH-INDI

B) Transverse

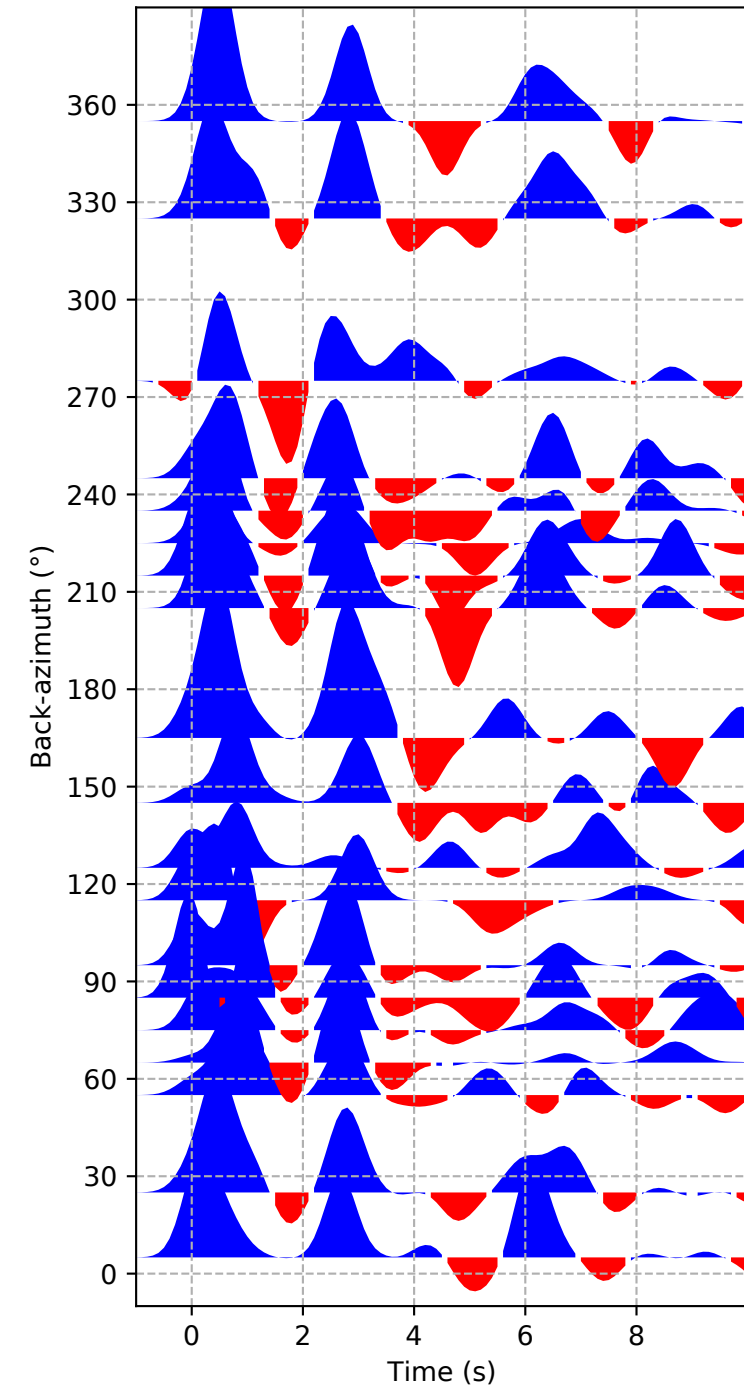
C) Harmonics components

A) Radial

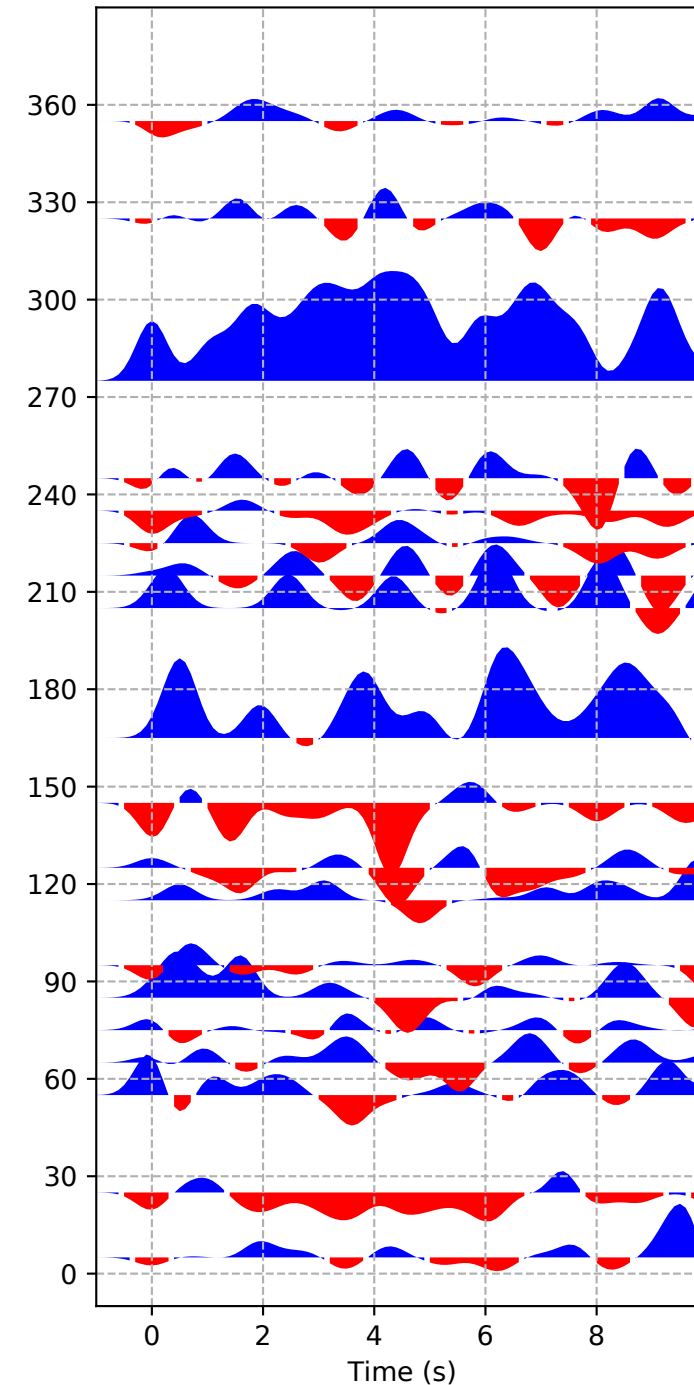


# YH-MANG

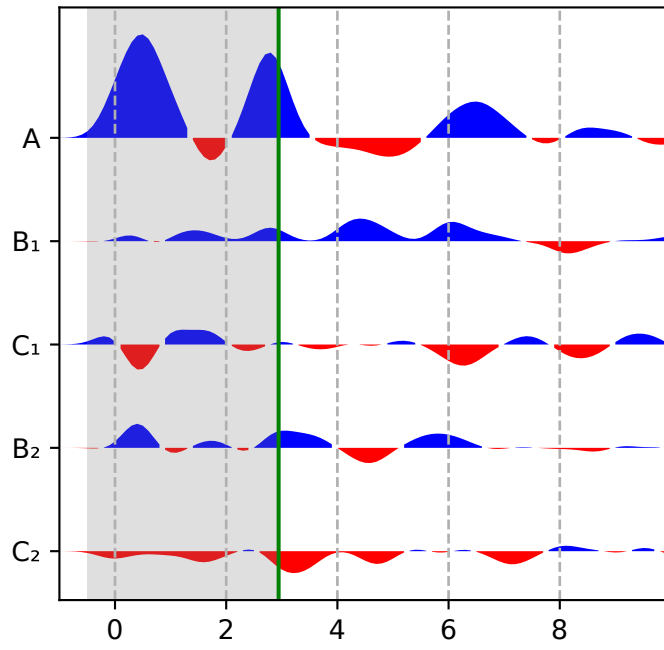
A) Radial



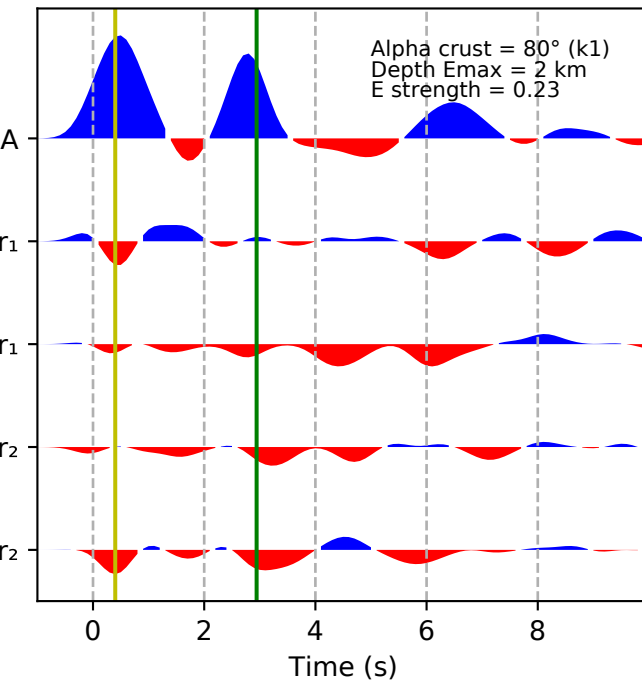
B) Transverse



C) Harmonics components

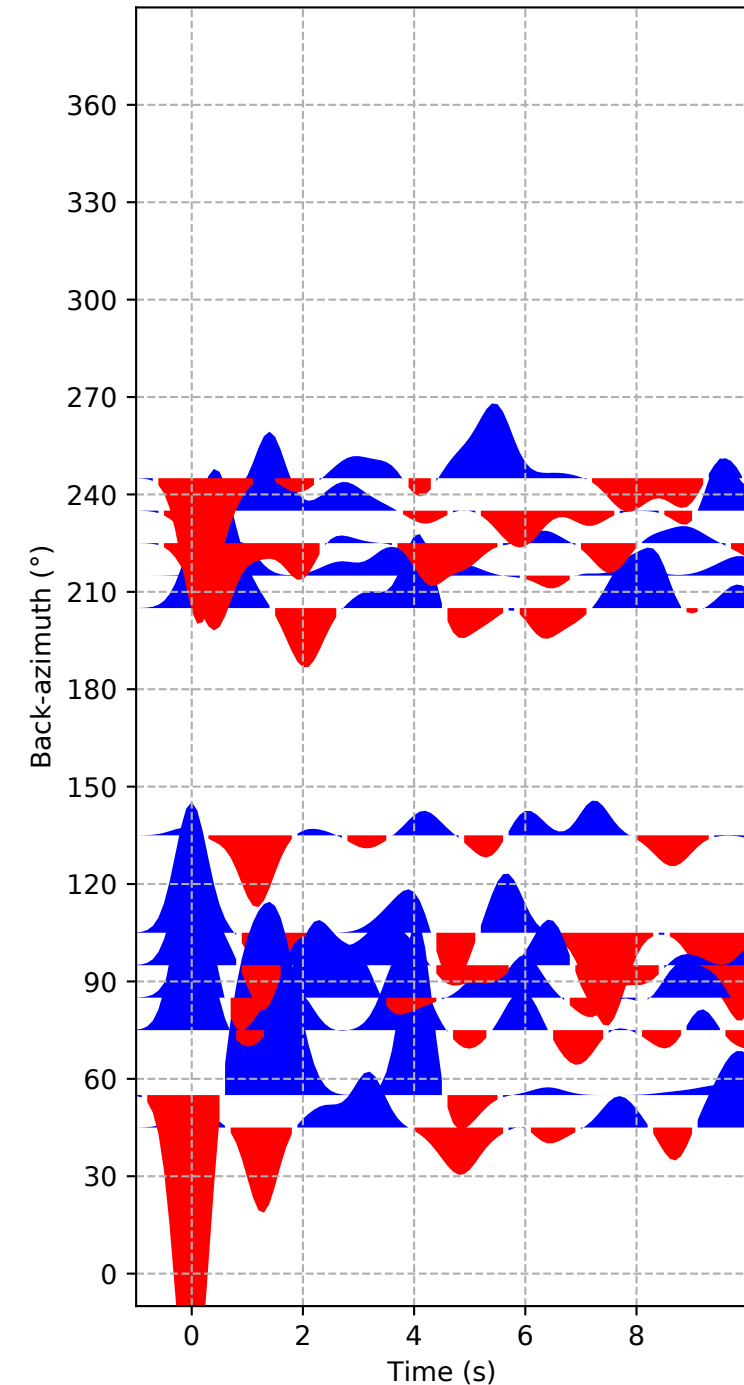


D) Rotated Harmonics components

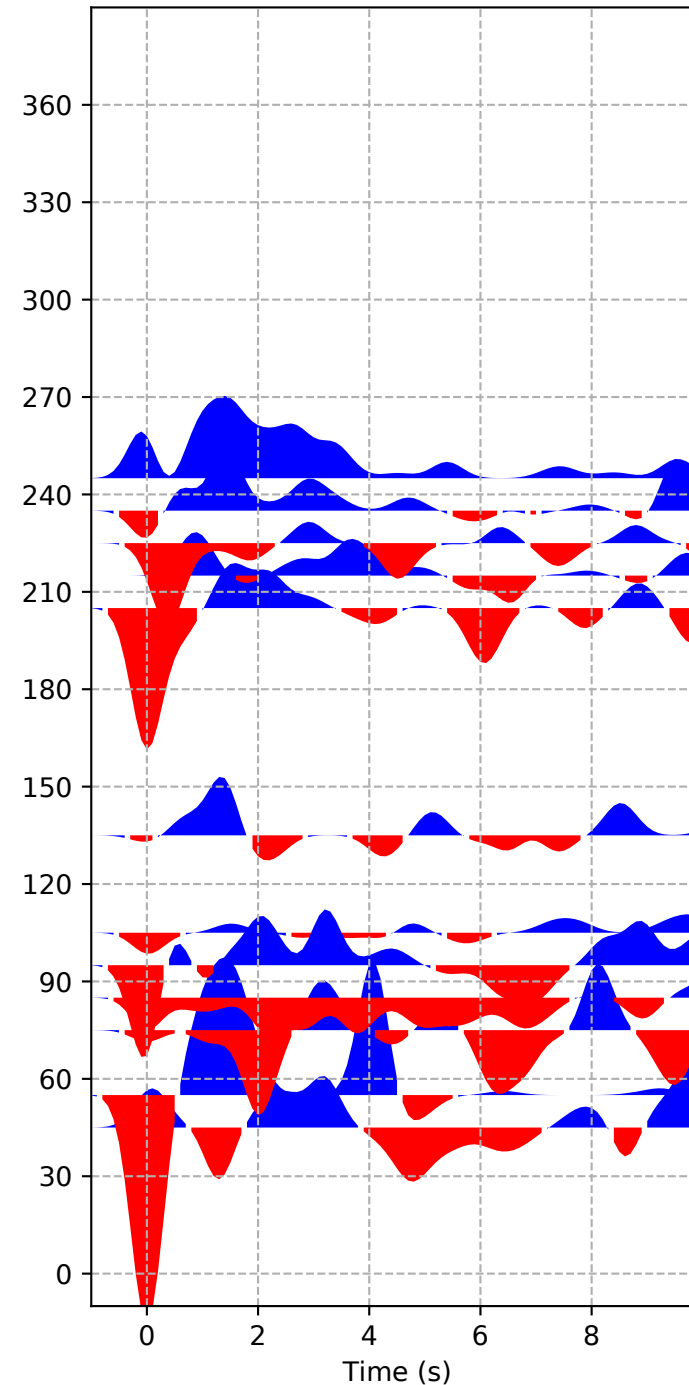


# YH-MOHO

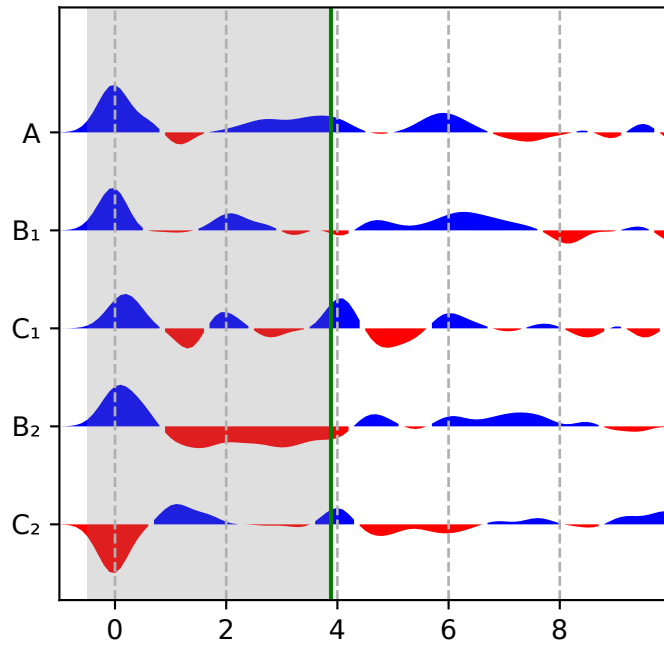
A) Radial



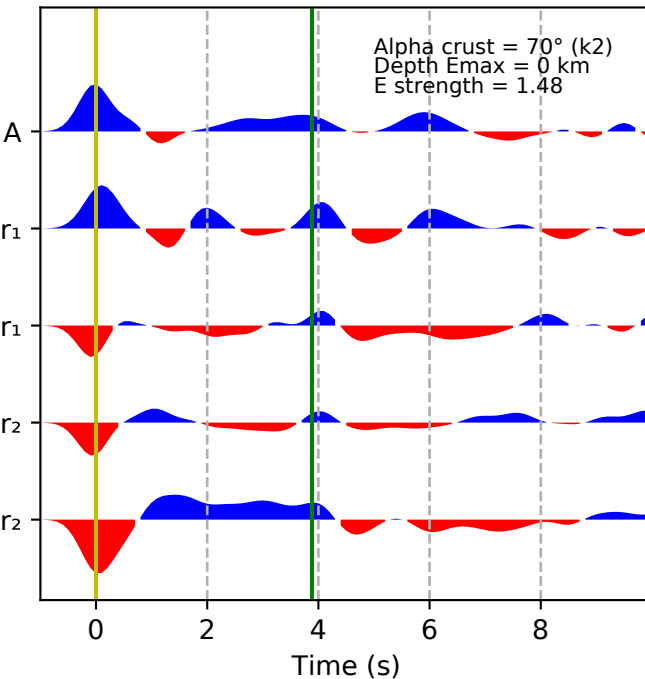
B) Transverse



C) Harmonics components

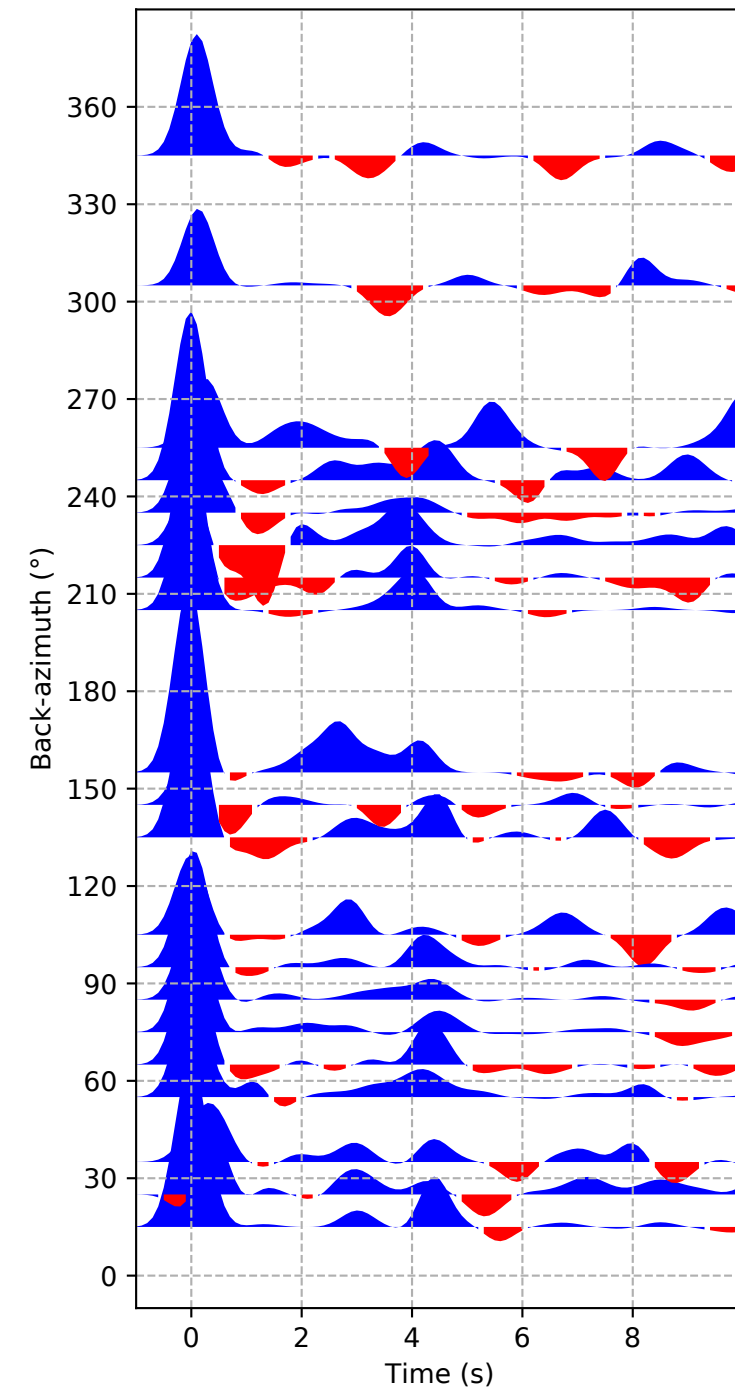


D) Rotated Harmonics components

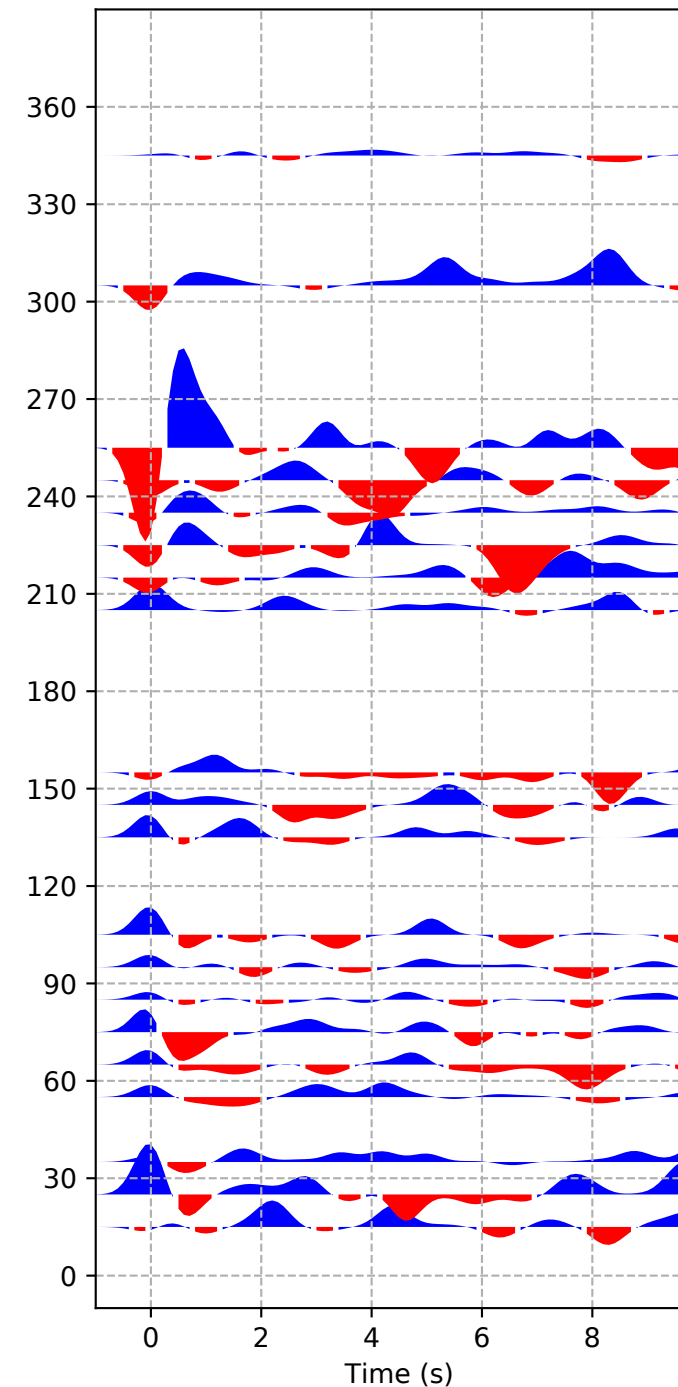


# YH-WALE

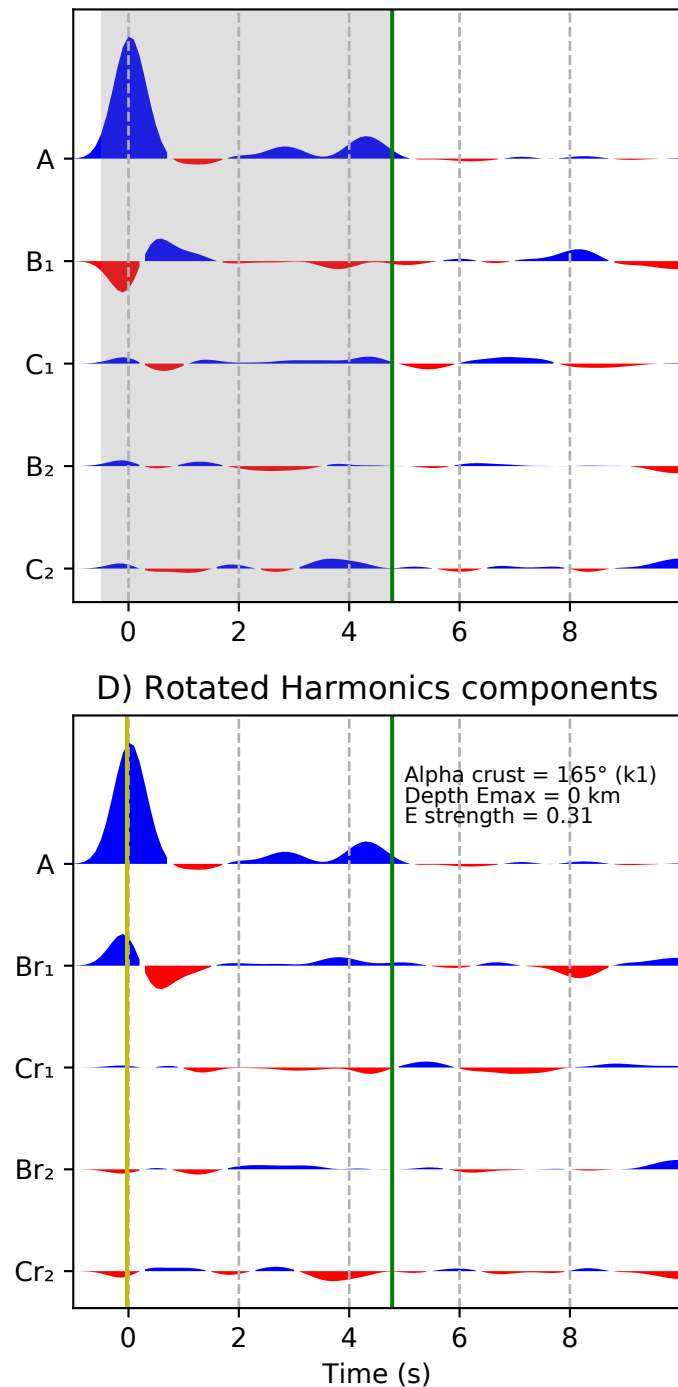
A) Radial



B) Transverse



C) Harmonics components



D) Rotated Harmonics components

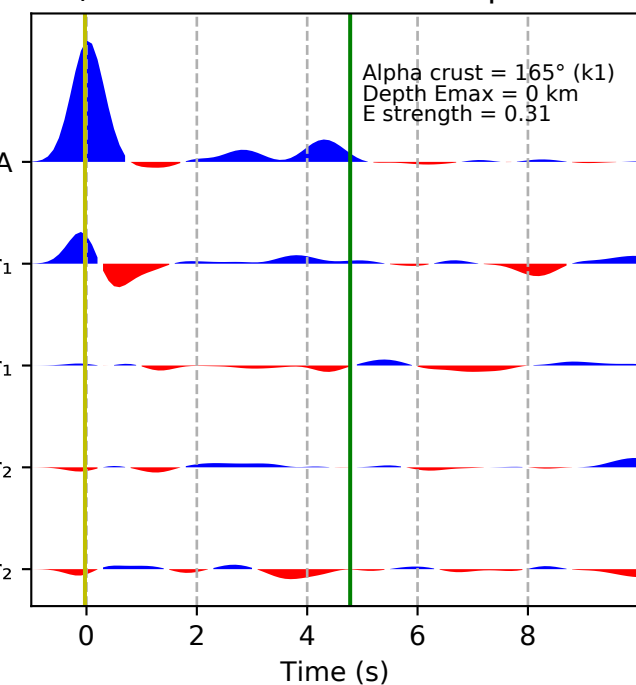


**Table S2.** Results and uncertainties of the h-k stacking method.

Station (network)	# RF used	Parameters set	H (km)	vp/vs	Corr (%)
CNG (AF)	8	1	37+/-0.9	1.84+/-0.03	-97.1
GRM (AF)	12	2	38+/-17.4	1.7+/-0.11	-86.2
HVD (AF)	41	2	40+/-1.2	1.72+/-0.05	-93.6
MOPA	29	1	42+/-3.7	1.72+/-0.08	-98.8
MZM (AF)	19	1	43+/-0.8	1.67+/-0.03	-96.4
SEK (AF)	39	2	40+/-1.6	1.68+/-0.05	-88.3
TETE (AF)	7	1	40+/-0.3	1.75+/-0.01	-85.5
WDLM (AF)	17	1	40+/-1.9	1.69+/-0.04	-84.0
ZOMB (AF)	49	1	39+/-0.6	1.75+/-0.02	-86.8
MOCU (XV)	6	1	37+/-0.5	1.72+/-0.02	-93.7
NAPU (XV)	8	2	42+/-4.1	1.68+/-0.05	-97.7
TETE (XV)	6	1	40+/-5.3	1.75+/-0.08	-99.5
MANG (YH)	22	1	21+/-0.4	1.79+/-0.02	-94.4
WALE (YH)	26	1	38+/-0.3	1.68+/-0.01	-86.7